Racemization of Chiral Sulfoxide Using an Immobilized Oxovanadium Catalyst

Tomoya Nishio,[1] Hajime Shigemitsu,[2,3] Toshiyuki Kida,[2,3] Shuji Akai,*[1] Kyohei Kanomata*[1]

[1]Graduate School of Pharmaceutical Sciences, Osaka University, 1-6 Yamadaoka, Suita, Osaka 565-0871, Japan

[2]Department of Applied Chemistry, Graduate School of Engineering, Osaka University, 2-1 Yamadaoka, Suita, Osaka 565-0871, Japan

[3]Integrated Frontier Research for Medical Science Division, Institute for Open and Transdisciplinary Research Initiatives (OTRI), Osaka University, 2-1 Yamadaoka, Suita Osaka 565-0871, Japan

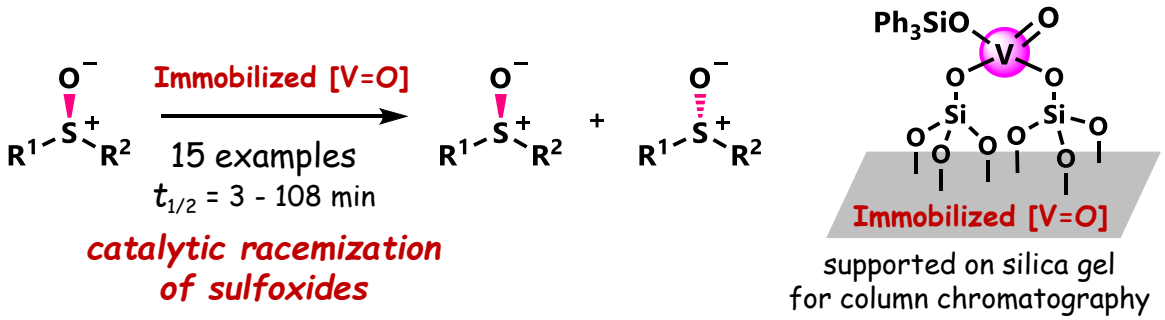

Abstract

Racemization of optically active compounds is an essential process in asymmetric transformations such as dynamic kinetic resolution and deracemization. In this study, the racemization of chiral sulfoxides under mild thermal conditions was realized using a novel silica-gel-supported oxovanadium catalyst. Specifically, we screened reaction conditions, analyzed the substrate scope, and conducted mechanistic studies of the silica-gel-supported oxovanadium-catalyzed racemization of sulfoxides. The racemization reaction has a wide substrate scope, including alkyl aryl sulfoxides and diaryl sulfoxides. The catalyst could be reused by exploiting its heterogeneous nature. Mechanistic studies suggested that racemization proceeds via the formation of a radical cation intermediate mediated by the oxovanadium(V)/(IV) redox cycle.

Keywords: heterogeneous catalysis, redox catalysis, radical cation

1. Introduction

Sulfoxides have stable chiral centers, and their optically active forms are commonly found in pharmaceuticals[1–4] and chiral ligands for asymmetric reactions.[5–8] Although the pyramidal inversion of sulfoxides requires high temperature (>200 °C),[9] rapid racemization under mild conditions using photocatalysts has been reported in recent years. In particular, *N*-methylquinolinium[10] and 2,4,6-triphenylpyridinium[11,12] salts catalyze the rapid racemization of sulfoxides upon photoirradiation, in which stereoinversion via the radical cations of sulfoxides was proposed. Moreover, thermal racemization via Ru(II)/Ru(III) redox catalysis[10] and [2,3]-sigmatropic rearrangement of allylic sulfoxides[13] have been reported, and the latter was coupled with Rh-catalyzed asymmetric hydrogenation to achieve dynamic kinetic resolution.[14]

Previously, we developed mesoporous silica-supported oxovanadium catalysts and used them in the racemization of alcohols (Figures 1a and 1b).[15–17] We utilized a redox-neutral process via V–O bond formation between the alcohol and oxovanadium center of the catalyst, followed by the formation of a carbocation intermediate. Moreover, we achieved oxidative cross-coupling reactions of aromatic C–H bonds using the same catalyst utilizing the redox nature of oxovanadium (Figure 1c).[18] During our continuous research, we discovered that silica-supported oxovanadium catalysts facilitate the racemization of sulfoxides under mild thermal conditions (Figure 1d). Considering the importance of racemization in asymmetric transformations, such as dynamic kinetic resolution and deracemization,[19–21] we investigated the unprecedented catalytic racemization of optically active sulfoxides in detail. This study reports the screening of reaction conditions, substrate scope, and mechanistic studies of the silica-supported-oxovanadium-catalyzed racemization of sulfoxides.

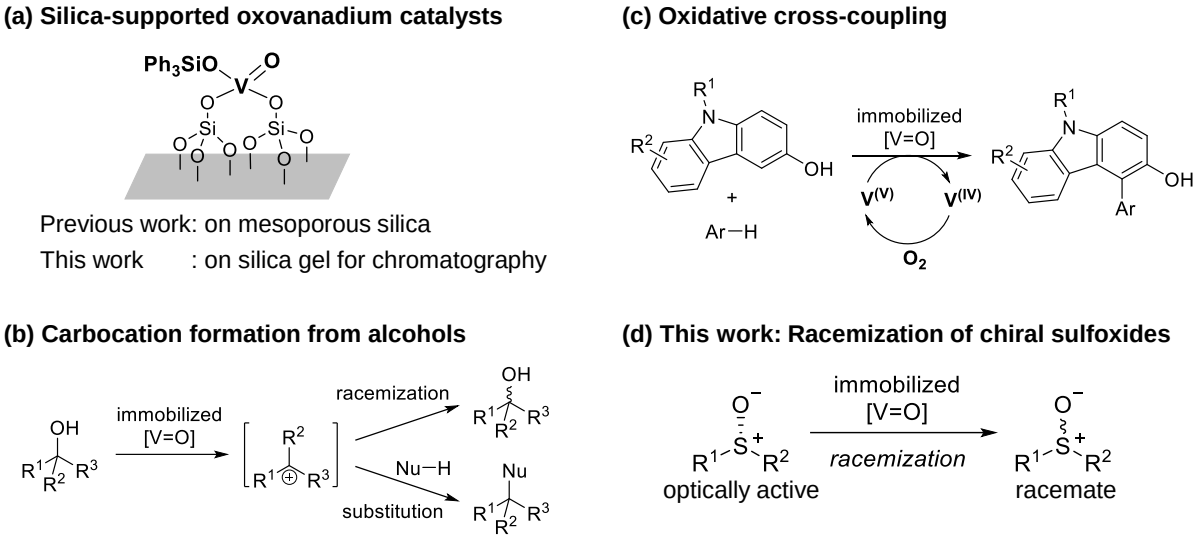

Fig. 1. Silica-supported oxovanadium species and their application in catalytic reactions: (a) structure of the silica-supported oxovanadium catalysts; (b) redox-neutral carbocation formation from alcohols; (c) oxidative cross-coupling reaction; (d) racemization of chiral sulfoxides.

2. Results and discussion

In this study, oxovanadium species were investigated for the racemization of enantiomerically pure alkyl aryl sulfoxide (*R*)-**1a** as a typical substrate (Table 1). When the reaction was conducted using mesoporous-silica-supported oxovanadium V-MPS4[15,16] as the catalyst (containing 5 mol% vanadium relative to **1a**), the racemization proceeded smoothly in 1,2-dichloroethane at 50 °C, and the decay in enantiomeric excess (% ee) followed first-order kinetics with a half-life ($t_{1/2}$) of 11 h (Entry 1). The immobilization of oxovanadium on a commercially available silica gel for column chromatography with particle size of 40–50 μm (V-SilicaGel) showed a 3.6-fold increase in the rate constant (k_{rac}) under the same reaction conditions as those utilized for V-MPS4 (Entry 2). In V-MPS4, the vanadium species are immobilized on the inner surface of the mesoporous silica with a pore diameter of 4 nm. Consequently, the reduced reactivity of V-MPS4 compared to V-SilicaGel is probably attributed to the restricted diffusion of substrates within the porous structure. Moreover, upon using $VO(SiPh_3)_3$, the precursor for preparing V-MPS4 and V-SilicaGel, significantly slower racemization was observed (approximately one hundredth in the rate constant) although the reaction mixture was homogeneous (Entry 3 vs Entry1). Although these catalysts have an oxovanadium(V) oxidation state, $VO(acac)_2$ and $VOSO_4$—both of which contain the oxovanadium(IV) oxidation state—were found to be ineffective for the racemization of **1a** (Entries 4 and 5). Notably, the decomposition of **1a** was not observed during the reaction and **1a** was recovered quantitatively under all conditions.

Table 1. Oxovanadium-catalyzed racemization of (*R*)-**1a**[a].

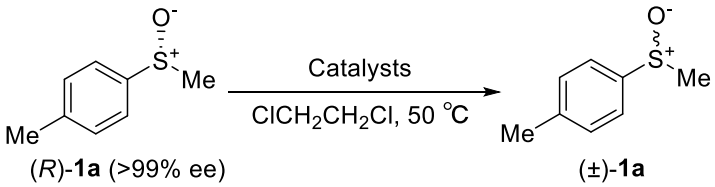

(*R*)-**1a** (>99% ee) (±)-**1a**

Entry	Catalyst	$t_{1/2}$/h	k_{rac}/h^{-1}
1	V-MPS4	1.1×10^{1}	6.4×10^{-2}
2	V-SilicaGel	3.0	2.3×10^{-1}
3	$VO(OSiPh_3)_3$	2.8×10^{2}	2.5×10^{-3}
4	$VOSO_4$	No racemization	
5	$VO(acac)_2$	No racemization	

[a] The reaction was conducted with (*R*)-**1a** (0.10 mmol) and oxovanadium catalyst (containing 5.0 mol% of vanadium relative to **1a**) in 1, 2-dichloroethane (0.1 M) at 50 °C. The time course of % ee was monitored by analyzing aliquots of the reaction mixture using chiral HPLC.

The effects of the solvent on the racemization of **1a** were investigated using V-SilicaGel as the catalyst (Table 2). The racemization rate increased with the solvent dielectric constant (relative permittivity). Thus, racemization was slow in a low-polarity aromatic hydrocarbon, namely, toluene (Entry 1), whereas it was faster in the higher-polarity solvent, THF (Entry 2). The racemization rates in acetone and nitromethane (Entries 3 and 4) were comparable, and the highest rate was observed in acetonitrile, with $t_{1/2}$ of 0.88 h (Entry 5). Conducting the reaction under dark conditions did not affect the racemization rate, indicating that a photocatalytic mechanism is not involved in the oxovanadium-catalyzed racemization (Entry 6). The racemization rate significantly increased at the elevated temperature (Entry 7; 80 °C). By contrast, no racemization occurred in Lewis basic solvents such as EtOH, DMF, and DMSO (Entries 8–10).

Table 2. Solvent effects on the racemization of (*R*)-**1a**[a].

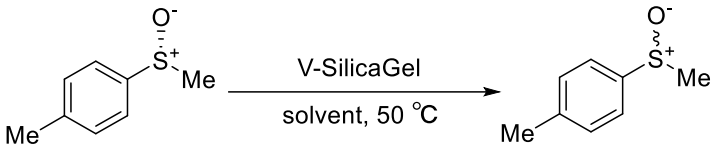

(*R*)-**1a** (>99% ee) (±)-**1a**

Entry	Solvent (0.1 M) [dielectric constant][22,23]	$t_{1/2}$/h	k_{rac}/h^{-1}
1	toluene [2.4][22]	9.0	7.7×10^{-2}
2	THF [7.6] [22]	5.8	1.2×10^{-1}
3	acetone [20.6] [22]	1.9	3.7×10^{-1}
4	$MeNO_2$ [22.7] [23]	2.0	3.5×10^{-1}
5	MeCN [35.9] [22]	8.8×10^{-1}	7.9×10^{-1}
6[b]	MeCN	8.8×10^{-1}	7.9×10^{-1}
7[c]	MeCN	5.8×10^{-2} (3.5 min)	1.2×10^{1}
8	EtOH	No racemization	
9	DMF	No racemization	
10	DMSO	No racemization	

[a] Unless otherwise noted, the reaction was conducted using (*R*)-**1a** (0.10 mmol) and V-SilicaGel (5.0 mol%) in the indicated solvent (0.1 M) at 50 °C. [b] Reaction conducted in dark. [c] The reaction was conducted at 80 °C.

With the optimal racemization conditions in hand (Table 2, Entry 7), we investigated the scope and limitations of the V-SilicaGel-catalyzed racemization of alkyl/aryl and aryl/aryl sulfoxides **1** (Scheme 1). The introduction of electron-donating groups at the *para*-position of the phenyl group increased the racemization rate. Thus, **1a**, bearing the *para*-Me group, exhibited a shorter half-life of % ee (3.6 min) than non-substituted **1b** (4.5 min), while **1c**, bearing a *para*-OMe group, had a much shorter half-life of % ee (2.7 min). By contrast, the presence of electron-withdrawing groups such as Br (**1d**), CN (**1e**), and NO_2 (**1f**) at the *para*-position cause a decrease in the racemization rate, resulting in half-lives of 7–15 min. Notably, **1g** having an NMe_2 group, was also racemized under these thermal conditions although some decomposition occurred, and the decay of % ee did not follow first-order kinetics. This resulted in a sharp contrast to the reported photocatalytic racemization, in which the racemization of **1g** did not proceed at all.[11] The steric effect had a significant impact on the racemization rate. In particular, the racemization rate decreased for *ortho*-iodo-substituted **1h**. The steric effect of the alkyl group (R^2) on the racemization rate was investigated. Although the racemization rate of **1i** (R^2 = Et) was comparable to that of **1a** ($t_{1/2}$ = 4.9 min), it decreased considerably as the R^2 group became bulkier. Although the racemization of **1j** (R^2 = ^{i}Pr) proceeded with a half-life of 41 min, **1k** (R^2 = ^{t}Bu) did not racemize under these conditions. The racemization of **1l** (R^2 = cyclopropyl) proceeded ($t_{1/2}$ = 72 min), with 99% recovery of **1l** upon the completion of racemization, and no ring-opened product was observed. The racemization rates of **1m** (R^2 = cyclopentyl) and **1n** (R^2 = vinyl) were comparable to that of **1j** at the initial stage of the reaction. However, the racemization rate of these two compounds decreased during the reaction, and complete racemization was not achieved even after 24 h. The racemization of diaryl sulfoxides **1o** and **1p** was also examined, which was much slower ($t_{1/2}$ > 100 min) than that of alkyl aryl sulfoxides. Although the initial racemization rates of **1o** (R^1 = *p*-tolyl, R^2 = Ph) and **1p** (R^1 = *p*-tolyl, R^2 = C_6H_4-4-OMe) were comparable, the racemization of **1p** decelerated during the reaction and was incomplete within 24 h, whereas **1o** smoothly racemized to afford a racemic mixture in 24 h. In all cases, **1** with a decreased enantiomeric excess, was isolated with a high recovery ratio. The reduced racemization rate of OMe-substituted **1p** compared to **1o** is explained by their transition-state structures. Due to steric hindrance from *ortho*-hydrogen atoms, the two benzene rings and the sulfoxide moiety in **1o** and **1p** are not coplanar in the transition state. As a result, the inductive effect of the OMe group dominates over the resonance effect, destabilizing the radical cation and decreasing the racemization rate of **1p**. In contrast, the racemization of alkyl-aryl sulfoxides **1a**–**1f**, in which the benzene ring and sulfoxide moiety are coplanar, follows the general substituent effect of the benzene ring, as indicated by the Hammett plot (Fig. 2). These structural features of the transition states were confirmed by DFT calculations (Table S3).

Scheme 1. Scope and limitation of racemization of **1**[a].

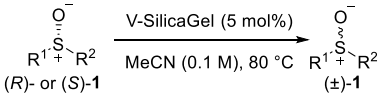

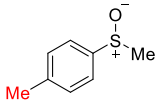

1a
>99% ee to <1% ee
in 0.5 h, 98% recov.
($t_{1/2}$ = 3.8 min)

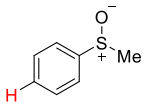

1b
66% ee to <1% ee
in 1.0 h, 97% recov.
($t_{1/2}$ = 4.7 min)

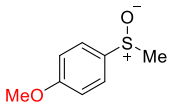

1c
89% ee to <1% ee
in 1.0 h, 98% recov.
($t_{1/2}$ = 2.9 min)

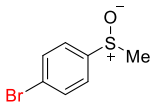

1d
84% ee to <1% ee
in 2.0 h, 99% recov.
($t_{1/2}$ = 8.5 min)

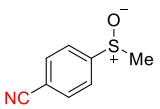

1e
57% ee to <1% ee
in 2.0 h, >99% recov.
($t_{1/2}$ = 14 min)

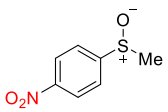

1f
83% ee to <1% ee
in 3.0 h, 99% recov.
($t_{1/2}$ = 16 min)

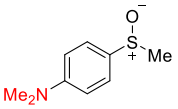

1g
51% ee to 39% ee
in 24 h, 84% recov.
($t_{1/2}$ = n.d.)[b]

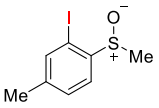

1h
94% ee to <1% ee
in 6.0 h, 99% recov.
($t_{1/2}$ = 25 min)

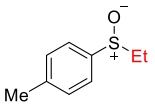

1i
97% ee to <1% ee
in 1.0 h, 98% recov.
($t_{1/2}$ = 5.0 min)

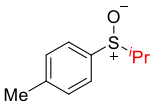

1j
97% ee to <1% ee
in 24 h, 96% recov.
($t_{1/2}$ = 41 min)

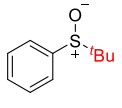

1k
No racemization

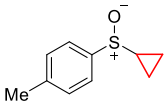

1l
95% ee to <1% ee
in 24 h, 99% recov.
($t_{1/2}$ = 69 min)

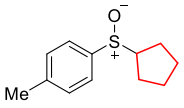

1m
88% ee to 17% ee
in 24 h, 94% recov.
($t_{1/2}$ = n.d.)[b]

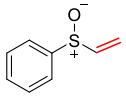

1n
44% ee to 25% ee
in 24 h, 93% recov.
($t_{1/2}$ = n.d.)[b]

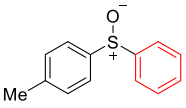

1o
98% ee to 3% ee
in 24 h, 99% recov.
($t_{1/2}$ = 110 min)

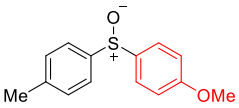

1p
98% ee to 49% ee
in 24 h, 98% recov.
($t_{1/2}$ = n.d.)[b]

[a] Unless otherwise noted, the reaction was conducted using **1** (0.10 mmol) and V-SilicaGel (containing 5.0 mol% of vanadium relative to **1**) in acetonitrile (0.1 M) at 80 °C. The recovery ratio (%) is the isolated yield of **1** at the indicated time. [b] Half-life was not determined because decay of % ee did not follow the first-order kinetics. n.d.: not determined.

Furthermore, the functional group tolerance of the racemization reaction was investigated by performing the reaction in the presence of several additives (Table 3). The racemization of (*R*)-**1a** (E_{pa} = +2.01 V vs Ag|AgCl) proceeded without decreasing the reaction rate in the presence of electron-rich aromatic compounds 1,3,5-trimethoxybenzene (**2**) and thioanisole (**3**) (Entries 1 and 2). In addition, completely racemized **1a** and the additives were recovered in >90% after 3 h in both cases. These results are in sharp contrast to the reported photocatalytic racemization, in which the reaction was completely suppressed by additives with low oxidation potentials.[11] In contrast, the addition of alcohol **4** decelerated the racemization reaction to some extent although its oxidation potential E_{pa} (+2.10 V vs Ag|AgCl) is considerably higher than those of **2** (+1.40 V vs Ag|AgCl) and **3** (+1.39 V vs Ag|AgCl) (Entry 3, also see Figure S3 for cyclic voltammograms). These results indicate that coordinating heteroatoms negatively impact racemization, probably by competing with **1a** to react with oxovanadium to initiate racemization. Other coordinating additives, such as indole (**5**) and *N*-Me indole (**6**), significantly decreased the racemization rate (Entries 4 and 5), and 4-methoxybenzenethiol (**7**) completely suppressed racemization with the concomitant formation of the disulfide (Entry 6). The complete inhibition of

racemization by **7** was attributed to the reduction of oxovanadium(V) to oxovanadium(IV) via disulfide formation.

Table 3. V-SilicaGel-catalyzed racemization of (*R*)-**1a** in the presence of additives[a].

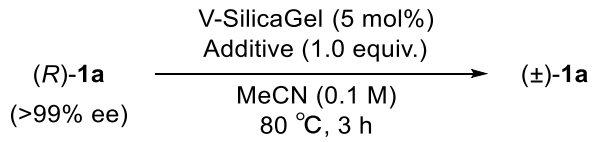

Entry	Additive (E_{pa} vs Ag|AgCl)		% ee of **1a**[b]	% Recovery of **1a**/additive[c]
1	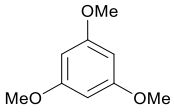 (+1.40 V)	**2**	<1	>95/>95
2	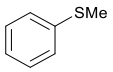 (+1.39 V)	**3**	<1	>95/91
3	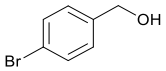 (+2.10 V)	**4**	23	>95/>95
4	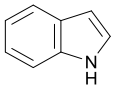 (+1.27 V)	**5**	89	>95/>95
5	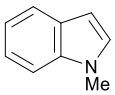 (+1.15 V)	**6**	58	>95/>95
6	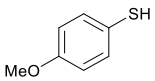 (+1.20 V)	**7**	>99	>95/71 (14)[d]

[a] The reaction was conducted using **1a** (0.10 mmol), the indicated additive (0.10 mmol), and V-SilicaGel (containing 5.0 mol% of vanadium relative to **1a**) in acetonitrile (0.10 M) at 80 °C for 3 h. [b] The % ee values were measured via HPLC conducted using a chiral stationary phase column. [c] The yield was determined through ^{1}H NMR analysis of the crude reaction mixture using trichloroethylene as an internal standard. [d] The disulfide (0.014 mmol) that corresponds to the additive was produced, and the yield of the disulfide is shown in parentheses.

Next, we investigated the reusability of the V-SilicaGel catalyst (Table 4). After 30 min of reaction using (*R*)-**1a**, the catalyst was recovered by centrifugation and reused for the next racemization reaction. While the catalyst was handled under ambient atmosphere, precautions were taken to minimize moisture exposure (See Supporting Information for the detailed procedure). The catalytic activity of V-SilicaGel was maintained for up to four runs, and completely racemized **1a** was quantitatively isolated in each reaction. However, in the fifth run, the racemization did not complete in 30 min.

Table 4. Reusability of V-SilicaGel[a].

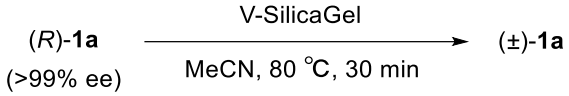

Run[a]	1	2	3	4	5
%ee of **1a**	<1	<1	<1	2	10
% recovery of **1a**	>95	>95	>95	>95	>95

[a] Each reaction was performed using **1a** (0.10 mmol) in acetnitrile (0.10 M). V-SilicaGel (39 mg, containing 5.0 mol% of vanadium relative to **1a**) was used for the first run. Following the reaction, the catalyst was recovered via centrifugation and reused for the next run. The yield was determined by ^{1}H NMR analysis of the crude reaction mixture using trichloroethylene as an internal standard.

To investigate the reaction mechanism, kinetic analyses of the oxovanadium-catalyzed thermal racemization of sulfoxides were performed. A Hammett plot of k_{rac} against σ^+_{para} values using sulfoxides **1a**–**1f** showed a good linear correlation (Figure 2a; $\rho = -0.50$, $R^2 = 0.94$, also see Table S1). The negative ρ value suggested that the rate-determining step involves a cationic intermediate. This result is in good agreement with a previous report by Lanzalunga et al., wherein $Ru(bpy)_3(PF_6)_2$ was used as a thermal redox catalyst.[10] They proposed that racemization proceeded via the reversible formation of a sulfoxide radical cation intermediate. The temperature dependence of the rate constant was also investigated to obtain the thermodynamic parameters of the reaction. The rate constant of pyramidal inversion $k_{enant.}$ (= $k_{rac}/2$) obtained for **1a** was applied to an Eyring plot to determine the activation parameters (Figure 2b; $\Delta H^{\ddagger} = 78.0$ kJ mol^{-1}, $\Delta S^{\ddagger} = -34.6$ J mol^{-1} K^{-1}, also see Supporting Information). A relatively small $\Delta S^{\ddagger}$ value indicates that the transition state is an intramolecular process. Thus, a sulfoxide radical cation would be generated by inner-sphere electron transfer following the complexation of **1** with an oxovanadium center of the V-SilicaGel catalyst.

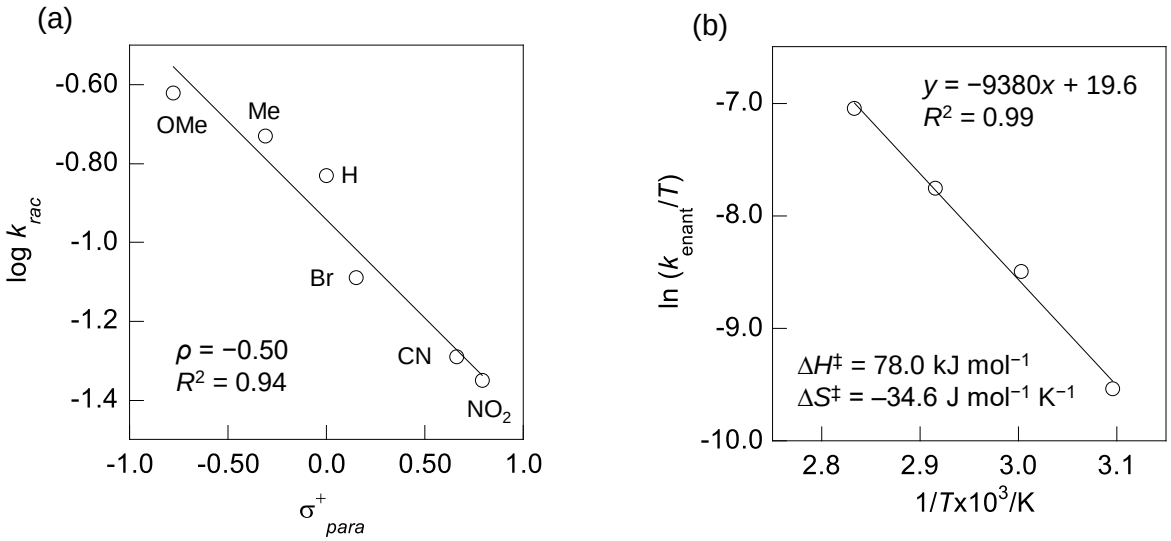

Fig. 2. a) Hammet plot of log k_{rac} vs σ^+_{para}; b) Eyring plot for the racemization of **1a**.

Density functional theory (DFT) calculations were performed to obtain further insights into the reaction mechanism. The transition state structures of pyramidal inversion were identified for both **1** and its corresponding radical cations at the M05-2X/6-311+G(d,p) level of theory (Scheme 2).[11] The activation energies for the pyramidal inversion calculated for some representative sulfoxides **1** were all approximately 170 kJ mol^{-1}, regardless of the substituents, suggesting that enantiomerization would hardly occur under the present reaction conditions (Scheme 2a, also see Table S3). Conversely, the activation energy of inversion for the radical cations was approximately 40 kJ mol^{-1}, which is in good agreement with a previous report (Scheme 2b).[10] Thus, enantiomerization would proceed via radical cation intermediates, which was also suggested in the Hammett plot analysis (Figure 2a). Considering that the activation free energy ($\Delta G^‡$) experimentally obtained from the Eyring plot was 90 kJ mol^{-1} at 353 K (see Table S2), the rate-determining step is not the pyramidal inversion step, but rather the generation of the radical cation intermediate through the reaction between the oxovanadium(V) catalyst and **1**. Thus, the significant electronic and steric effects observed in the substrate scope are attributable to the redox process and/or V–O bond formation between **1** and V-SilicaGel, rather than the enantiomerization process.

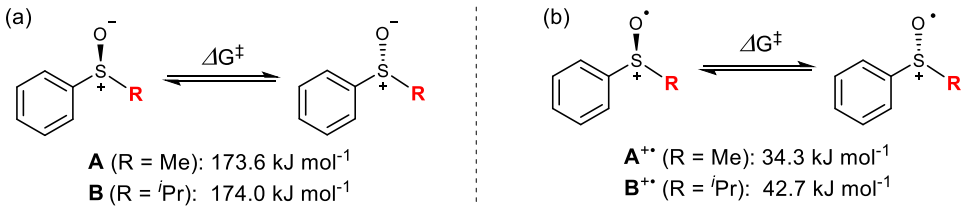

Scheme 2. DFT calculation of the activation free energy ($\Delta G^‡$) of pyramidal inversion. All calculations were performed at M05-2X/6-311+G(d,p).

A plausible mechanism for the V-SilicaGel-catalyzed enantiomerization of (*S*)-**1** is illustrated in Scheme 3. Initially, the oxygen of sulfoxide (*S*)-**1** attacks to the oxovanadium(V) center of the catalyst to form intermediate **I** with concomitant release of a triphenylsiloxy anion (Ph_3SiO^-). The subsequent ligand-to-metal charge transfer (LMTC) under thermal conditions forms complex **II** with oxovanadium(IV), in which the sulfoxide moiety is a radical cation. Complex **II** is in rapid enantiomerization equilibrium with the sulfoxide moiety of *ent*-**II**. Subsequently, metal-to-ligand charge transfer (MLCT) in *ent*-**II** forms *ent*-**I**, which undergoes substituent exchange with another (*S*)-**1** to release (*R*)-**1**.

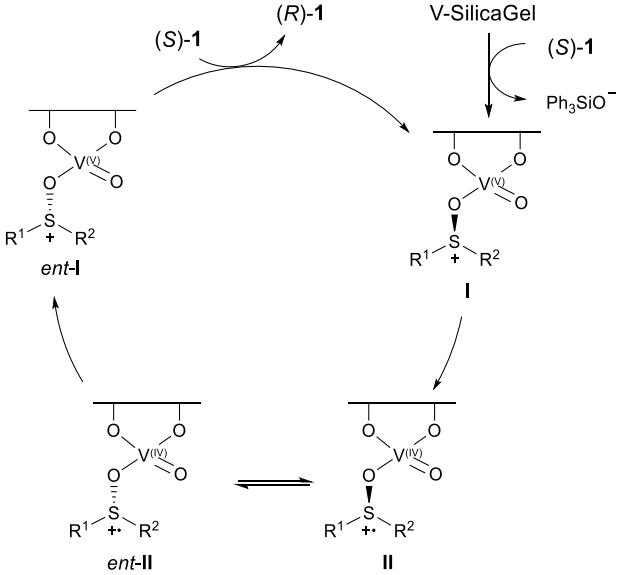

Scheme 3. Plausible reaction mechanism of V-SilicaGel-catalyzed enantiomerization of **1**.

3. Conclusion

We developed a thermal racemization method for optically active sulfoxides catalyzed by silica-gel-supported oxovanadium under mild thermal conditions. The racemization reaction exhibited a wide substrate scope, including alkyl aryl sulfoxides and diaryl sulfoxides. Notably, racemization was tolerated by oxidation-labile functional groups, such as electron-rich aromatic rings, which were not applicable in the previously reported photocatalytic racemization.[11] Additionally, taking advantage of the heterogeneous catalyst, it was repeatedly reused without a significant loss of catalytic activity. Mechanistic studies suggested that enantiomerization proceeds via a radical cation species of sulfoxide in the inner sphere of the oxovanadium catalyst. Further application of the catalytic racemization of sulfoxides at dynamic kinetic resolution is currently underway in our laboratory.

Acknowledgement

The computation was performed using Research Center for Computational Science, Okazaki, Japan (Project: 24-IMS-C216).

Supplementary data

Supplementary material is available at *Bulletin of the Chemical Society of Japan.*

Funding

This work was supported by JSPS KAKENHI Grant Numbers 24K02148 (S.A.) and 24K08410 (K.K.), JSPS Research Fellowship for Young Scientists 24KJ1586 (T.N.), JST SPRING Grant Number JPMJSP2138 (T.N.), The Research Foundation for Pharmaceutical Sciences (K.K.), Amano Institute of Technology (K.K.), Tokuyama Science Foundation (K.K.), the Nissan Chemical Award in the Society of Synthetic Organic Chemistry Japan (K.K.), Japan Foundation for Applied Enzymology (K.K.), "Innovation inspired by Nature" Research Support Program, SEKISUI CHEMICAL CO., LTD. (K.K.), and Research Support Project for Life Science and Drug Discovery (Basis for Supporting Innovative Drug Discovery and Life Science Research (BINDS)) from AMED under Grant Number JP24ama121054.

Conflict of interest statement. None declared.

References

(1) I. Fernández, N. Khiar, *Chem. Rev.* **2003**, *103*, 3651.
(2) R. Bentley, *Chem. Soc. Rev.* **2005**, *34*, 609.
(3) T. Matsui, Y. Dekishima, M. Ueda, *Appl. Microbiol. Biotechnol.* **2014**, *98*, 7699.
(4) W. R. F. Goundry, B. Adams, H. Benson, J. Demeritt, S. McKown, K. Mulholland, A. Robertson, P. Siedlecki, P. Tomlin, K. Vare, *Org. Process Res. Dev.* **2017**, *21*, 107.
(5) B. M. Trost, M. Rao, *Angew. Chem. Int. Ed.* **2015**, *54*, 5026.
(6) S. Otocka, M. Kwiatkowska, L. Madalińska, P. Kiełbasiński, *Chem. Rev.* **2017**, *117*, 4147.
(7) M. M. Yang, S. Wang, Z. B. Dong, *Synthesis* **2022**, *54*, 5168.
(8) E. Wojaczyńska, J. Wojaczyński, *Chem. Rev.* **2020**, *120*, 4578.
(9) D. R. Rayner, A. J. Gordon, K. Mislow, *J. Am. Chem. Soc.* **1968**, *90*, 4854.
(10) C. Aurisicchio, E. Baciocchi, M. F. Gerini, O. Lanzalunga, *Org. Lett.* **2007**, *9*, 1939.
(11) K. Makino, K. Tozawa, Y. Tanaka, A. Inagaki, H. Tabata, T. Oshitari, H. Natsugari, H. Takahashi, *J. Org. Chem.* **2021**, *86*, 17249.
(12) K. Tozawa, K. Makino, Y. Tanaka, K. Nakamura, A. Inagaki, H. Tabata, T. Oshitari, H. Natsugari, N. Kuroda, K. Kanemaru, Y. Oda, H. Takahashi, *J. Org. Chem.* **2023**, *88*, 6955.
(13) R. Tang, K. Mislow, *J. Am. Chem. Soc.* **1970**, *92*, 2100.
(14) P. K. Dornan, K. G. M. Kou, K. N. Houk, V. M. Dong, *J. Am. Chem. Soc.* **2014**, *136*, 291.

(15) M. Egi, K. Sugiyama, M. Saneto, R. Hanada, K. Kato, S. Akai, *Angew. Chem. Int. Ed.* **2013**, *52*, 3654.
(16) K. Sugiyama, Y. Oki, S. Kawanishi, K. Kato, T. Ikawa, M. Egi, S. Akai, *Catal. Sci. Technol.* **2016**, *6*, 5023.
(17) T. Nishio, S. Yoshioka, K. Hasegawa, K. Yahata, K. Kanomata, S. Akai, *Eur. J. Org. Chem.* **2021**, *2021*, 4417.
(18) K. Kasama, K. Kanomata, Y. Hinami, K. Mizuno, Y. Uetake, T. Amaya, M. Sako, S. Takizawa, H. Sasai, S. Akai, *RSC Adv.* **2021**, *11*, 35342.
(19) J. Zhang, Z. Zheng, C. Zhu, *Chinese Chem. Lett.* **2024**, *35*, 109160.
(20) J. A. Carmona, C. Rodríguez-Franco, R. Fernández, J. M. Lassaletta, V. Hornillos, *ChemCatChem* **2024**, *16*, e202400701.
(21) H. Gröger, S. Horino, K. Kanomata, S. Akai, *Chem. Eur. J.* **2024**, *30*, e202304028.
(22) Kanto Chemical Co.,Inc, https://www.kanto.co.jp/products/siyaku/reagent_property/solvent_physical_property.html (2024, December 21).
(23) Chemical Book, https://www.chemicalbook.com/ProductIndex_EN.aspx (2024, December 21).

Supporting information

Table of contents

1. General information 2
2. Preparation of V-SilicaGel 2
3. Substrate synthesis 3
4. Racemization of optically active sulfoxides 9
6. Catalyst recycle experiment 19
7. Kinetic analysis 19
8. DFT calculation 21
9. Refarence 29
10. HPLC and NMR chart 30

1. General information

Infrared (IR) absorption spectra were recorded on a SHIMADZU IRAffinity-1S spectrophotometer. ^{1}H and ^{13}C NMR spectra were measured on a JEOL JNM-ECA500 (^{1}H: 500 MHz, ^{13}C: 125 MHz) and a JEOL JMN-ECS400 (^{1}H: 400 MHz, ^{13}C: 100 MHz) instruments. Chemical shifts were reported in δ (ppm) relative to the deuterated solvents (7.26 ppm (^{1}H) and 77.0 ppm (^{13}C) for $CDCl_3$). Data are reported as follows: chemical shift, multiplicity (s = singlet, d = doublet, t = triplet, q = quartet, quint = quintet, sext = sextet, sept = septet, m = multiplet, brs = broad singlet), coupling constants (Hz) and integration. High-resolution mass spectra (HRMS) were measured on a JEOL JMS-3000 (MALDI) instrument. Chiral HPLC analysis was carried out using a JASCO LC-2000Plus system (HPLC pump: PU-2080, UV detector: MD-2018) equipped with a chiral stationary phase column (4.6 mm x 250 mm). Optical rotations were measured on a JASCO P-1020 polarimeter. Reagents and solvents were purchased from Tokyo Chemical Industry Co., Ltd. (Tokyo, Japan), Nacalai TesqueInc. (Kyoto, Japan), Sigma-Aldrich Co., LLC (Tokyo, Japan), FUJIFILM Wako Pure Chemical Co., Ltd. (Tokyo, Japan), Kanto Chemical Co., Inc. (Tokyo, Japan), and Kishida Chemical Co., Ltd. (Osaka, Japan), and used without further purification. Unless otherwise noted, the reactions were carried out in anhydrous solvents under argon atmosphere. Silica gel chromatography was performed on silica gel 60N (particle size 40–50 μm) purchased from Kanto Chemical Co., Inc. The same silica gel was used to prepare V-SilicaGel. Mesoporous silica (TMPS-4R) used to prepare V-MPS4 was purchased from Taiyo Kagaku Co., Ltd. (Tokyo, Japan).

2. Preparation of V-SilicaGel

2.1 Preparation of $VO(OSiPh_3)_3$

$VO(OSiPh_3)_3$ was prepared according to the literature method.[1] In brief, Ph_3SiOH (18 g, 65 mmol) was weighed into a two-neck flask (1 L) and the atmosphere was replaced with argon. Dry toluene (200 mL) was added to the flask, followed by $VO(O^iPr)_3$ (5.1 mL, 21 mmol), and the resultant mixture was refluxed for 4 h using a Dean-Stark apparatus. After that, toluene was removed under reduced pressure, and the resulting residue was dried further in vacuo to afford $VO(OSiPh_3)_3$ (19.7 g, quant), which was used in the next reaction without purification.

2.2 Preparation of V-SilicaGel

V-SilicaGel was prepared by a similar procedure for V-MPS4 described in the previous report.[1] In brief, silica gel 60N (10 g, particle size 40–50 μm) was placed in a two-neck flask (1 L) and dried overnight at 150°C in vacuo. The flask was then allowed to cool to room temperature under argon atmosphere. To the flask, $VO(OSiPh_3)_3$ (11 g, 12 mmol) was added, followed by anhydrous toluene (0.80 L, 0.015 M), and the resultant mixture was refluxed at 120 °C for 8 h. After that, toluene was removed under reduced pressure. The residue was divided into 5-g batches in 50-mL glass centrifuging

tubes equipped with a rubber septum. Each batch was suspended in hexane/CH_2Cl_2 (2:3 ratio, 30 mL) and centrifuged (5000 rpm, 5 min). After removing the supernatant by cannulation, the suspending/centrifuging process was repeated four more times. After that, each precipitate was dried overnight in vacuo at room temperature to afford V-SilicaGel. The vanadium content of V-SilicaGel was determined by inductively coupled plasma-optical emission spectrometry (ICP-OES) using an Agilent 720 ICP-OES instrument. The vanadium content of V-SilicaGel was 0.13 mmol per gram of silica gel (0.13 mmol/g).

3. Substrate synthesis

Optically active sulfoxide (*R*)-**1a** (>99% ee) was purchased from a commercial supplier. Sulfoxide (*S*)-**1b** and (*S*)-**1d**–**1g** were synthesized by asymmetric oxidation using $VO(acac)_2$/chiral Shiff base ligand **S2** from the corresponding sulfides **S1** (General procedure A).[2] Sulfoxide (*R*)-**1c**, (*R*)-**1k** and (*R*)-**1n** were synthesized by asymmetric oxidation using $Ti(^iPrO)_4$/(*R*)-BINOL from the corresponding sulfides **S1** (General procedure B).[3] Sulfides **S1b**–**S1d**, **S1f**, and **S1n** were purchased from commercial suppliers, and **S1e**,[4] **S1g**,[5] and **S1k**[6] were synthesized according to the literature. Optically active sulfoxide (*S*)-**1i**, (*S*)-**1j**, (*S*)-**1l**, (*S*)-**1m**, and (*S*)-**1o**, (*S*)-**1p** were synthesized according to the Andersen synthesis (General procedure C).[7]

General procedure A[2]: asymmetric oxidation using $VO(acac)_2$/chiral Shiff base ligand (1b and 1d–1g)

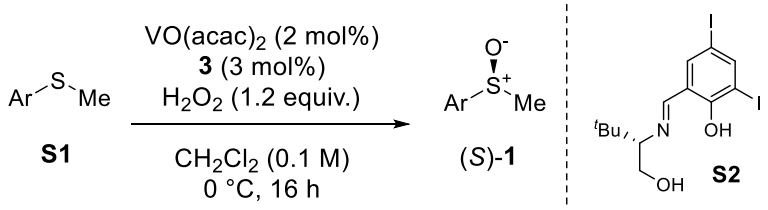

Under argon atmosphere, $VO(acac)_2$ (10.6 mg, 2.0 mol%) was added to a CH_2Cl_2 solution (8.0 mL) of **S2** (30.4 mg, 3.0 mol%)[5] at room temperature. The reaction solution was stirred at room temperature for 30 min. After that, the CH_2Cl_2 solution of sulfide **S1** (2.0 mmol) was added to the reaction solution. The reaction solution was cooled to 0 °C then, H_2O_2 (30% in H_2O, 0.544 mL, 1.2 mmol) was added dropwise to the reaction solution at 0 °C. The reaction solution was stirred at 0 °C for 16 h. After that, the reaction solution was quenched with sat. $Na_2S_2O_3$ aq. and raised to room temperature, and the product was extracted with $CHCl_3$ (x3). The combined organic layers were dried over $MgSO_4$ and concentrated under reduced pressure. The residue was purified by silica gel chromatography to give (*S*)-**1**. The ^1H NMR spectra of **1b**, **1d**–**1f** were in good agreement with those reported in the literature. Sulfoxide **1g** was fully characterized by TF-IR, ^1H and ^{13}C NMR, and HRMS because they are not reported in the literature.

General procedure B[3]: asymmetric oxidation using Ti(^{i}PrO)$_4$/(*R*)-BINOL (1c, 1k, and 1n)

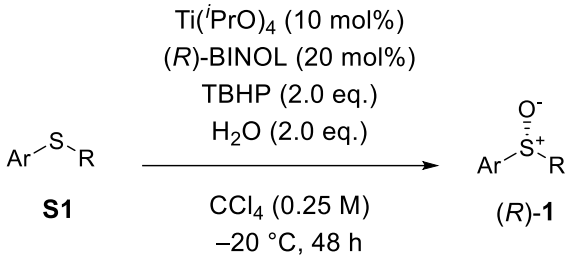

Under argon atmosphere, Ti(^{i}PrO)$_4$ (57 mg, 0.20 mmol) was added to a CCl_4 solution (8.0 mL, 0.25 M) of sulfide **S1** (2.0 mmol), (*R*)-BINOL (114 mg, 0.40 mmol) and H_2O (72 mg, 4.0 mmol) at room temperature. The reaction solution was stirred at room temperature for 1 h. After that, the reaction solution was cooled to –20 °C then, *tert*-butyl hydroperoxide (TBHP) (5.5 M in decane, 0.72 mL, 4.0 mmol) was added dropwise to the reaction solution at –20 °C. The reaction solution was stirred at –20 °C for 48 h. After that, the reaction solution was raised to room temperature and quenched with sat. $Na_2S_2O_3$ aq., and the product was extracted with EtOAc (x3). The combined organic layers were dried over $MgSO_4$ and concentrated under reduced pressure. The residue was purified by silica gel chromatography to give (*R*)-**1**. The ^{1}H NMR spectra were consistent with those in the literature.

General procedure C[7]: Andersen synthesis (1i, 1j, 1l, 1m, 1o, and 1p)

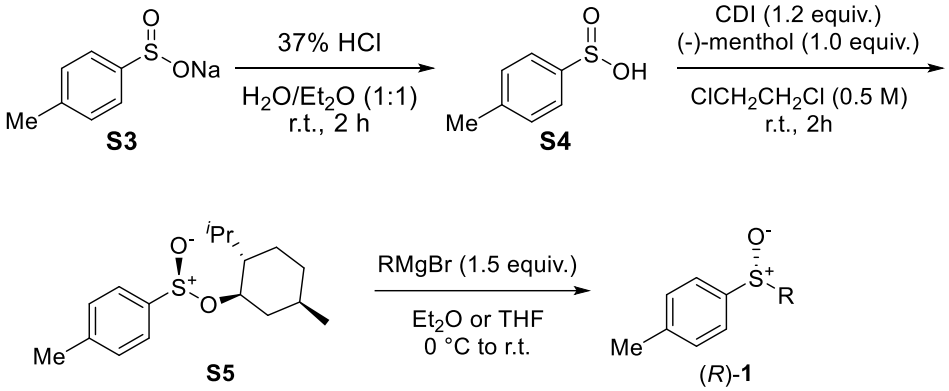

Sodium sulfinate **S3** (18 g, 100 mmol) was dissolved to a 1:1 solution of H_2O/Et_2O (25 mL) at room temperature. An aq. HCl solution (37% in H_2O, 9.0 mL) was added to the solution, and the resultant mixture was stirred at room temperature for 2 h. After that, the product was extracted with EtOAc (x3). The combined organic layers were dried over $MgSO_4$ and concentrated under reduced pressure to give **S4** as a white solid (15 g, 95% yield),[8] which was used to the next step without purification.

Sulfinate **S4** (2.0 g, 1.3 mmol) was added to a dichloroethane solution (20 mL) of 1,1'-carbonyldiimidazole (2.1 g, 1.3 mmol) at room temperature. The resultant solution was stirred at room temperature for 30 min. After that, (-)-menthol (1.6 g, 10 mmol) was added and the solution was

stirring at room temperature for another 2 h. The reaction was quenched with water, and the solution was extracted with EtOAc (x3). The combined organic layers were dried over $MgSO_4$ and concentrated under reduced pressure. The residue was purified by silica gel chromatography (hexane/EtOAc=4:1), and the resultant white solid was recrystallized in hexane to give **S5** as colorless needle crystals (1.02 g, 35% yield).[9] The ^{1}H NMR spectra of **S5** was in good agreement with those reported in the literature.

Under argon atmosphere, RMgBr (Et_2O or THF solution, 0.75 mmol) was added to a solution of **S5** (147 mg, 0.5 mmol) in anhydrous Et_2O (5.0 mL) at 0 °C. After stirring for 30 min at the same temperature, the reaction mixture was warmed to room temperature and quenched with saturated aq. NH_4Cl solution. The resultant mixture was extracted with EtOAc (x3), and the combined organic phases were washed with brine, dried over $MgSO_4$, and concentrated under reduced pressure. The residue was purified by silica gel column chromatography to give (*R*)-**1**. The ^{1}H NMR spectra of **1i**, **1j**, **1o**, and **1p** were in good agreement with those reported in the literature. Sulfoxide **1l** and **1m** were fully characterized by TF-IR, ^{1}H and ^{13}C NMR, and HRMS because they are not reported in the literature.

Synthesis of (*R*)-1h[10]

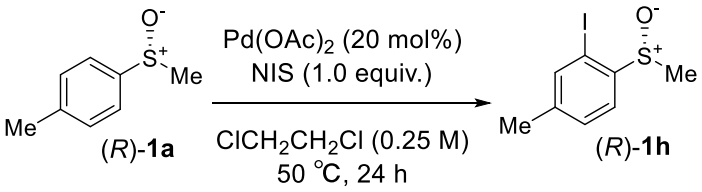

Under air atmosphere, *N*-iodosuccinimide (225 mg, 1.0 mmol) was added to a solution of (*R*)-**1a** (154 mg, 1.0 mmol) and $Pd(OAc)_2$ (45 mg, 20 mol%) in anhydrous 1,2-dichloroethane (4 mL) at room temperature. The reaction mixture was warmed to 90 °C and stirred for 24 h at the same temperature. After that, the reaction was cooled to room temperature and added H_2O (3 mL). Two phases were separated, and the aqueous phase was extracted with EtOAc (x3). The combined organic phases were washed with brine, dried over $MgSO_4$, and concentrated under reduced pressure. The residue was purified by silica gel column chromatography (hexane/EtOAc=1:1) to give (*R*)-**1h** as white solid (93 mg, 33% yield, 94% ee).

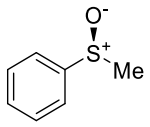

(*S*)-(methylsulfinyl)benzene (1b)[11]: General procedure A; a colorless oil (103 mg, 37% yield, 66% ee) after purification by silica gel chromatography (hexane/EtOAc=1:1); ^{1}H NMR (500 MHz, $CDCl_3$): δ 7.66-7.64 (m, 2H), 7.55-7.48 (m, 3H), 2.73 (s, 3H).

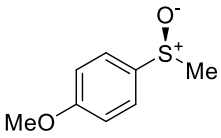

(*R*)-1-methoxy-4-(methylsulfinyl)benzene (1c)[11]: General procedure B; a white solid (190 mg, 56% yield, 89% ee) after purification by silica gel chromatography (hexane/EtOAc=1:4); ^{1}H NMR (400 MHz, $CDCl_3$): δ 7.59 (d, *J* = 9.0 Hz, 2H), 7.02 (d, *J* = 9.0 Hz, 2H), 3.85 (s, 3H), 2.69 (s, 3H).

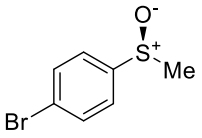

(*S*)-1-bromo-4-(methylsulfinyl)benzene (1d)[11]: General procedure A; a white solid (125 mg, 29% yield, 84% ee) after purification by silica gel chromatography (hexane/EtOAc=1:1); ^{1}H NMR (400 MHz, $CDCl_3$): δ 7.67 (d, *J* = 8.5 Hz, 2H), 7.52 (d, *J* = 8.5 Hz, 2H), 2.71 (s, 3H).

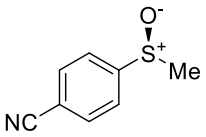

(*S*)-4-(methylsulfinyl)benzonitrile (1e)[11]: General procedure A; a white solid (83 mg, 25% yield, 57% ee) after purification by silica gel chromatography (hexane/EtOAc=2:3); ^{1}H NMR (400 MHz, $CDCl_3$): δ 7.83 (d, *J* = 8.7 Hz, 2H), 7.77 (d, *J* = 8.7 Hz, 2H), 2.76 (s, 3H).

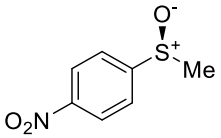

(*S*)-1-(methylsulfinyl)-4-nitrobenzene (1f)[11]: General procedure A; a white solid (63 mg, 17% yield, 83% ee) after purification by silica gel chromatography (hexane/EtOAc=2:3); ^{1}H NMR (400 MHz, $CDCl_3$): δ 8.40 (d, *J* = 9.0 Hz, 2H), 7.84 (d, *J* = 9.0 Hz, 2H), 2.79 (s, 3H).

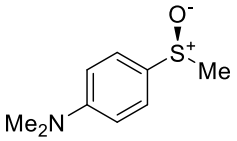

(*S*)- *N*,*N*-dimethyl-4-(methylsulfinyl)aniline (1g): General procedure A; a white solid (81 mg, 32% yield, 51% ee) after purification by silica gel chromatography (hexane/EtOAc=1:4); IR (NaCl): 1597, 1512, 1366, 1093, 1046, 815 cm^{-1}; ^{1}H NMR (400 MHz, $CDCl_3$): δ 7.52 (d, *J* = 9.0 Hz, 2H), 6.76 (d, *J*

= 9.0 Hz, 2H), 3.02 (s, 6H), 2.69 (s, 3H); ^{13}C NMR (100 MHz, $CDCl_3$): δ 152.5, 130.6, 125.6, 112.2, 43.8, 40.4; HRMS(MALDI) m/z calcd. for $C_9H_{14}NOS$ $[M+H]^+$: 184.0791, found: 184.0792.

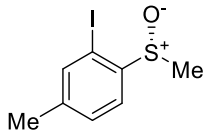

(*R*)-2-iodo-4-methyl-1-(methylsulfinyl)benzene (1h): IR (NaCl): 1458, 1098, 1057, 1018, 823 cm^{-1}; ^{1}H NMR (400 MHz, $CDCl_3$): δ 7.78 (d, *J* = 8.0 Hz, 1H), 7.66 (s, 1H), 7.42 (d, *J* = 8.0 Hz, 1H), 2.76 (s, 3H), 2.37 (s, 3H); ^{13}C NMR (100 MHz, $CDCl_3$): δ 145.2, 143.4, 140.0, 130.6, 125.7, 91.5, 42.5, 21.0; HRMS(MALDI) m/z calcd. for $C_8H_{10}OSI$ $[M+H]^+$: 280.9492, found: 280.9494.

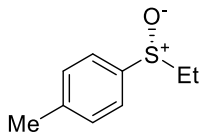

(*R*)-1-(ethylsulfinyl)-4-methylbenzene (1i)[9]: General procedure C; a colorless oil (78 mg, 93% yield, 97% ee) after purification by silica gel column chromatography (hexane/EtOAc=1:1); ^{1}H NMR (400 MHz, $CDCl_3$): δ 7.49 (d, *J* = 8.2 Hz, 2H), 7.31 (d, *J* = 8.2 Hz, 2H), 2.91-2.71 (m, 2H), 2.41 (s, 3H), 1.18 (t, *J* = 7.6 Hz, 3H).

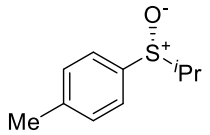

(*R*)- 1-(*iso*-propylsulfinyl)-4-methylbenzene (1j)[9]: General procedure C; a white solid (83 mg, 91% yield, 97% ee) after purification by silica gel column chromatography (hexane/EtOAc=1:1); ^{1}H NMR (400 MHz, $CDCl_3$): δ 7.47 (d, *J* = 7.8 Hz, 2H), 7.30 (d, *J* = 7.8 Hz, 2H), 2.80 (sept, *J* = 6.9 Hz, 1H), 2.41 (s, 3H), 1.19 (d, *J* = 6.9 Hz, 3H), 1.14 (d, *J* = 6.9 Hz, 3H).

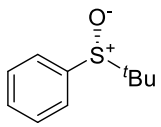

(*R*)-(*tert*-butylsulfinyl)benzene (1k)[9]: General procedure B; a white solid; (138 mg, 38% yield, 96% ee) after purification by silica gel column chromatography (hexane/EtOAc=3:2); ^{1}H NMR (400 MHz, $CDCl_3$): δ 7.63-7.56 (m, 2H), 7.52-7.47 (m, 3H), 1.17 (s, 9H).

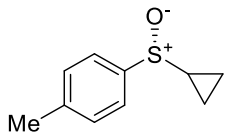

(*R*)-1-(*cyclo*-propylsulfinyl)-4-methylbenzene (1l): General procedure C; a colorless oil (85 mg, 94% yield, 95% ee) after purification by silica gel column chromatography (hexane/EtOAc=1:1); IR (NaCl): 1494, 1088, 1054, 881, 810 cm^{-1}; ^1H NMR (400 MHz, $CDCl_3$): δ 7.55 (d, *J* = 8.0 Hz, 2H), 7.32 (d, *J* = 8.0 Hz, 2H), 2.41 (s, 3H), 2.27-2.21 (m, 1H), 1.27-1.18 (m, 1H), 1.03-0.89 (m, 3H); ^{13}C NMR (100 MHz, $CDCl_3$): δ 141.8, 141.5, 130.0, 124.2, 34.0, 21.6, 3.5, 3.0; HRMS (MALDI) m/z calcd. for $C_{10}H_{13}OS$ $[M+H]^+$: 181.0682, found: 181.0682.

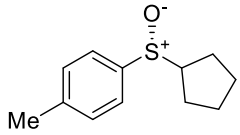

(*R*)-1-(*cyclo*-pentylsulfinyl)-4-methylbenzene (1m): General procedure C; a colorless oil (102 mg, 99% yield, 88% ee) after purification by silica gel column chromatography (hexane/EtOAc=1:1); IR (NaCl): 1494, 1085, 1043, 810, 752 cm^{-1}; ^1H NMR (400 MHz, $CDCl_3$): δ 7.51 (d, *J* = 7.8 Hz, 2H), 7.29 (d, *J* = 7.8 Hz, 2H), 3.13-3.05 (m, 1H), 2.40 (s, 3H), 2.14-2.05 (m, 1H), 1.78-1.52 (m, 7H); ^{13}C NMR (100 MHz, $CDCl_3$): δ 141.4, 140.5, 129.8, 124.8, 64.5, 27.7, 26.2, 25.8, 25.3, 21.6; HRMS(MALDI) m/z calcd. for $C_{12}H_{17}OS$ $[M+H]^+$: 209.0995, found: 209.0993.

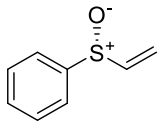

(*R*)-(vinylsulfinyl)benzene (1n)[12]: General procedure B; a white solid (96 mg, 32% yield, 44% ee) after purification by silica gel column chromatography (hexane/EtOAc=3:2); ^1H NMR (400 MHz, $CDCl_3$): δ 7.64-7.60 (m, 2H), 7.54-7.47 (m, 3H), 6.60 (dd, *J* = 16.5, 9.6 Hz, 1H), 6.21 (d, *J* = 16.5 Hz, 1H), 5.90 (d, *J* = 9.6 Hz, 1H).

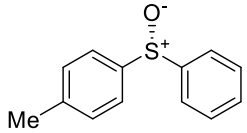

(*R*)-1-methyl-4-(phenylsulfinyl)benzene (1o)[9]; General procedure C; a white solid (103 mg, 95% yield, 98% ee) after purification by silica gel column chromatography (hexane/EtOAc=1:1); ^1H NMR (400 MHz, $CDCl_3$): δ 7.65-7.61 (m, 2H), 7.53 (d, *J* = 8.0 Hz, 2H), 7.48-7.40 (m, 3H), 7.26 (d, *J* = 8.0 Hz, 2H), 2.36 (s, 3H).

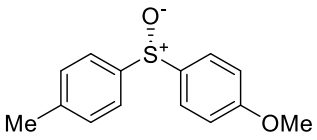

(*S*)-1-methoxy-4-(*p*-tolylsulfinyl)benzene (1p); General procedure C; a white solid (97 mg, 79% yield, 98% ee) after purification by silica gel column chromatography (hexane/EtOAc=1:1); IR (NaCl): 1593, 1495, 1253, 1090, 1044 cm^{-1}; ^1H NMR (400 MHz, $CDCl_3$): δ 7.55 (d, J = 8.7 Hz, 2H), 7.49 (d, J = 7.7 Hz, 2H), 7.25 (d, J = 7.7 Hz, 2H), 6.95 (d, J = 8.7 Hz, 2H), 3.81 (s, 3H), 2.37 (s, 3H); ^{13}C NMR (100 MHz, $CDCl_3$): δ 162.0, 142.8, 141.4, 137.1, 130.0, 127.2, 124.9, 114.9, 55.6, 21.5; HRMS(MALDI) m/z calcd. for $C_{14}H_{15}O_2S$ $[M+H]^+$: 247.0787, found: 247.0776.

4. Racemization of optically active sulfoxides

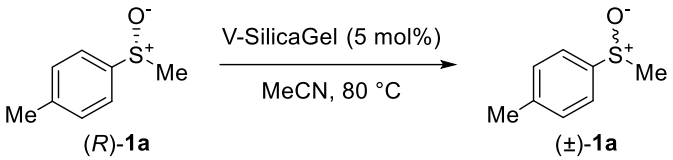

(*R*)-**1a** (±)-**1a**

[**General procedure**] Under argon atmosphere, V-SilicaGel (39.4 mg, containing 5.0 μmol of vanadium, 5 mol% relative to **1**) was added to a MeCN solution (1.0 mL, 0.1 M) of sulfoxide (*R*)-**1** 0.10 mmol), and the mixture was stirred at 80 ℃. After stirring for the indicated time in Scheme 1, the reaction mixture was filtered through a pad of Celite, and the filtrate was concentrated under reduced pressure. The residue was purified by silica gel chromatography to determine the recovery ratio of **1**. The ^1H NMR spectrua were in good agreement with those of the corresponding optically active isomers. Compound *rac*-**1l** was unknown in literature and fully characterized by ^1H and ^{13}C NMR, FT-IR, and HRMS.

For the time course analysis, an aliquot sample of the reaction mixture was analyzed by chiral HPLC to determine the enantiomeric excess. Racemization rates were shown to follow first-order kinetics, and the pseudo-rate constants k_{rac} were determined from the slope of the plot of −ln (% ee_t) against time.[13]

$$-\ln (\%\ ee_t) = k_{rac}\, t$$

$$t_{1/2} = \ln 2 / k_{rac}$$

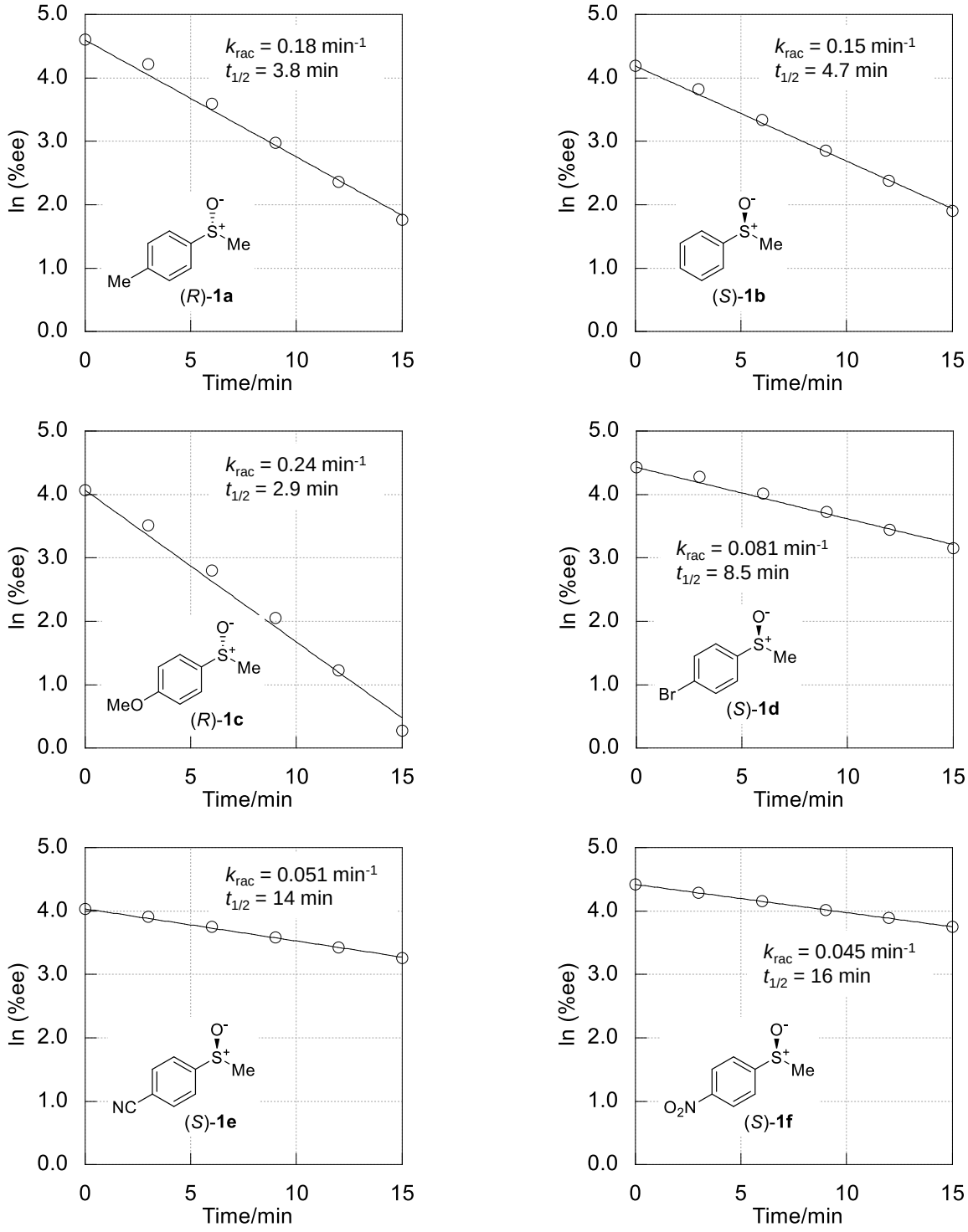

Figure S1. Log plots of the time course of % ee in the racemization. Numerical data are provided in a separate csv file.

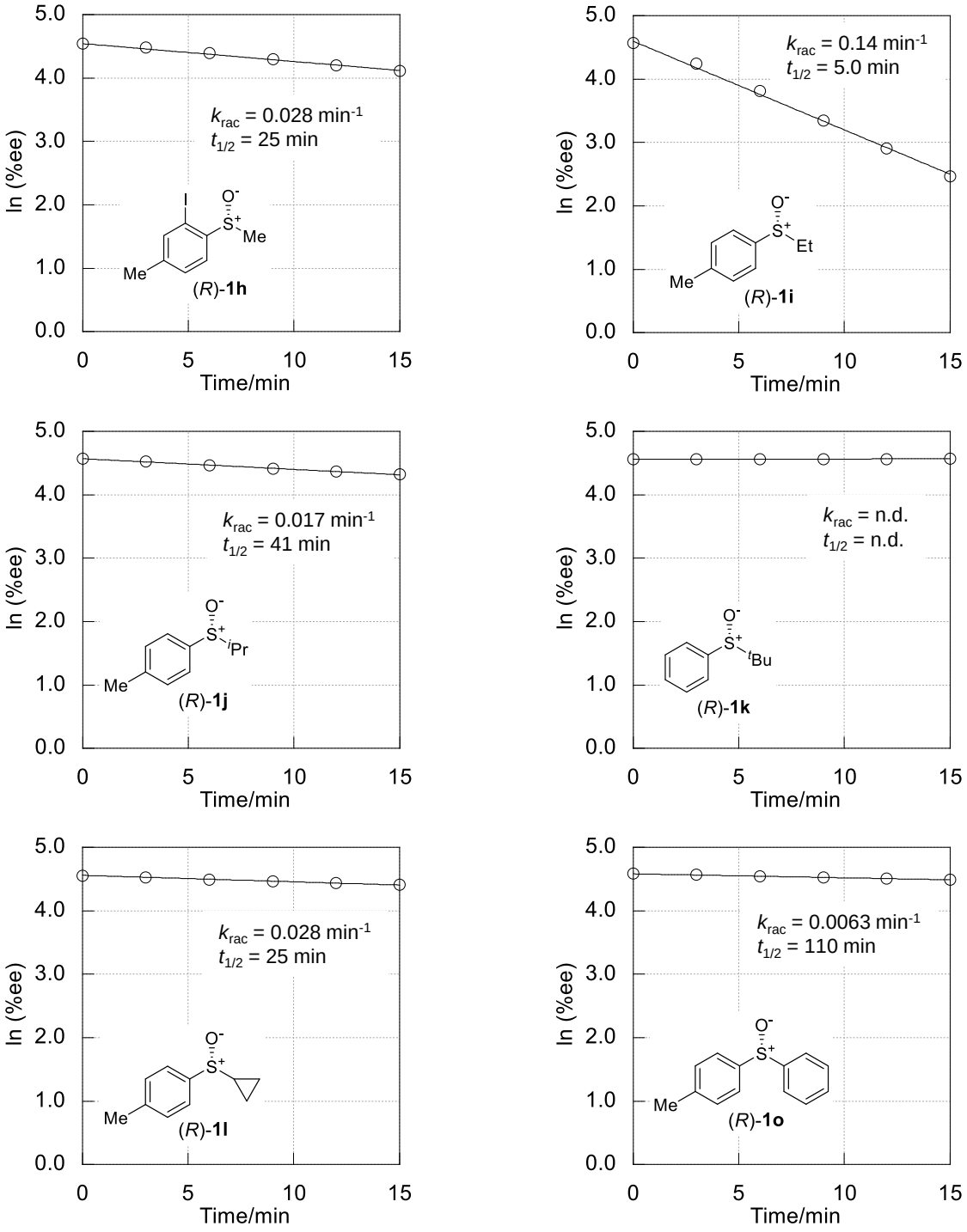

Figure S1 (continued): Log plots of the time course of % ee in the racemization. Numerical data are provided in a separate csv file.

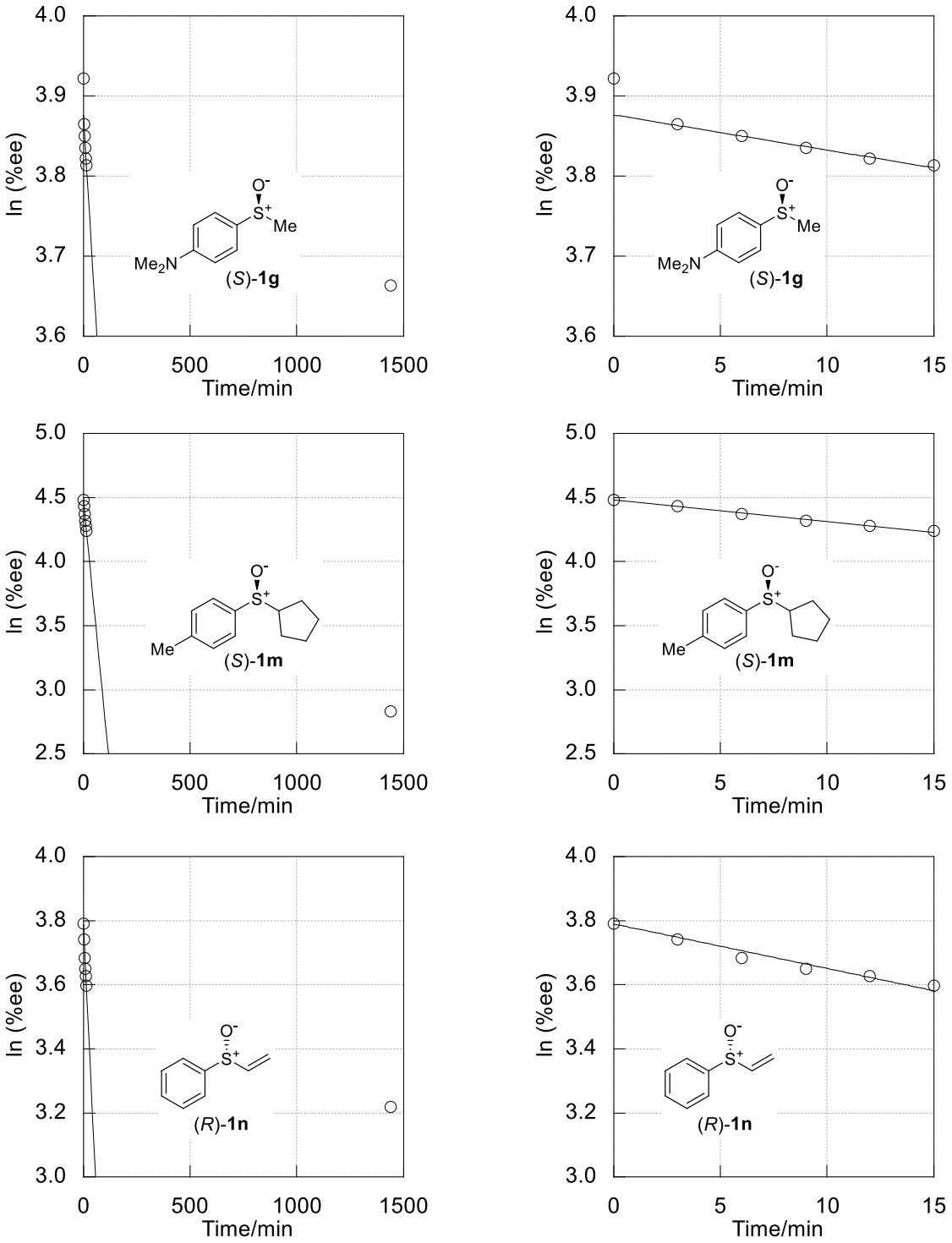

Figure S2. Log plots of % ee that do not follow the first order kinetics; left: overall time course; right: magnified view of the initial stage of the reaction. Numerical data are provided in a separate csv file.

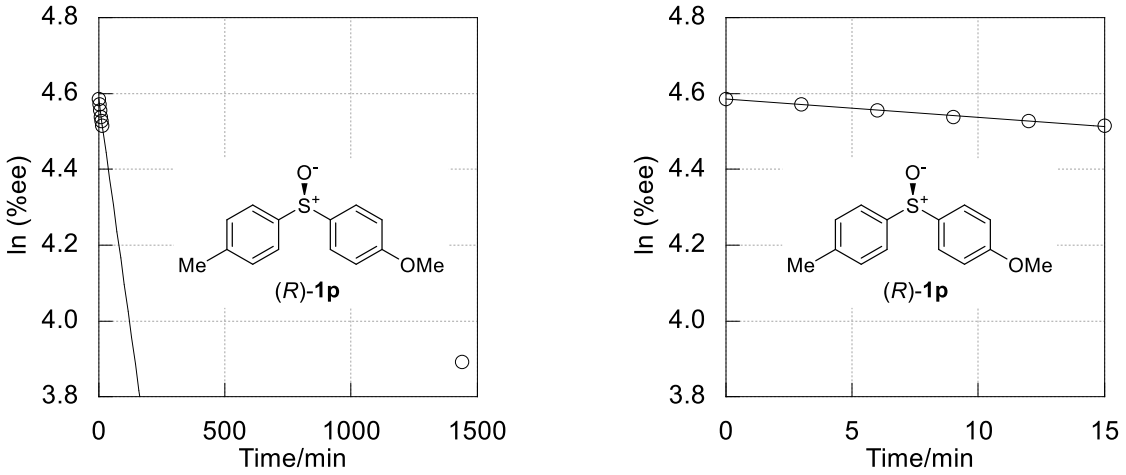

Figure S2 (continued): Log plots of % ee that do not follow the first order kinetics; left: overall time course; right: magnified view of the initial stage of the reaction. Numerical data are provided in a separate csv file.

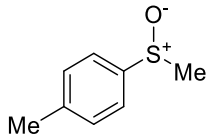

[*rac*-1a]: Purified by column chromatography using hexane to hexane/EtOAc=1:1 as an eluant; 98% yield (15.1 mg, <1% ee); a white solid; the ^{1}H NMR spectrum was in good agreement with that of the corresponding optically active isomer; ^{1}H NMR (500 MHz, $CDCl_3$): δ 7.52 (d, J = 8.0 Hz, 2H), 7.32 (d, J = 8.0 Hz, 2H), 2.69 (s, 3H), 2.40 (s, 3H); HPLC analysis DAICEL CHIRALPAK ID-3 (Hexane/*i*-PrOH = 70/30, 1.0 mL/min, 254 nm, 30 ºC), 9.9 min, 10.7 min.

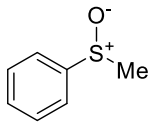

[*rac*-1b]: Purified by column chromatography using hexane to hexane/EtOAc=1:1 as an eluant; 97% yield (13.6 mg, <1% ee); a colorless oil; the ^{1}H NMR spectrum was in good agreement with that of the corresponding optically active isomer; ^{1}H NMR (500 MHz, $CDCl_3$): δ 7.66-7.64 (m, 2H), 7.55-7.48 (m, 3H), 2.73 (s, 3H); HPLC analysis DAICEL CHIRALPAK IC-3 (Hexane/*i*-PrOH = 70/30, 1.0 mL/min, 254 nm, 30 ºC), 15.3 min, 17.0 min.

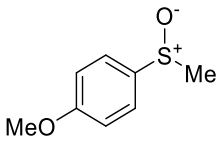

[*rac*-1c]: Purified by column chromatography using hexane to hexane/EtOAc=1:4 as an eluant; 98% yield (16.7 mg, <1% ee); a white solid; the ^{1}H NMR spectrum was in good agreement with that of the corresponding optically active isomer; ^{1}H NMR (400 MHz, $CDCl_3$): δ 7.59 (d, J = 9.0 Hz, 2H), 7.02 (d, J = 9.0 Hz, 2H), 3.85 (s, 3H), 2.69 (s, 3H); HPLC analysis DAICEL CHIRALPAK IF-3 (Hexane/*i*-PrOH = 70/30, 1.0 mL/min, 254 nm, 30 ºC), 29.9 min, 33.1 min.

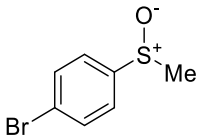

[*rac*-1d]: Purified by column chromatography using hexane to hexane/EtOAc=1:1 as an eluant; 99% yield (21.6 mg, <1% ee); a white solid; the ^{1}H NMR spectrum was in good agreement with that of the corresponding optically active isomer; ^{1}H NMR (400 MHz, $CDCl_3$): δ 7.67 (d, J = 8.5 Hz, 2H), 7.52 (d, J = 8.5 Hz, 2H), 2.71 (s, 3H); HPLC analysis DAICEL CHIRALPAK IE-3 (Hexane/*i*-PrOH = 80/20, 1.0 mL/min, 254 nm, 30 ºC), 12.1 min, 13.1 min.

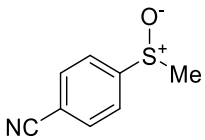

[*rac*-1e]: Purified by column chromatography using hexane to hexane/EtOAc=1:4 as an eluant; >99% yield (16.5 mg, <1% ee); a white solid; the ^{1}H NMR spectrum was in good agreement with that of the corresponding optically active isomer; ^{1}H NMR (400 MHz, $CDCl_3$): δ 7.83 (d, J = 8.7 Hz, 2H), 7.77 (d, J = 8.7 Hz, 2H), 2.76 (s, 3H); HPLC analysis DAICEL CHIRALPAK IE-3 (Hexane/*i*-PrOH = 70/30, 1.0 mL/min, 254 nm, 30 ºC), 11.6 min, 12.5 min.

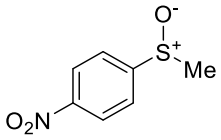

[*rac*-1f]: Purified by column chromatography using hexane to hexane/EtOAc=1:4 as an eluant; 99% yield (18.4 mg, <1% ee); a white solid; the ^{1}H NMR spectrum was in good agreement with that of the corresponding optically active isomer; ^{1}H NMR (400 MHz, $CDCl_3$): δ 8.40 (d, J = 9.0 Hz, 2H), 7.84 (d, J = 9.0 Hz, 2H), 2.79 (s, 3H); HPLC analysis DAICEL CHIRALPAK ID-3 (Hexane/*i*-PrOH = 70/30, 1.0 mL/min, 254 nm, 30 ºC), 13.0 min, 14.4 min.

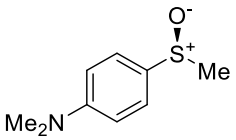

[(*S*)-1g]: Purified by column chromatography using hexane to hexane/EtOAc=1:4 as an eluant; 84% yield (15.3 mg, 39% ee); a white solid; the ^{1}H NMR spectrum was in good agreement with that of the corresponding optically active isomer; ^{1}H NMR (400 MHz, $CDCl_3$): δ 7.52 (d, *J* = 9.3 Hz, 2H), 6.76 (d, *J* = 9.3 Hz, 2H), 3.02 (s, 6H), 2.69 (s, 3H); HPLC analysis DAICEL CHIRALPAK IE-3 (Hexane/*i*-PrOH = 60/40, 1.0 mL/min, 254 nm, 30 ºC), 22.5 min, 24.5 min.

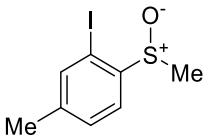

[*rac*-1h]: Purified by column chromatography using hexane to hexane/EtOAc=1:1 as an eluant; 99% yield (27.7 mg, <1% ee); a white solid; the ^{1}H NMR spectrum was in good agreement with that of the corresponding optically active isomer; ^{1}H NMR (300 MHz, CDCl3): δ 7.77 (d, *J* = 8.4 Hz, 1H), 7.65 (s, 1H), 7.41 (d, *J* = 8.4 Hz, 1H), 2.75 (s, 3H), 2.36 (s, 3H); HPLC analysis DAICEL CHIRALPAK IA-3 (Hexane/*i*-PrOH = 95/5, 1.0 mL/min, 254 nm, 30 ºC), 13.7 min, 14.5 min.

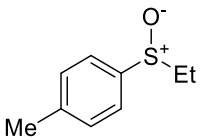

[*rac*-1i]: Purified by column chromatography using hexane to hexane/EtOAc=1:1 as an eluant; 98% yield (16.4 mg, <1% ee); a colorless oil; the ^{1}H NMR spectrum was in good agreement with that of the corresponding optically active isomer; ^{1}H NMR (400 MHz, $CDCl_3$): δ 7.49 (d, *J* = 8.2 Hz, 2H), 7.31 (d, *J* = 8.2 Hz, 2H), 2.91-2.71 (m, 2H), 2.41 (s, 3H), 1.18 (t, *J* = 7.6 Hz, 3H); HPLC analysis DAICEL CHIRALPAK IK-3 (Hexane/*i*-PrOH = 80/20, 1.0 mL/min, 254 nm, 30 ºC), 27.1 min, 29.8 min.

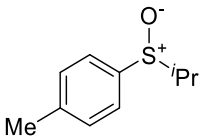

[*rac*-1j]: Purified by column chromatography using hexane to hexane/EtOAc=1:1 as an eluant; 96% yield (17.5 mg, <1% ee); a white solid; the ^{1}H NMR spectrum was in good agreement with that of the corresponding optically active isomer; ^{1}H NMR (400 MHz, $CDCl_3$): δ 7.47 (d, *J* = 7.8 Hz, 2H), 7.30 (d, *J* = 7.8 Hz, 2H), 2.80 (sept, *J* = 6.9 Hz, 1H), 2.41 (s, 3H), 1.19 (d, *J* = 6.9 Hz, 3H), 1.14 (d, *J* = 6.9 Hz, 3H); HPLC analysis DAICEL CHIRALPAK IG-3 (Hexane/*i*-PrOH = 90/10, 1.0 mL/min, 254 nm,

30 ºC), 19.3 min, 20.7 min.

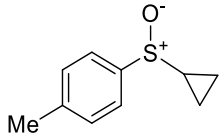

[*rac*-1l]: Purified by column chromatography using hexane to hexane/EtOAc=1:1 as an eluant; 99% yield (17.9 mg, <1% ee); a colorless oil; IR (NaCl): 1494, 1088, 1054, 881, 810 cm^{-1}; ^1H NMR (400 MHz, $CDCl_3$): δ 7.55 (d, *J* = 8.0 Hz, 2H), 7.32 (d, *J* = 8.0 Hz, 2H), 2.42 (s, 3H), 2.27-2.21 (m, 1H), 1.28-1.18 (m, 1H), 1.03-0.89 (m, 3H); ^{13}C NMR (100 MHz, $CDCl_3$): δ 141.8, 141.5, 130.0, 124.2, 77.5, 77.2, 76.8, 34.0, 21.6, 3.4, 3.0; HPLC analysis DAICEL CHIRALPAK IA-3 (Hexane/*i*-PrOH = 80/20, 1.0 mL/min, 254 nm, 30 ºC), 6.3 min, 7.1 min; HRMS(MALDI) m/z calcd. for $C_{10}H_{13}OS$ $[M+H]^+$: 181.0682, found: 181.0684.

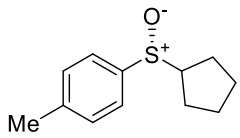

[(*R*)-1m]: Purified by column chromatography using hexane to hexane/EtOAc=1:1 as an eluant; 94% yield (19.6 mg, 17% ee); a colorless oil; the ^1H NMR spectrum was in good agreement with that of the corresponding optically active isomer; ^1H NMR (400 MHz, $CDCl_3$): δ 7.51 (d, *J* = 8.2 Hz, 2H), 7.29 (d, *J* = 8.2 Hz, 2H), 3.13-3.05 (m, 1H), 2.40 (s, 3H), 2.14-2.04 (m, 1H), 1.78-1.51 (m, 7H); HPLC analysis DAICEL CHIRALPAK IK-3 (Hexane/*i*-PrOH = 80/20, 1.0 mL/min, 254 nm, 30 ºC), 13.2 min, 14.4 min.

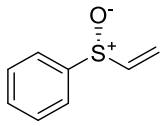

[(*R*)-1n]: Purified by column chromatography using hexane to hexane/EtOAc=1:1 as an eluant; 93% yield (17.0 mg, 25% ee); a white solid; the ^1H NMR spectrum was in good agreement with that of the corresponding optically active isomer; ^1H NMR (400 MHz, $CDCl_3$): δ 7.64-7.60 (m, 2H), 7.54-7.47 (m, 3H), 6.60 (dd, *J* = 16.5, 9.6 Hz, 1H), 6.21 (d, *J* = 16.5 Hz, 1H), 5.90 (d, *J* = 9.6 Hz, 1H); HPLC analysis DAICEL CHIRALPAK ID-3 (Hexane/*i*-PrOH = 70/30, 1.0 mL/min, 254 nm, 30 ºC), 8.0 min, 8.7 min.

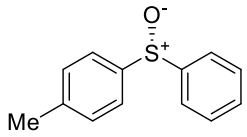

[(*R*)-1o]: Purified by column chromatography using hexane to hexane/EtOAc=1:1 as an eluant; 99% yield (21.3 mg, 3% ee); a white solid; the ^{1}H NMR spectrum was in good agreement with that of the corresponding optically active isomer; ^{1}H NMR (400 MHz, $CDCl_3$): δ 7.65-7.61 (m, 2H), 7.53 (d, J = 8.0 Hz, 2H), 7.48-7.40 (m, 3H), 7.26 (d, J = 8.0 Hz, 2H), 2.36 (s, 3H); HPLC analysis DAICEL CHIRALPAK IH-3 (Hexane/*i*-PrOH = 80/20, 1.0 mL/min, 254 nm, 30 ºC), 25.7 min, 34.2 min.

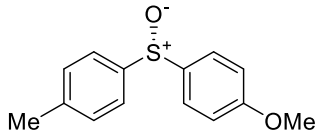

[(*S*)-1p]: Purified by column chromatography using hexane to hexane/EtOAc=1:1 as an eluant; 98% yield (24.1 mg, 49% ee); a white solid; the ^{1}H NMR spectrum was in good agreement with that of the corresponding optically active isomer; ^{1}H NMR (400 MHz, $CDCl_3$): δ 7.55 (d, J = 8.7 Hz, 2H), 7.49 (d, J = 7.7 Hz, 2H), 7.25 (d, J = 7.7 Hz, 2H), 6.95 (d, J = 8.7 Hz, 2H), 3.81 (s, 3H), 2.37 (s, 3H); HPLC analysis DAICEL CHIRALPAK IK-3 (Hexane/*i*-PrOH = 85/15, 1.0 mL/min, 254 nm, 30 ºC), 37.6 min, 39.6 min.

5. Cyclic voltammetry

Cyclic voltammetry was performed using a ALS/CH Instruments Model 610 Es using a glassy carbon working electrode, a platinum wire counter electrode, and an Ag|AgCl (sat. KCl) reference electrode in MeCN (Infinity Pure grade, FUJIFILM Wako Pure Chemical Co., Ltd.) containing the analyte (3.0 mM) and Bu_4NClO_4 (0.1 M, recrystallized from EtOH) as an electrolyte. The solution was degassed by bubbling argon prior to the measurement. The sweep scan was 100 mV/s. The glassy carbon electrode was polished between each scan.

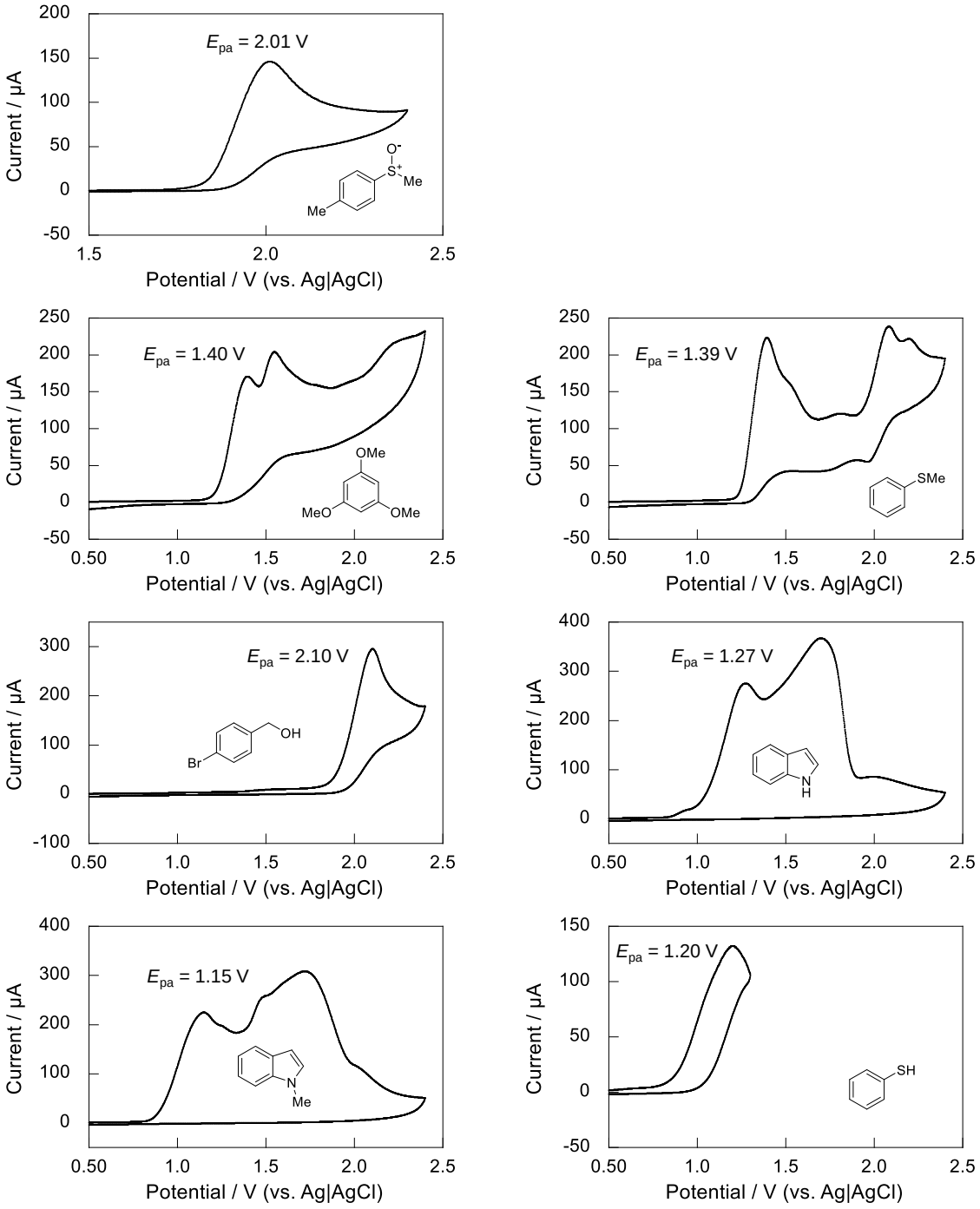

Figure S3. Cyclic voltammograms of **1a** and **2**–**7**

6. Catalyst recycle experiment

To a 15-mL centrifuging tube, V-SilicaGel (39 mg, 5 mol%), MeCN (1.0 mL, 0.1 M), sulfoxide (*R*)-**1a** (0.1 mmol) were added in this order. The reaction mixture was stirred at 80 ℃, under argon atomosphere for 30 min. After that, the reaction mixture was centrifuged (5000 rpm, 1 min) and the supernatant containing the product was collected by decantation. The precipitate was resuspended in EtOAc (2 mL), centrifuged, and the supernatant was removed by decantation. After this process was repeated twice, the catalyst was recovered as the precipitate. The precipitate was dried in vacuo for 3 h prior to the next use, as water contamination diminishes the catalytic activity.

Leaching examination of V-SilicaGel

To a 15 mL centrifuged tube, V-SilicaGel (39 mg, 0.005 mmol based on vanadium content) and MeCN (1.0 mL) were added. The suspension was stirred for 30 min at 80 °C. After that, the suspension was centrifuged (5000 rpm, 2 min) and the precipitated V-SilicaGel was filtered off on a membrane filter (0.2 μm pore). The filtrate was added to another 15 mL centrifuging tube containing (*R*)-**1a** (15.4 mg, 0.10 mmol). After the tube was purged with argon, the mixture was stirred at 80 °C for 30 min. After the reaction, the mixture was filtered off through a short pad of silica gel with EtOAc as eluent and the filtrate was evaporated under reduced pressure. No racemization of (*R*)-**1a** (>99%ee) was detected by HPLC analysis of the crude mixture.

7. Kinetic analysis

7.1. Hammett plot analysis

Table S1. Hammett plot parameters[14]

	σ^{+}_{para}	k_{rac} / min^{-1}[a]	log (k_{rac})
1c (OMe)	–0.78	0.24	–0.62
1a (Me)	–0.31	0.18	–0.73
1b (H)	0	0.15	–0.83
1d (Br)	0.15	0.081	–1.09
1e (CN)	0.66	0.051	–1.29
1f (NO_2)	0.79	0.045	–1.35
[a] The k_{rac} values are calculated in Figure S1.			

7.2 Temperature dependence of racemization kinetics

The racemization reaction of (*R*)-**1a** (0.10 mmol) using V-SilicaGel (5 mol%) was performed in MeCN (0.1 M) at different temperature (50, 60, 70, and 80 °C), and the time courses of ln (%ee) were plotted to determine the racemization rate constant k_{rac} (Figure S4).

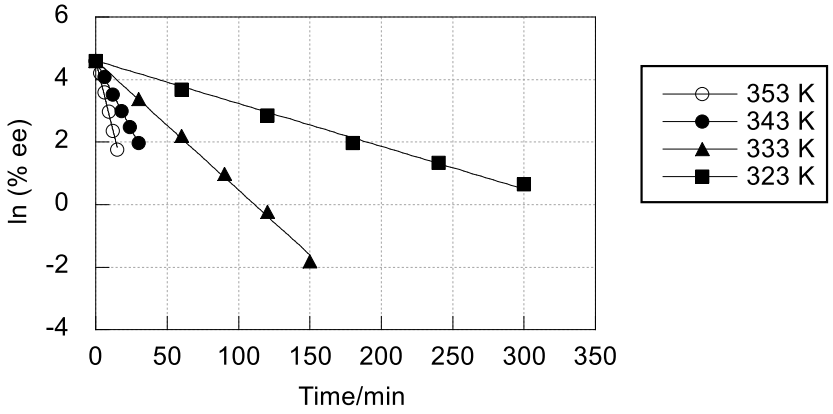

Figure S4. Kinetic analysis of racemization of **1a** at different temperature. Numerical data are provided in a separate csv file.

Table S2. Kinetic parameters for Eyring plot

T/K	k_{rac}/min^{-1}	k_{enant}/M^{-1} s^{-1}
353	0.185	0.308
343	0.088	0.147
333	0.041	0.068
323	0.014	0.023

Assuming that the racemization follows pseudo first-order kinetics, the observed rate constant (k_{obs} = k_{rac}) is expressed as k_{rac} = 2k_{enant} [V], whereas k_{enant} is the rate constant of enantiomerization (stereoinversion)[15] and [V] is the molar concentration of vanadium catalyst (= 0.005 M):

racemization rate (mol s^{-1}) = k_{rac}[**1a**] = 2k_{enant}[V][**1a**]

According to the Eyring equation; $ln\frac{k_{enant}}{T} = -\frac{\Delta H^{\ddagger}}{R}\frac{1}{T} + \left(\frac{\Delta S^{\ddagger}}{R} + ln\frac{k_B}{h}\right)$

whereas,

R = 8.31 J K^{-1} mol^{-1} (ideal gas constant)

h = 6.63 × 10^{-34} J s (Plank constant)

k_B = 1.38 × 10^{-23} J K^{-1} (Boltzmann constant)

$\Delta H^{\ddagger}$ = 78.0 kJ mol^{-1}

$\Delta S^{\ddagger}$ = –34.6 J mol^{-1} K^{-1}

8. DFT calculation

DFT calculation of enantiomerization barrier

The calculations were performed with the Gaussian 16 Revision C.02 package. The geometries were fully optimized at the M05-2X/6-311+G(d,p) level of theory and characterized by frequency calculations. The 3D representations were prepared using CYLview20.

Gaussian 16, Revision C.02

M. J. Frisch, G. W. Trucks, H. B. Schlegel, G. E. Scuseria, M. A. Robb, J. R. Cheeseman, G. Scalmani, V. Barone, G. A. Petersson, H. Nakatsuji, X. Li, M. Caricato, A. V. Marenich, J. Bloino, B. G. Janesko, R. Gomperts, B. Mennucci, H. P. Hratchian, J. V. Ortiz, A. F. Izmaylov, J. L. Sonnenberg, D. Williams-Young, F. Ding, F. Lipparini, F. Egidi, J. Goings, B. Peng, A. Petrone, T. Henderson, D. Ranasinghe, V. G. Zakrzewski, J. Gao, N. Rega, G. Zheng, W. Liang, M. Hada, M. Ehara, K. Toyota, R. Fukuda, J. Hasegawa, M. Ishida, T. Nakajima, Y. Honda, O. Kitao, H. Nakai, T. Vreven, K. Throssell, J. A. Montgomery, Jr., J. E. Peralta, F. Ogliaro, M. J. Bearpark, J. J. Heyd, E. N. Brothers, K. N. Kudin, V. N. Staroverov, T. A. Keith, R. Kobayashi, J. Normand, K. Raghavachari, A. P. Rendell, J. C. Burant, S. S. Iyengar, J. Tomasi, M. Cossi, J. M. Millam, M. Klene, C. Adamo, R. Cammi, J. W. Ochterski, R. L. Martin, K. Morokuma, O. Farkas, J. B. Foresman, and D. J. Fox, Gaussian, Inc., Wallingford CT, 2019.

CYLview20

Legault, C. Y., Université de Sherbrooke, 2020 (http://www.cylview.org)

Table S3. Transition state structures and enantiomerization barriers of sulfoxides and their radical cations

Entry	Sulfoxide		$\Delta G^{\ddagger}$ (sulfoxide) /kJ mol^{-1}	$\Delta G^{\ddagger}$ (radical cation) /kJ mol^{-1}
1	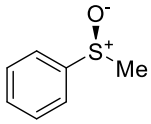	**1b**	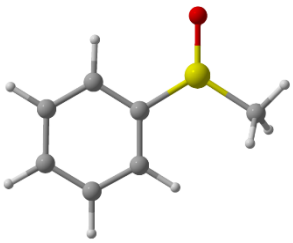 173.5	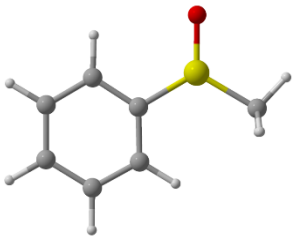 34.3
2	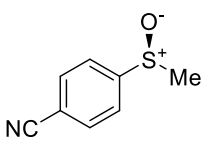	**1e**	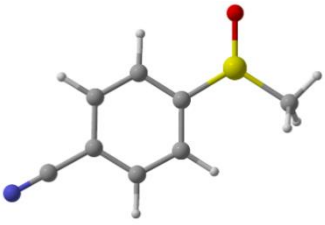 163.9	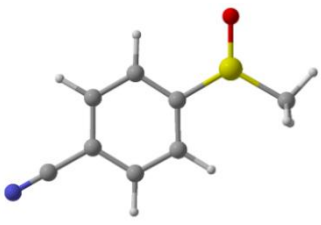 32.2

3	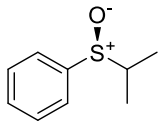	**1j'**	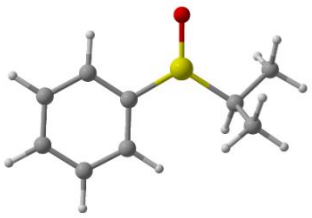 172.2	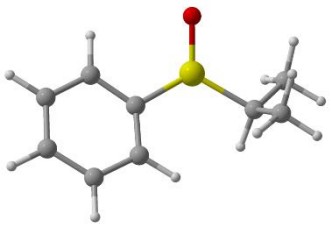 42.6
4	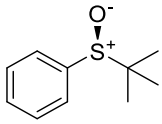	**1k**	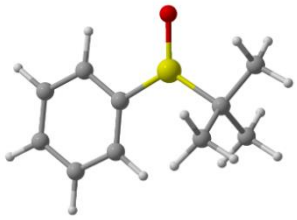 177.7	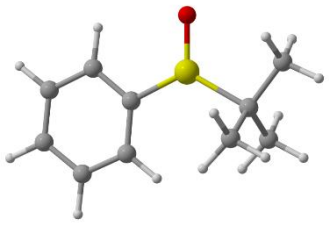 46.0
5	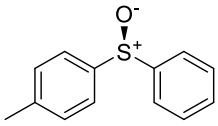	**1o**	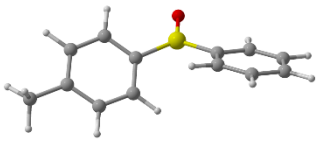 165.5	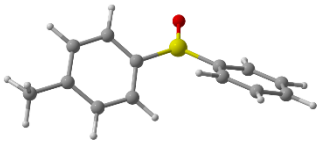 32.2

Cartesian coordinate of transition state

1b

Charge = 0; Spin = 1

Number of imaginary frequencies = 1

Sum of electronic and thermal Free Energies = –744.807479 a.u.

Center Number	Atomic Number	Atomic Type	Coordinates (Angstroms) X	Y	Z
1	6	0	0.807104	1.215291	-0.073377
2	6	0	0.169151	-0.024288	-0.014351
3	6	0	0.896555	-1.212281	0.049042
4	6	0	2.281367	-1.144980	0.061112
5	6	0	2.937696	0.080497	0.017295
6	6	0	2.194070	1.252963	-0.049193
7	1	0	0.240978	2.132792	-0.150553
8	1	0	0.372017	-2.156537	0.087449
9	1	0	2.850814	-2.062922	0.109426
10	1	0	4.017225	0.121387	0.029810
11	1	0	2.694158	2.210709	-0.093470
12	16	0	-1.560854	-0.153367	-0.017788
13	8	0	-2.265225	-1.514224	-0.090552
14	6	0	-2.467591	1.387460	0.103992
15	1	0	-2.565943	1.881973	-0.858294

16	1	0	-3.442564	1.086230	0.479876
17	1	0	-1.981346	2.026055	0.837662

1b (radical cation)

Charge = 1; Spin = 2
Number of imaginary frequencies = 1
Sum of electronic and thermal Free Energies = –744.548299 a.u.

Center Number	Atomic Number	Atomic Type	Coordinates (Angstroms) X	Y	Z
1	6	0	2.912461	0.116145	-0.000036
2	6	0	2.159058	1.288683	0.000151
3	6	0	0.776796	1.229786	0.000197
4	6	0	0.190680	-0.038303	0.000031
5	6	0	0.914984	-1.231379	-0.000153
6	6	0	2.295152	-1.133043	-0.000182
7	1	0	2.649396	2.251195	0.000279
8	1	0	0.188931	2.137216	0.000381
9	1	0	0.412552	-2.188652	-0.000272
10	1	0	2.890280	-2.034605	-0.000327
11	16	0	-1.538372	-0.163743	0.000048
12	8	0	-2.200834	-1.483379	0.000288
13	6	0	-2.535047	1.334917	-0.000314
14	1	0	-3.555269	0.953871	-0.000984
15	1	0	-2.321094	1.894644	0.906703
16	1	0	-2.319999	1.894849	-0.906947
17	1	0	3.991313	0.177559	-0.000067

1e

Charge = 0; Spin = 1
Number of imaginary frequencies = 1
Sum of electronic and thermal Free Energies = –837.073129 a.u.

Center Number	Atomic Number	Atomic Type	Coordinates (Angstroms) X	Y	Z
1	6	0	-0.119940	1.194451	0.055117
2	6	0	0.542998	-0.036873	0.016529
3	6	0	-0.164752	-1.242045	-0.023665
4	6	0	-1.545157	-1.206501	-0.030631
5	6	0	-2.222377	0.015545	-0.002469
6	6	0	-1.501514	1.210842	0.041167
7	1	0	0.427542	2.124388	0.107537
8	1	0	0.375864	-2.177369	-0.048987
9	1	0	-2.108093	-2.128302	-0.061622
10	1	0	-2.030197	2.152731	0.071163
11	16	0	2.262236	-0.135187	0.010794
12	8	0	2.983897	-1.481650	0.049761
13	6	0	3.142213	1.424469	-0.074059
14	1	0	3.176088	1.921132	0.891303

15	1	0	4.141776	1.133014	-0.388387
16	1	0	2.691016	2.051152	-0.839327
17	6	0	-3.653092	0.045586	-0.011024
18	7	0	-4.801603	0.072372	-0.018324

1e (radical cation)

Charge = 1; Spin = 2
Number of imaginary frequencies = 1
Sum of electronic and thermal Free Energies = –836.795451 a.u.

Center Number	Atomic Number	Atomic Type	Coordinates (Angstroms) X	Y	Z
1	6	0	2.209074	0.022799	0.000000
2	6	0	1.489263	1.222513	-0.000004
3	6	0	0.108450	1.196006	-0.000004
4	6	0	-0.513508	-0.054598	-0.000002
5	6	0	0.177197	-1.267479	0.000002
6	6	0	1.557574	-1.214988	0.000002
7	1	0	2.015560	2.165828	-0.000006
8	1	0	-0.451125	2.121032	-0.000008
9	1	0	-0.349668	-2.211608	0.000004
10	1	0	2.135588	-2.127659	0.000005
11	16	0	-2.246773	-0.135226	-0.000001
12	8	0	-2.931333	-1.442671	-0.000004
13	6	0	-3.210204	1.386783	0.000006
14	1	0	-4.238304	1.026462	0.000021
15	1	0	-2.983082	1.940134	0.907899
16	1	0	-2.983106	1.940129	-0.907896
17	6	0	3.640074	0.065543	0.000001
18	7	0	4.786522	0.101600	0.000002

1j'

Charge = 0; Spin = 1
Number of imaginary frequencies = 1
Sum of electronic and thermal Free Energies = –823.395758 a.u.

Center Number	Atomic Number	Atomic Type	Coordinates (Angstroms) X	Y	Z
1	6	0	1.202490	1.165918	-0.245603
2	6	0	0.806370	-0.155998	-0.033413
3	6	0	1.744909	-1.168795	0.162391
4	6	0	3.092887	-0.843791	0.138508
5	6	0	3.508487	0.466215	-0.073365
6	6	0	2.557673	1.462582	-0.264061
7	1	0	0.474517	1.951430	-0.391469
8	1	0	1.405744	-2.181992	0.325254
9	1	0	3.824075	-1.626342	0.288059
10	1	0	4.561127	0.709127	-0.088728
11	1	0	2.869290	2.485080	-0.428099

12	16	0	-0.869343	-0.612974	-0.000122
13	8	0	-1.264828	-2.080175	0.231398
14	6	0	-2.310893	1.540780	0.991710
15	1	0	-3.023709	2.340768	0.780703
16	1	0	-2.711392	0.915586	1.788827
17	1	0	-1.380020	1.986732	1.337981
18	6	0	-2.103275	0.708555	-0.264686
19	6	0	-3.370923	0.001030	-0.725340
20	1	0	-1.695191	1.307215	-1.078901
21	1	0	-3.209241	-0.540144	-1.654809
22	1	0	-3.705967	-0.708958	0.029063
23	1	0	-4.147485	0.751515	-0.873965

1j' (radical cation)
Charge = 1; Spin = 2
Number of imaginary frequencies = 1
Sum of electronic and thermal Free Energies = –823.144499 a.u.

Center Number	Atomic Number	Atomic Type	Coordinates (Angstroms) X	Y	Z
1	6	0	1.198531	-1.181628	0.213583
2	6	0	0.839040	0.169736	0.210792
3	6	0	1.761150	1.194712	-0.011803
4	6	0	3.100787	0.854029	-0.077568
5	6	0	3.491291	-0.479722	0.012297
6	6	0	2.545565	-1.492569	0.151755
7	1	0	0.461398	-1.967849	0.297863
8	1	0	1.436056	2.221738	-0.103624
9	1	0	3.839461	1.629971	-0.216481
10	1	0	4.540093	-0.734159	-0.044454
11	1	0	2.855580	-2.526848	0.184865
12	16	0	-0.845083	0.605579	0.068177
13	8	0	-1.179275	1.900776	-0.564986
14	6	0	-2.371536	-1.463243	-0.990305
15	1	0	-3.128972	-2.222801	-0.792550
16	1	0	-2.742131	-0.811580	-1.780041
17	1	0	-1.466244	-1.962803	-1.328747
18	6	0	-2.167299	-0.681102	0.298109
19	6	0	-3.394266	0.082423	0.770974
20	1	0	-1.726724	-1.279479	1.097024
21	1	0	-3.216846	0.613637	1.703332
22	1	0	-3.734839	0.783576	0.010957
23	1	0	-4.180895	-0.654699	0.933914

1k
Charge = 0; Spin = 1
Number of imaginary frequencies = 1
Sum of electronic and thermal Free Energies = –862.688776 a.u.

Center	Atomic	Atomic	Coordinates (Angstroms)

Number	Number	Type	X	Y	Z
1	6	0	1.347739	-1.165828	0.000004
2	6	0	0.987066	0.182992	0.000001
3	6	0	1.960404	1.183876	-0.000003
4	6	0	3.298461	0.820568	-0.000004
5	6	0	3.675890	-0.517610	-0.000001
6	6	0	2.694500	-1.501414	0.000003
7	1	0	0.603759	-1.946842	0.000007
8	1	0	1.651570	2.219406	-0.000005
9	1	0	4.051922	1.596331	-0.000006
10	1	0	4.721212	-0.790921	-0.000002
11	1	0	2.973844	-2.546210	0.000005
12	16	0	-0.665054	0.743320	0.000002
13	8	0	-0.895101	2.266184	0.000006
14	6	0	-3.300424	0.467649	-0.000007
15	1	0	-4.188283	-0.167313	-0.000005
16	1	0	-3.314326	1.104797	0.881854
17	1	0	-3.314323	1.104789	-0.881873
18	6	0	-2.084969	-0.453903	-0.000001
19	6	0	-2.046055	-1.300296	1.267642
20	1	0	-1.138447	-1.896518	1.338488
21	1	0	-2.112982	-0.667274	2.150322
22	1	0	-2.900134	-1.981713	1.255491
23	6	0	-2.046046	-1.300299	-1.267642
24	1	0	-1.138440	-1.896526	-1.338478
25	1	0	-2.900128	-1.981711	-1.255498
26	1	0	-2.112961	-0.667279	-2.150325

1k (radical cation)
Charge = 1; Spin = 2
Number of imaginary frequencies = 1
Sum of electronic and thermal Free Energies = –862.441976 a.u.

Center Number	Atomic Number	Atomic Type	Coordinates (Angstroms) X	Y	Z
1	6	0	1.367343	-1.173087	0.016673
2	6	0	1.054513	0.186763	0.003919
3	6	0	2.020562	1.192486	-0.012035
4	6	0	3.350417	0.805649	-0.015995
5	6	0	3.691922	-0.543799	-0.004395
6	6	0	2.706116	-1.526897	0.011923
7	1	0	0.604169	-1.936260	0.031569
8	1	0	1.733230	2.234208	-0.020751
9	1	0	4.121461	1.562376	-0.028457
10	1	0	4.733309	-0.832170	-0.007795
11	1	0	2.979885	-2.571896	0.021955
12	16	0	-0.619062	0.712282	0.007784
13	8	0	-0.815294	2.185465	0.024547
14	6	0	-3.326376	0.578543	-0.022092
15	1	0	-4.260378	0.010408	-0.030701
16	1	0	-3.317490	1.207407	0.865471

17	1	0	-3.297675	1.201901	-0.913140
18	6	0	-2.224486	-0.457373	-0.006685
19	6	0	-2.161206	-1.265143	1.272145
20	1	0	-1.304193	-1.933881	1.309027
21	1	0	-2.169750	-0.628837	2.154591
22	1	0	-3.063137	-1.882547	1.288963
23	6	0	-2.130440	-1.271013	-1.279829
24	1	0	-1.270844	-1.937284	-1.294812
25	1	0	-3.029818	-1.891455	-1.313294
26	1	0	-2.121609	-0.638967	-2.165330

1o
Charge = 0; Spin = 1
Number of imaginary frequencies = 1
Sum of electronic and thermal Free Energies = –975.824653 a.u.

Center Number	Atomic Number	Atomic Type	Coordinates (Angstroms) X	Y	Z
1	6	0	1.303703	-0.733694	0.691455
2	6	0	1.064071	0.476045	0.043601
3	6	0	2.096813	1.177255	-0.571285
4	6	0	3.377030	0.645351	-0.544764
5	6	0	3.640407	-0.584868	0.055617
6	6	0	2.585416	-1.261487	0.668123
7	1	0	0.506976	-1.243013	1.215226
8	1	0	1.892317	2.127554	-1.044535
9	1	0	4.184942	1.194523	-1.010975
10	1	0	2.775352	-2.204664	1.164494
11	16	0	-0.522999	1.205336	0.040414
12	8	0	-0.715075	2.721467	0.099802
13	6	0	-1.897148	0.136028	-0.032642
14	6	0	-1.794567	-1.156798	-0.545626
15	6	0	-3.116229	0.652704	0.400428
16	6	0	-2.931905	-1.949413	-0.580601
17	1	0	-0.851530	-1.527725	-0.920894
18	6	0	-4.243965	-0.152537	0.331069
19	1	0	-3.164927	1.667033	0.770884
20	6	0	-4.157730	-1.455001	-0.146408
21	1	0	-2.861093	-2.954935	-0.971949
22	1	0	-5.194704	0.242742	0.660962
23	1	0	-5.039550	-2.078064	-0.188781
24	6	0	5.024210	-1.175274	0.033089
25	1	0	5.200536	-1.791081	0.913807
26	1	0	5.158065	-1.805734	-0.847957
27	1	0	5.781570	-0.393620	0.002339

1o (radical cation)
Charge = 1; Spin = 2
Number of imaginary frequencies = 1
Sum of electronic and thermal Free Energies = –975.575949 a.u.

Center Number	Atomic Number	Atomic Type	Coordinates (Angstroms) X	Y	Z
1	6	0	1.267835	-0.769738	0.651907
2	6	0	1.072707	0.462280	0.022343
3	6	0	2.111408	1.192869	-0.557870
4	6	0	3.380638	0.650596	-0.512152
5	6	0	3.619509	-0.591794	0.087148
6	6	0	2.549295	-1.285405	0.665199
7	1	0	0.452894	-1.292993	1.132364
8	1	0	1.925037	2.152874	-1.019234
9	1	0	4.203526	1.197453	-0.951841
10	1	0	2.730786	-2.233706	1.152288
11	16	0	-0.505363	1.178416	0.005349
12	8	0	-0.665641	2.647246	0.024592
13	6	0	-1.907136	0.147346	-0.036335
14	6	0	-1.828975	-1.089804	-0.678116
15	6	0	-3.072055	0.643658	0.547710
16	6	0	-2.974936	-1.866267	-0.704334
17	1	0	-0.917319	-1.421538	-1.154735
18	6	0	-4.203258	-0.152891	0.491701
19	1	0	-3.086507	1.615830	1.020526
20	6	0	-4.152624	-1.400795	-0.123848
21	1	0	-2.954105	-2.828133	-1.195732
22	1	0	-5.123636	0.199671	0.933943
23	1	0	-5.041474	-2.014541	-0.158081
24	6	0	4.998959	-1.176134	0.096386
25	1	0	5.134224	-1.854605	0.935785
26	1	0	5.164746	-1.741578	-0.823278
27	1	0	5.754549	-0.394876	0.147241

9. Refarence

1 K. Sugiyama, Y. Oki, S. Kawanishi, K. Kato, T. Ikawa, M. Egi, S. Akai, *Catal. Sci. Technol.* **2016**, *6*, 5023.

2 B. Pelotier, M. S. Anson, I. B. Campbell, S. J. F. Macdonald, G. Priem, R. F. W. Jackson, *Synlett* **2002**, *2002*, 1055.

3 N. Komatsu, Y. Nishibayashi, T. Sugita, S. Uemura, *Tetrahedron Lett.* **1992**, *33*, 5391.

4 M. Laube, C. Gassner, S. K. Sharma, R. Günther, A. Pigorsch, J. König, M. Köckerling, F. Wuest, J. Pietzsch, T. Kniess, *J. Org. Chem.* **2015**, *80*, 5611.

5 M. G. Cabiddu, S. Cabiddu, E. Cadoni, R. Cannas, S. De Montis, C. Fattuoni, S. Melis, *J. Organomet. Chem.* **2001**, *620*, 263.

6 S. R. Mangaonkar, P. B. Kole, F. V. Singh, *Synlett* **2018**, *29*, 199.

7 K. K. Andersen, *Tetrahedron Lett.* **1962**, *3*, 93.

8 Y. Li, F. Ma, P. Li, T. Miao, L. Wang, *Adv. Synth. Catal.* **2019**, *361*, 1606.

9 H. Gholami, J. Zhang, M. Anyika, B. Borhan, *Org. Lett.* **2017**, *19*, 1722.

10 H. Saito, K. Yamamoto, Y. Sumiya, L. J. Liu, K. Nogi, S. Maeda, H. Yorimitsu, *Chem. Asian J.* **2020**, *15*, 2442.

11 P. J. Gilissen, X. Chen, J. De Graaf, P. Tinnemans, B. L. Feringa, J. A. A. W. Elemans, R. J. M. Nolte, *Chem. Eur. J.* **2023**, *29*, e202203539.

12 A. Jalba, N. Régnier, T. Ollevier, *Eur. J. Org. Chem.* **2017**, *2017*, 1628.

13 C. Wolf, *Dynamic Stereochemistry of Chiral Compounds*, The Royal Society of Chemistry, Cambridge, **2008**.

14 C. Hansch, A. Leo, R. W. Taft, *Chem. Rev.* **1991**, *91*, 165.

15 M. Reist, B. Testa, P.-A. Carrupt, M. Jung, V. Schurig, *Chirality* **1995**, *7*, 396.

10. HPLC and NMR chart

[Condition For **1a**]

Column: CHIRALPAK ID-3 (4.6 mm x 250 mm)

Eluent: hexane/^{i}PrOH = 70:30

Flow rate: 1.0 mL/min

Detection: 254 nm

Temperature: 30 ˚C

Peaks: (*R*) t_R = 9.9 min, (*S*) t_R = 10.7 min

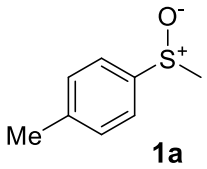

1a

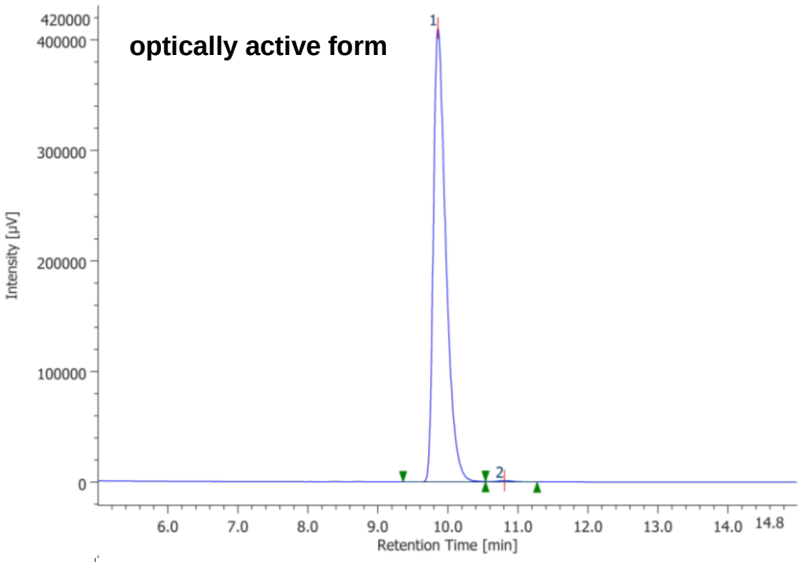

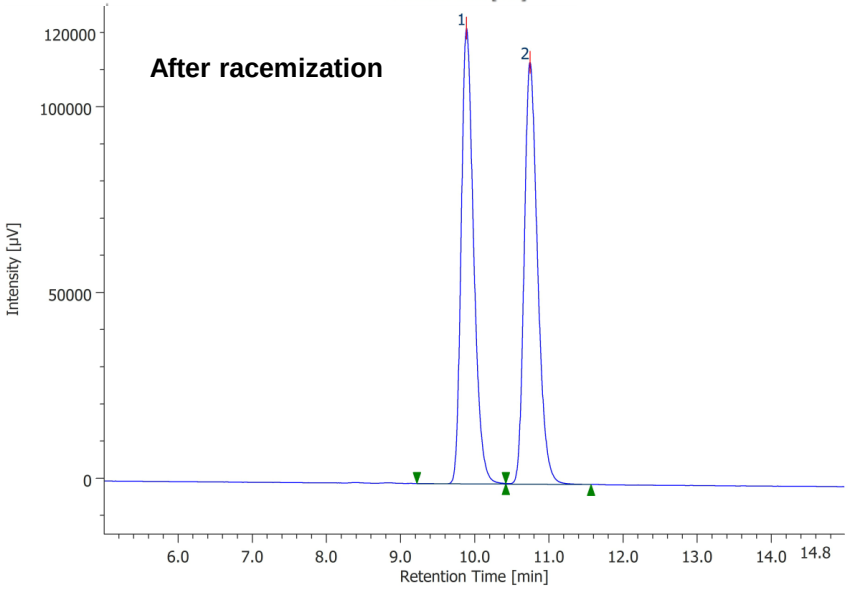

#	Peak Name	CH	tR [min]	Area [μV·sec]	Height [μV]	Area%	Height%	Quantity	NTP	Resolution	Symmetry Factor	Warning
1	Unknown	5	9.857	5092392	410254	99.607	99.683	N/A	15339	2.823	1.595	
2	Unknown	5	10.807	20114	1303	0.393	0.317	N/A	14712	N/A	N/A	

#	Peak Name	CH	tR [min]	Area [μV·sec]	Height [μV]	Area%	Height%	Quantity	NTP	Resolution	Symmetry Factor	Warning
1	Unknown	5	9.887	1426891	122680	50.072	51.939	N/A	17271	2.747	1.304	
2	Unknown	5	10.743	1422778	113521	49.928	48.061	N/A	17546	N/A	1.277	

[Condition For **1b**]

Column: CHIRALPAK IC-3 (4.6 mm x 250 mm)

Eluent: hexane/^{i}PrOH = 70:30

Flow rate: 1.0 mL/min

Detection: 254 nm

Temperature: 30 ℃

Peaks: (*R*) t_R = 15.3 min, (*S*) t_R = 17.0 min

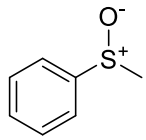

1b

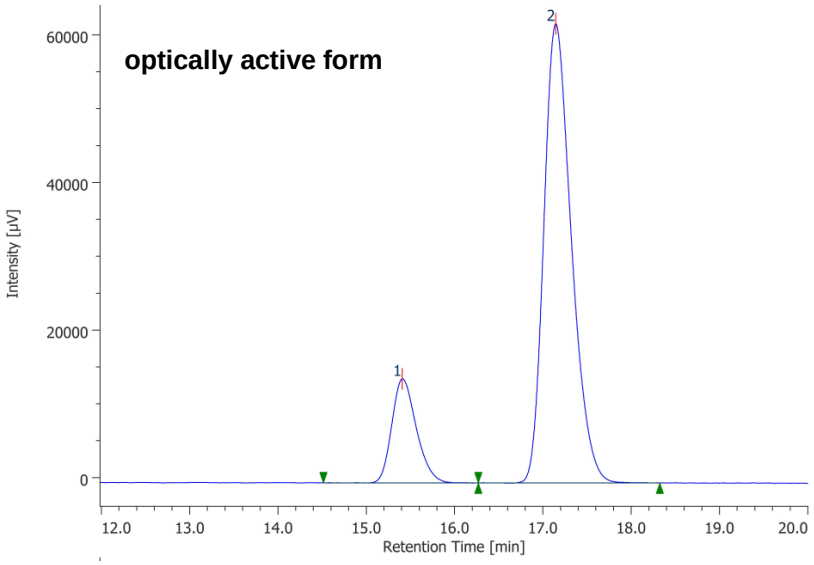

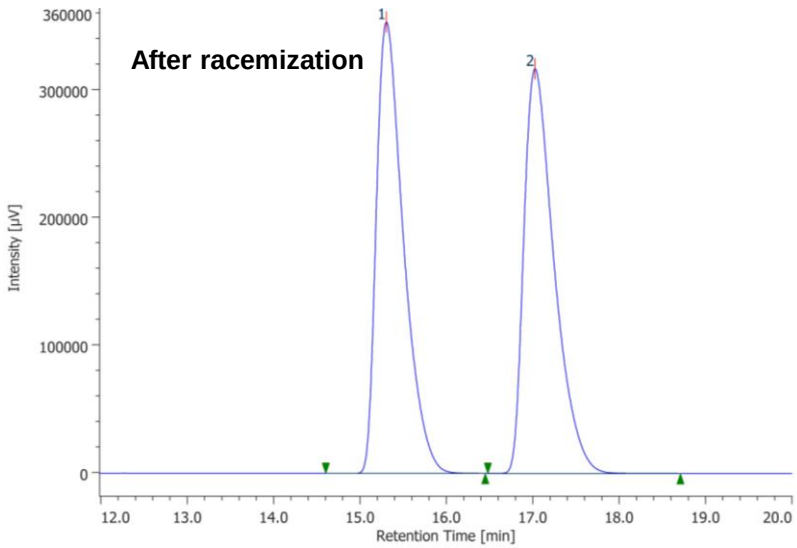

#	Peak Name	CH	tR [min]	Area [μV·sec]	Height [μV]	Area%	Height%	Quantity	NTP	Resolution	Symmetry Factor	Warning
1	Unknown	5	15.407	272343	14111	16.837	18.489	N/A	14948	3.258	1.258	
2	Unknown	5	17.143	1345230	62211	83.163	81.511	N/A	14730	N/A	1.284	

#	Peak Name	CH	tR [min]	Area [μV·sec]	Height [μV]	Area%	Height%	Quantity	NTP	Resolution	Symmetry Factor	Warning
1	Unknown	5	15.303	7716636	353631	49.967	52.730	N/A	11678	2.875	1.626	
2	Unknown	5	17.023	7726905	317018	50.033	47.270	N/A	11569	N/A	1.638	

[Condition For **1c**]

Column: CHIRALPAK IF-3 (4.6 mm x 250 mm)

Eluent: hexane/^{i}PrOH = 70:30

Flow rate: 1.0 mL/min

Detection: 254 nm

Temperature: 30 ℃

Peaks: (*S*) t_R = 29.9 min, (*R*) t_R = 33.1 min

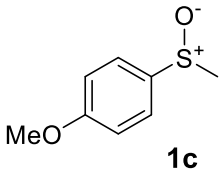

1c

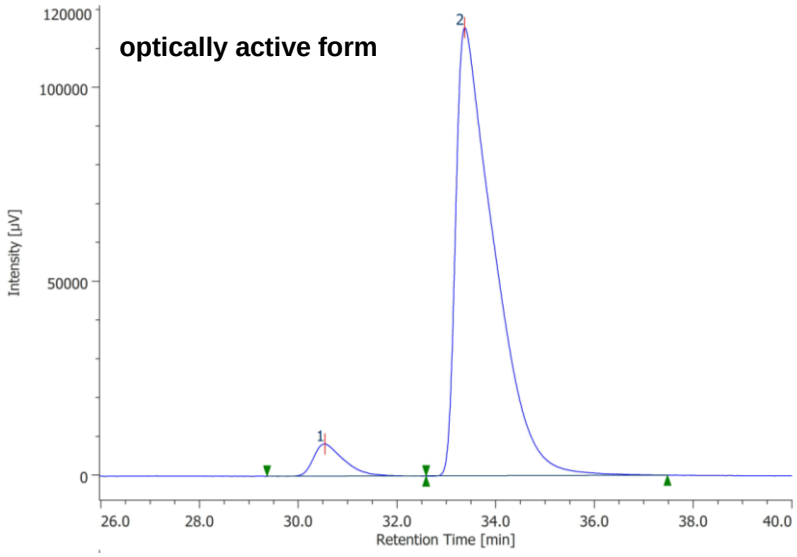

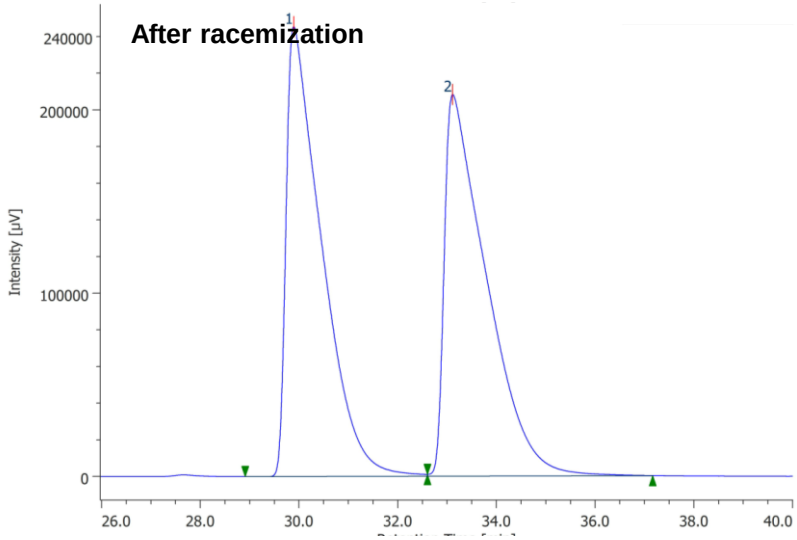

#	Peak Name	CH	tR [min]	Area [μV·sec]	Height [μV]	Area%	Height%	Quantity	NTP	Resolution	Symmetry Factor	Warning
1	Unknown	5	30.540	351525	8287	5.354	6.697	N/A	12527	2.289	1.562	
2	Unknown	5	33.370	6214681	115466	94.646	93.303	N/A	9251	N/A	2.617	

#	Peak Name	CH	tR [min]	Area [μV·sec]	Height [μV]	Area%	Height%	Quantity	NTP	Resolution	Symmetry Factor	Warning
1	Unknown	5	29.893	12247215	245334	49.840	54.106	N/A	8585	2.280	2.881	
2	Unknown	5	33.110	12325834	208098	50.160	45.894	N/A	7407	N/A	3.127	

[Condition For **1d**]

Column: CHIRALPAK IE-3 (4.6 mm x 250 mm)

Eluent: hexane/^{i}PrOH = 80:20

Flow rate: 1.0 mL/min

Detection: 254 nm

Temperature: 30 ℃

Peaks: (*S*) t_R = 12.1 min, (*R*) t_R = 13.1 min

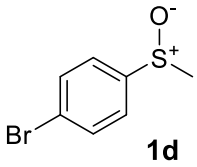

1d

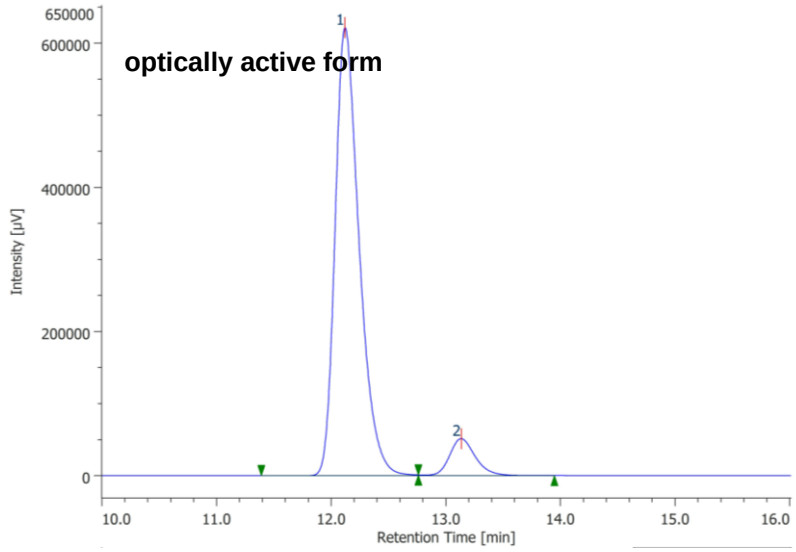

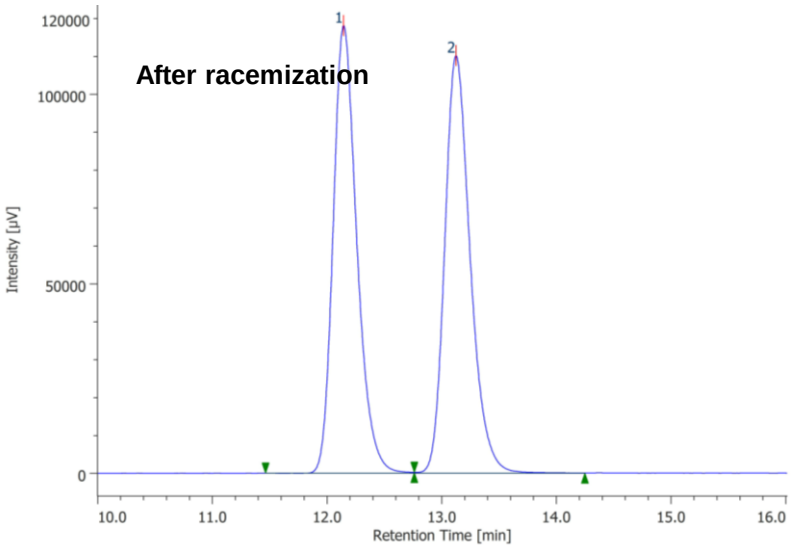

#	Peak Name	CH	tR [min]	Area [μV·sec]	Height [μV]	Area%	Height%	Quantity	NTP	Resolution	Symmetry Factor	Warning
1	Unknown	5	12.120	9063397	621450	91.863	92.374	N/A	16699	2.629	1.362	
2	Unknown	5	13.133	802774	51304	8.137	7.626	N/A	17444	N/A	1.219	

#	Peak Name	CH	tR [min]	Area [μV·sec]	Height [μV]	Area%	Height%	Quantity	NTP	Resolution	Symmetry Factor	Warning
1	Unknown	5	12.143	1692191	118053	49.929	51.743	N/A	17353	2.571	1.256	
2	Unknown	5	13.123	1696992	110100	50.071	48.257	N/A	17596	N/A	1.250	

[Condition For **1e**]

Column: CHIRALPAK IE-3 (4.6 mm x 250 mm)

Eluent: hexane/^{i}PrOH = 70:30

Flow rate: 1.0 mL/min

Detection: 254 nm

Temperature: 30 ℃

Peaks: (*R*) t_R = 11.6 min, (*S*) t_R = 12.5 min

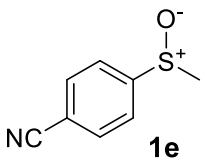

1e

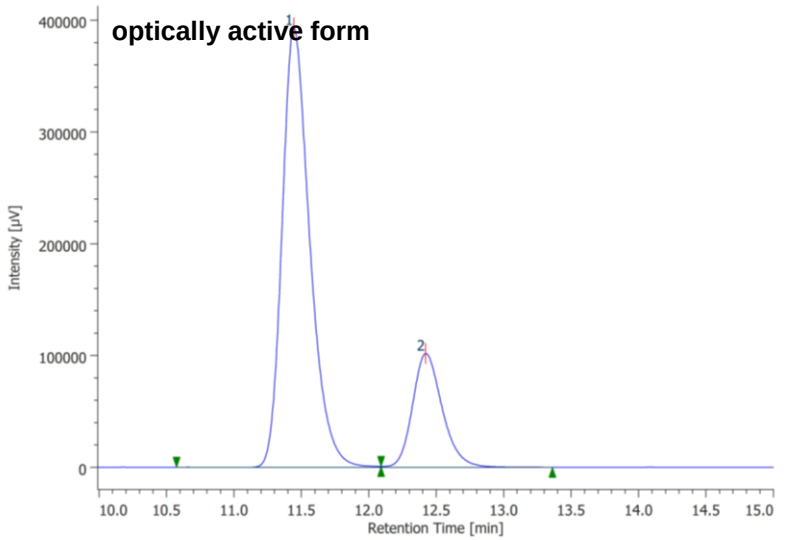

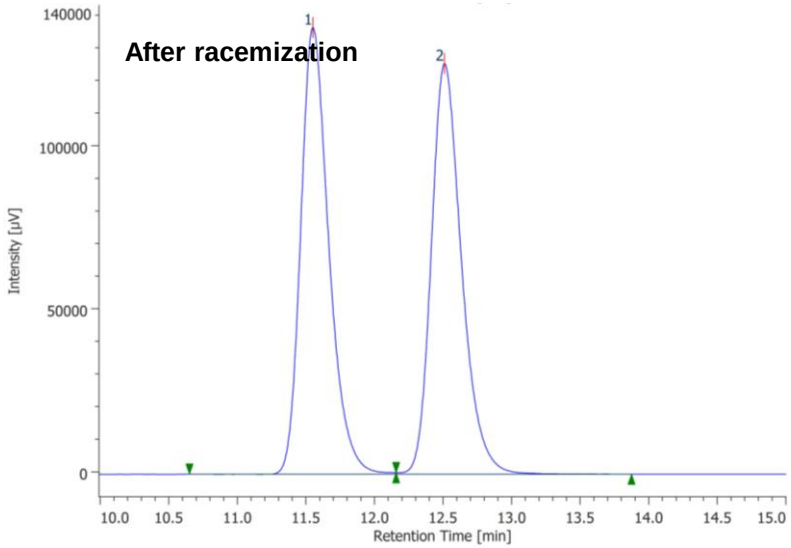

#	Peak Name	CH	tR [min]	Area [μV·sec]	Height [μV]	Area%	Height%	Quantity	NTP	Resolution	Symmetry Factor	Warning
1	Unknown	5	11.443	5610856	393087	78.278	79.421	N/A	15648	2.585	1.309	
2	Unknown	5	12.420	1557001	101857	21.722	20.579	N/A	16088	N/A	1.230	

#	Peak Name	CH	tR [min]	Area [μV·sec]	Height [μV]	Area%	Height%	Quantity	NTP	Resolution	Symmetry Factor	Warning
1	Unknown	5	11.550	1947336	136935	50.229	52.109	N/A	16086	2.546	1.288	
2	Unknown	5	12.510	1929589	125849	49.771	47.891	N/A	16299	N/A	1.272	

[Condition For **1f**]

Column: CHIRALPAK ID-3 (4.6 mm x 250 mm)

Eluent: hexane/^{i}PrOH = 70:30

Flow rate: 1.0 mL/min

Detection: 254 nm

Temperature: 30 ℃

Peaks: (*S*) t_R = 13.0 min, (*R*) t_R = 14.4 min

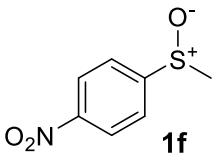

1f

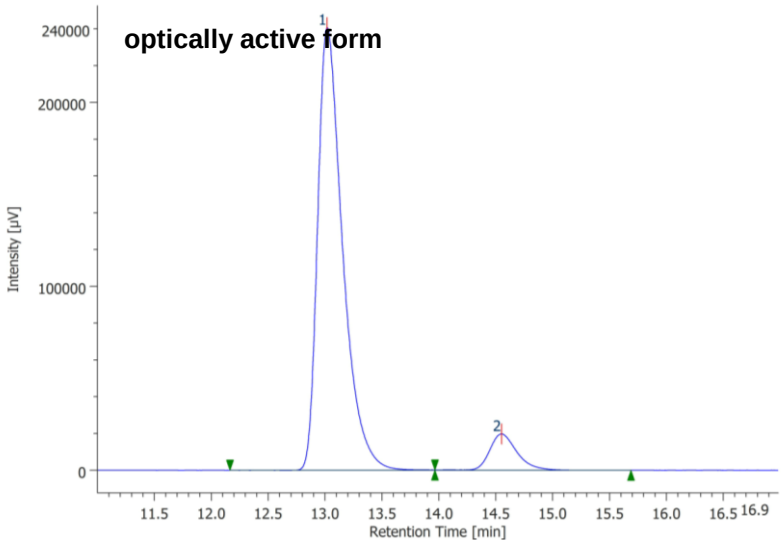

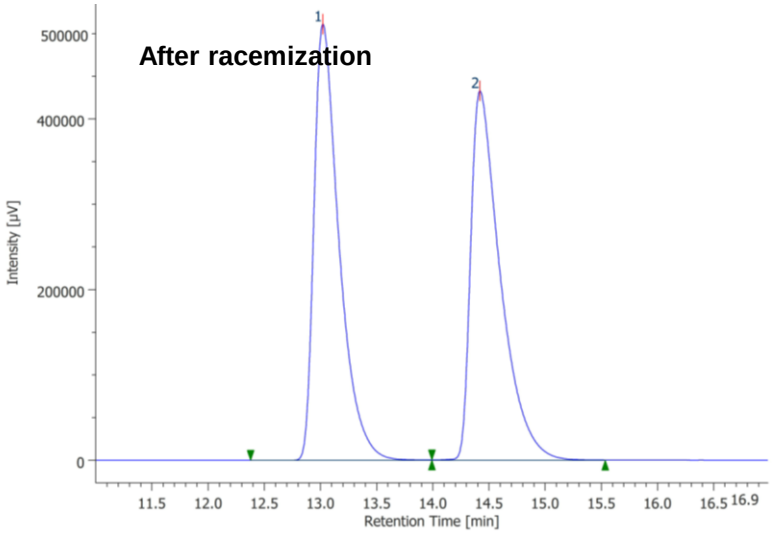

#	Peak Name	CH	tR [min]	Area [μV·sec]	Height [μV]	Area%	Height%	Quantity	NTP	Resolution	Symmetry Factor	Warning
1	Unknown	5	13.017	3673651	240743	91.661	92.394	N/A	18157	3.800	1.573	
2	Unknown	5	14.550	334204	19818	8.339	7.606	N/A	18953	N/A	1.306	

#	Peak Name	CH	tR [min]	Area [μV·sec]	Height [μV]	Area%	Height%	Quantity	NTP	Resolution	Symmetry Factor	Warning
1	Unknown	5	13.020	7933111	510978	50.000	54.156	N/A	17657	3.278	1.729	
2	Unknown	5	14.417	7933029	432556	50.000	45.844	N/A	15551	N/A	2.031	

[Condition For **1g**]

Column: CHIRALPAK IE-3 (4.6 mm x 250 mm)

Eluent: hexane/^{i}PrOH = 60:40

Flow rate: 0.7 mL/min

Detection: 254 nm

Temperature: 30 ℃

Peaks: (*S*) t_R = 22.5 min, (*R*) t_R = 24.5 min

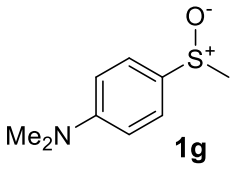

1g

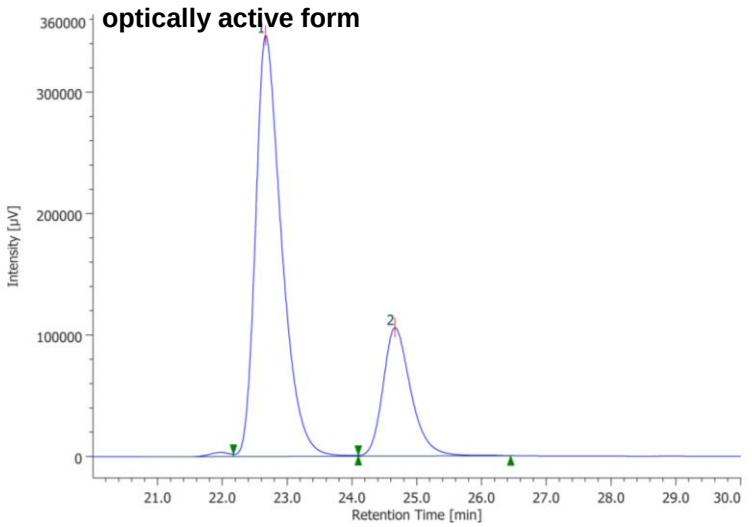

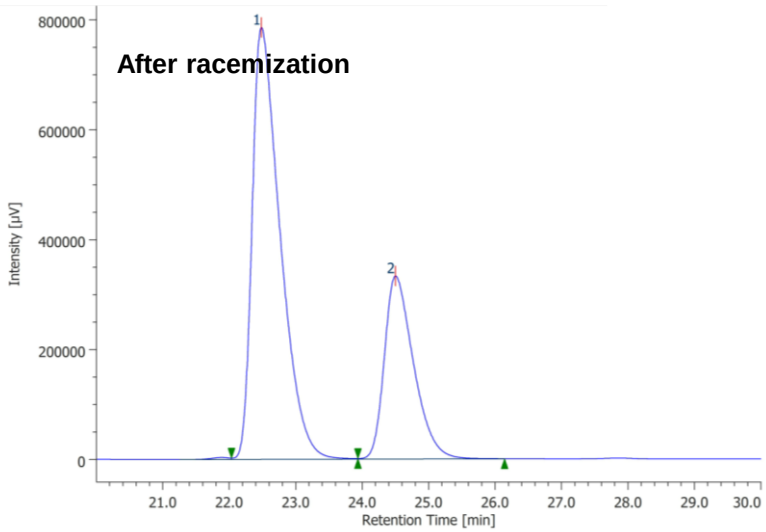

#	Peak Name	CH	tR [min]	Area [μV*sec]	Height [μV]	Area%	Height%	Quantity	NTP	Resolution	Symmetry Factor	Warning
1	Unknown	5	22.667	9668340	346490	75.346	76.625	N/A	16222	2.723	1.441	
2	Unknown	5	24.663	3163557	105700	24.654	23.375	N/A	16902	N/A	1.290	

#	Peak Name	CH	tR [min]	Area [μV*sec]	Height [μV]	Area%	Height%	Quantity	NTP	Resolution	Symmetry Factor	Warning
1	Unknown	5	22.483	22997139	785607	69.355	70.234	N/A	14133	2.618	1.709	
2	Unknown	5	24.500	10161402	332942	30.645	29.766	N/A	15466	N/A	1.448	

[Condition For **1h**]

Column: CHIRALPAK IA-3 (4.6 mm x 250 mm)

Eluent: hexane/^{i}PrOH = 95:5

Flow rate: 1.0 mL/min

Detection: 254 nm

Temperature: 30 ℃

Peaks: (*R*) t_R = 13.7 min, (*S*) t_R = 14.5 min

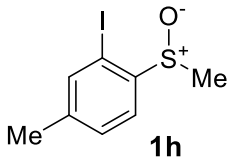

1h

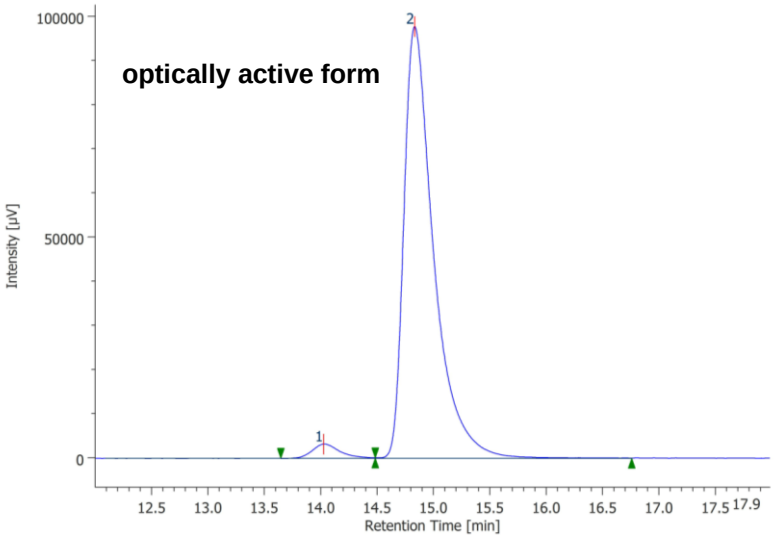

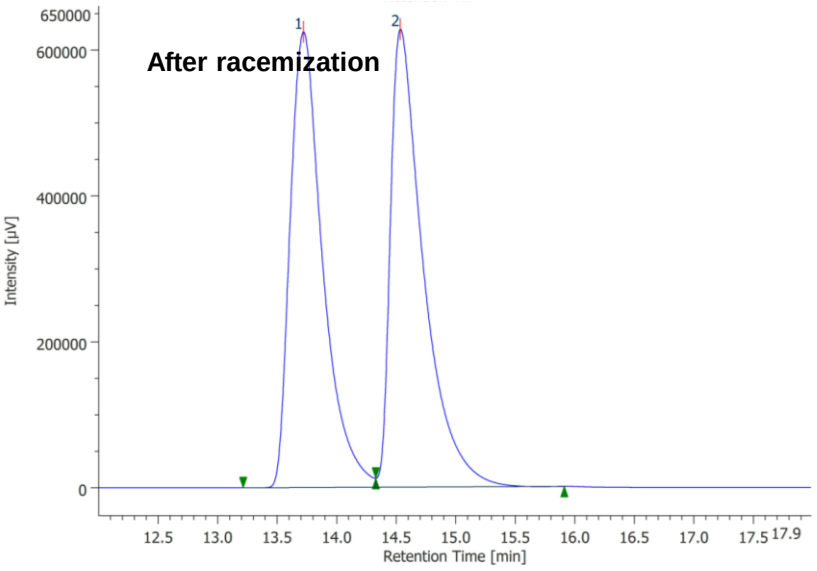

#	Peak Name	CH	tR [min]	Area [μV·sec]	Height [μV]	Area%	Height%	Quantity	NTP	Resolution	Symmetry Factor	Warning
1	Unknown	5	14.027	54581	3221	2.960	3.190	N/A	17590	1.856	1.358	
2	Unknown	5	14.833	1789174	97748	97.040	96.810	N/A	17516	N/A	1.768	

#	Peak Name	CH	tR [min]	Area [μV·sec]	Height [μV]	Area%	Height%	Quantity	NTP	Resolution	Symmetry Factor	Warning
1	Unknown	5	13.720	11858293	624435	49.616	49.877	N/A	12900	1.707	1.586	
2	Unknown	5	14.533	12042050	627505	50.384	50.123	N/A	15155	N/A	2.205	

[Condition For **1i**]

Column: CHIRALPAK IK-3 (4.6 mm x 250 mm)

Eluent: hexane/^{i}PrOH = 80:20

Flow rate: 1.0 mL/min

Detection: 254 nm

Temperature: 30 ℃

Peaks: (*R*) t_R = 27.1 min, (*S*) t_R = 29.8 min

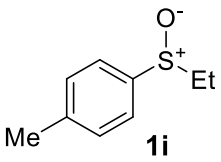

1i

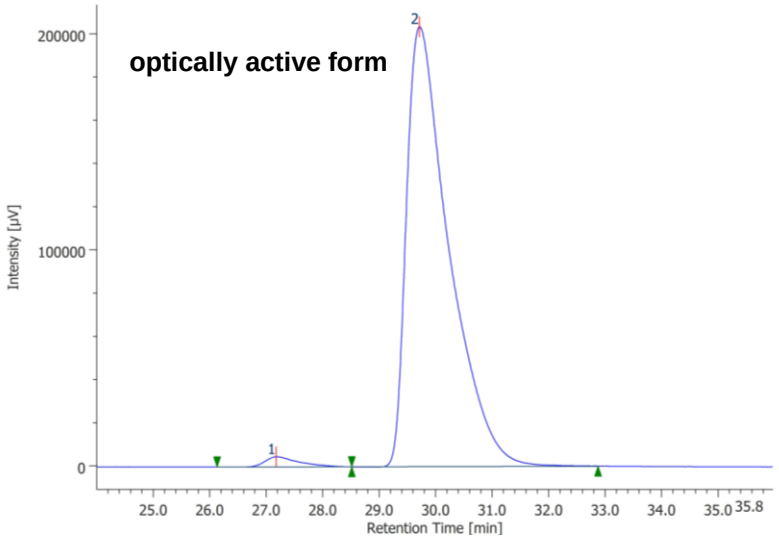

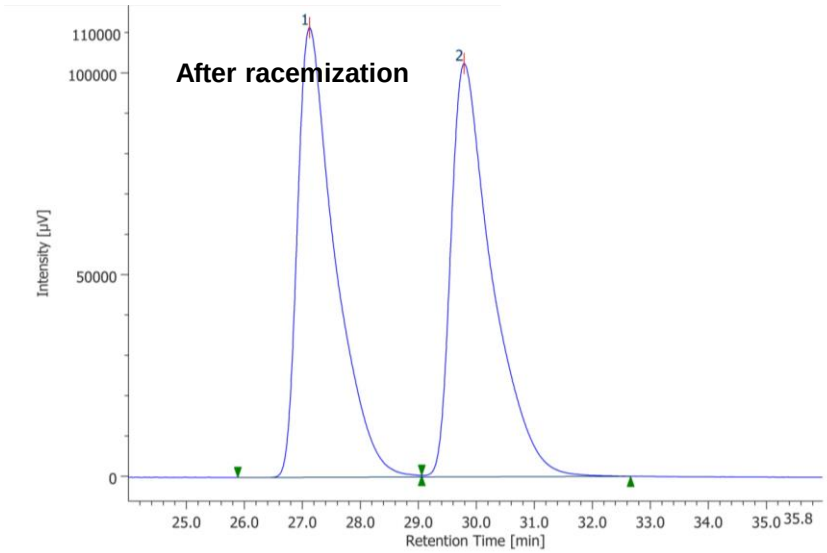

#	Peak Name	CH	tR [min]	Area [μV·sec]	Height [μV]	Area%	Height%	Quantity	NTP	Resolution	Symmetry Factor	Warning
1	Unknown	5	27.177	187981	4634	1.743	2.227	N/A	11475	2.188	1.715	
2	Unknown	5	29.713	10594419	203451	98.257	97.773	N/A	8233	N/A	2.045	

#	Peak Name	CH	tR [min]	Area [μV·sec]	Height [μV]	Area%	Height%	Quantity	NTP	Resolution	Symmetry Factor	Warning
1	Unknown	5	27.123	4996839	111470	49.793	52.116	N/A	9495	2.297	1.910	
2	Unknown	5	29.787	5038372	102419	50.207	47.884	N/A	9675	N/A	1.925	

[Condition For **1j**]

Column: CHIRALPAK IG-3 (4.6 mm x 250 mm)

Eluent: hexane/^{i}PrOH = 90:10

Flow rate: 1.0 mL/min

Detection: 254 nm

Temperature: 30 ℃

Peaks: (*S*) t_R = 19.3 min, (*R*) t_R = 20.7 min

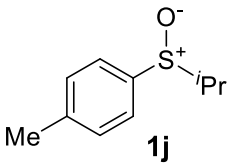

1j

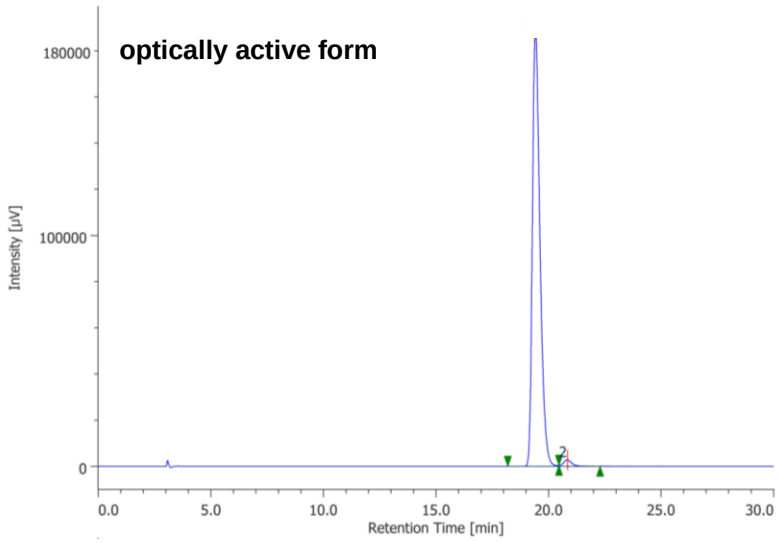

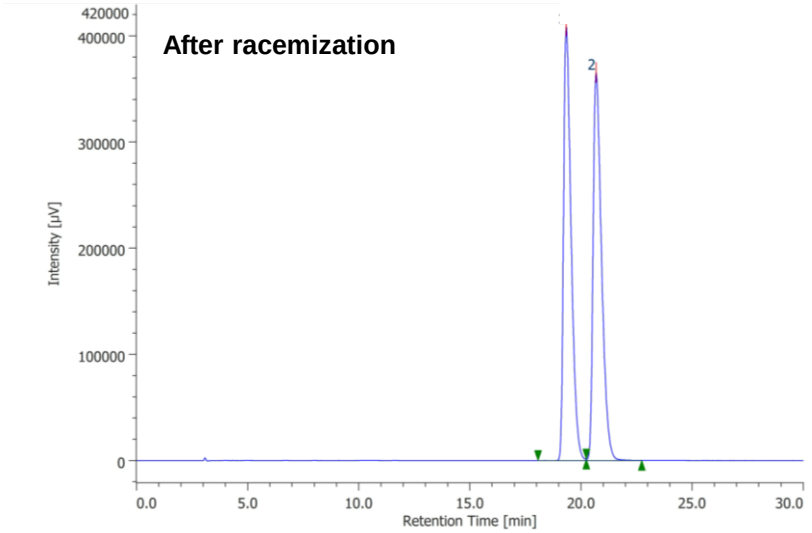

#	Peak Name	CH	tR [min]	Area [μV·sec]	Height [μV]	Area%	Height%	Quantity	NTP	Resolution	Symmetry Factor	Warning
1	Unknown	5	19.410	4407613	189754	98.420	98.552	N/A	16757	2.300	1.407	
2	Unknown	5	20.833	70757	2788	1.580	1.448	N/A	16902	N/A	N/A	

#	Peak Name	CH	tR [min]	Area [μV·sec]	Height [μV]	Area%	Height%	Quantity	NTP	Resolution	Symmetry Factor	Warning
1	Unknown	5	19.330	9681109	408949	50.081	52.812	N/A	15779	2.070	1.617	
2	Unknown	5	20.673	9649706	365403	49.919	47.188	N/A	14547	N/A	1.614	

[Condition For **1l**]

Column: CHIRALPAK IA-3 (4.6 mm x 250 mm)

Eluent: hexane/^{i}PrOH = 80:20

Flow rate: 1.0 mL/min

Detection: 254 nm

Temperature: 30 ℃

Peaks: (*S*) t_R = 6.3 min, (*R*) t_R = 7.1 min

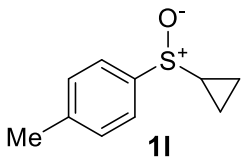

1l

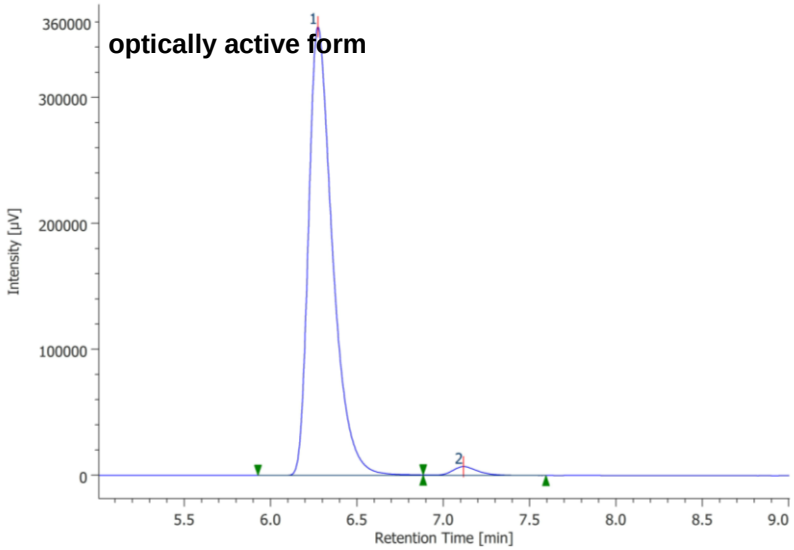

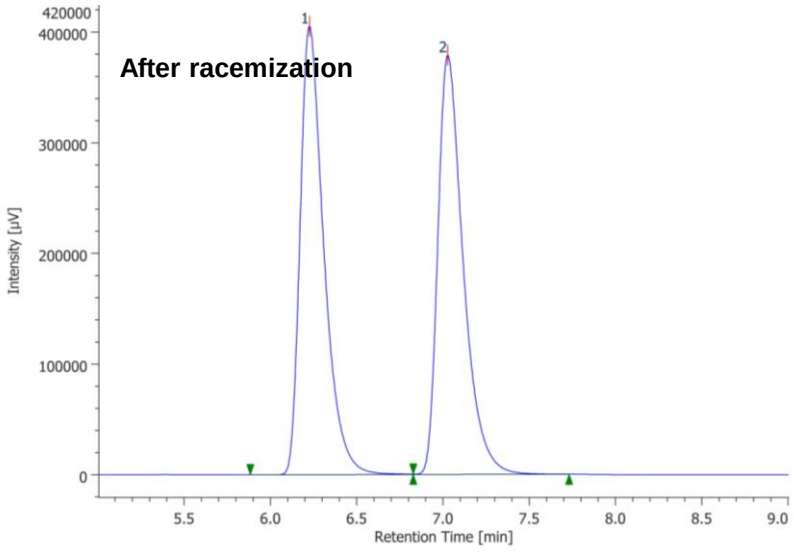

#	Peak Name	CH	tR [min]	Area [μV·sec]	Height [μV]	Area%	Height%	Quantity	NTP	Resolution	Symmetry Factor	Warning
1	Unknown	5	6.273	3430250	356378	97.861	98.054	N/A	10567	3.339	1.516	
2	Unknown	5	7.117	74977	7072	2.139	1.946	N/A	11764	N/A	N/A	

#	Peak Name	CH	tR [min]	Area [μV·sec]	Height [μV]	Area%	Height%	Quantity	NTP	Resolution	Symmetry Factor	Warning
1	Unknown	5	6.227	3865853	405147	49.987	51.677	N/A	10578	3.201	1.497	
2	Unknown	5	7.027	3867831	378849	50.013	48.323	N/A	11778	N/A	1.531	

[Condition For **1m**]

Column: CHIRALPAK IK-3 (4.6 mm x 250 mm)

Eluent: hexane/^{i}PrOH = 80:20

Flow rate: 1.0 mL/min

Detection: 254 nm

Temperature: 30 ℃

Peaks: (*R*) t_R = 13.2 min, (*S*) t_R = 14.4. min

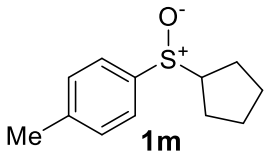

1m

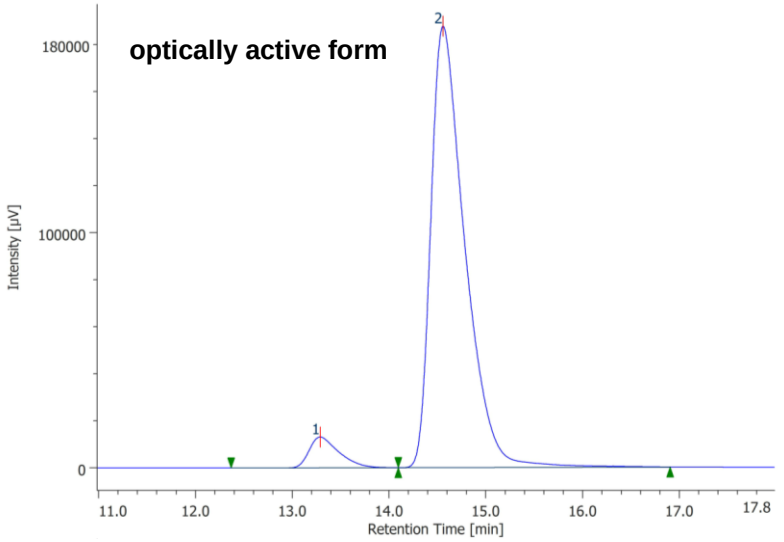

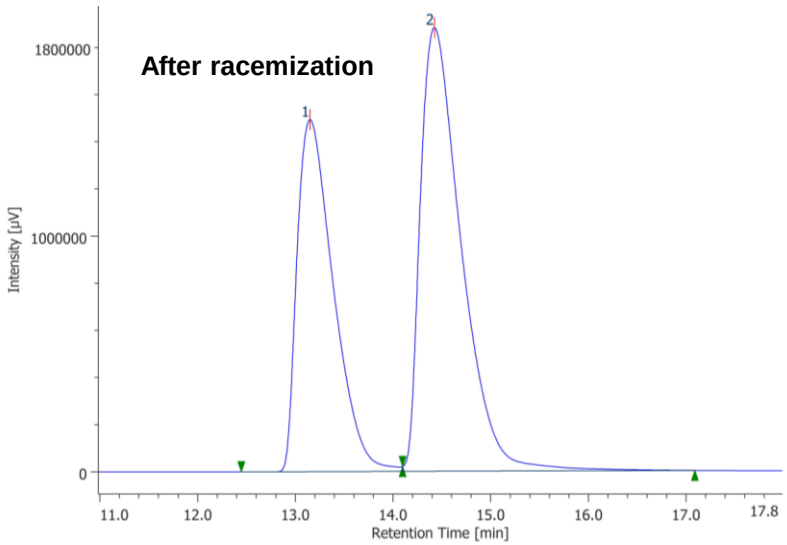

#	Peak Name	CH	tR [min]	Area [μV·sec]	Height [μV]	Area%	Height%	Quantity	NTP	Resolution	Symmetry Factor	Warning
1	Unknown	5	13.290	277761	13088	5.731	6.522	N/A	9344	2.171	1.510	
2	Unknown	5	14.557	4569059	187600	94.269	93.478	N/A	8824	N/A	1.600	

#	Peak Name	CH	tR [min]	Area [μV·sec]	Height [μV]	Area%	Height%	Quantity	NTP	Resolution	Symmetry Factor	Warning
1	Unknown	5	13.150	38470414	1492512	41.279	44.242	N/A	5927	1.779	1.713	
2	Unknown	5	14.423	54724906	1881003	58.721	55.758	N/A	5889	N/A	1.788	

[Condition For **1n**]

Column: CHIRALPAK ID-3 (4.6 mm x 250 mm)

Eluent: hexane/^{i}PrOH = 70:30

Flow rate: 1.0 mL/min

Detection: 254 nm

Temperature: 30 ℃

Peaks: (*R*) t_R = 8.0 min, (*S*) t_R = 8.7 min

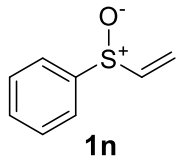

1n

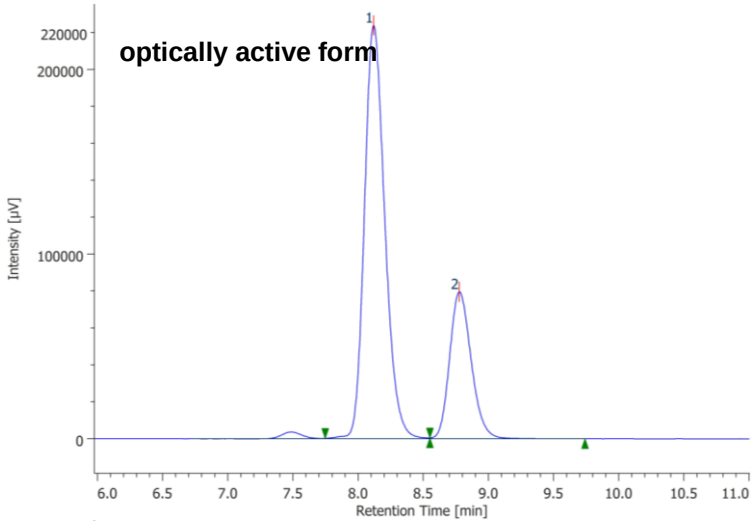

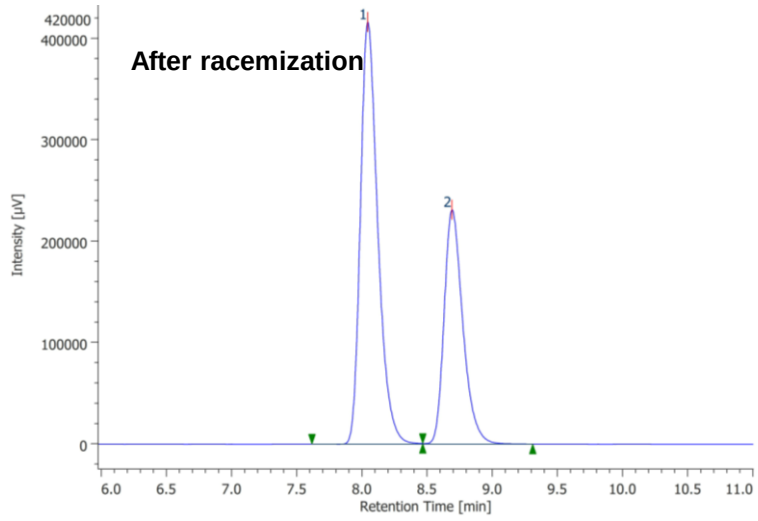

#	Peak Name	CH	tR [min]	Area [μV·sec]	Height [μV]	Area%	Height%	Quantity	NTP	Resolution	Symmetry Factor	Warning
1	Unknown	5	8.120	2435393	223888	72.630	73.763	N/A	13235	2.260	1.200	
2	Unknown	5	8.777	917761	79634	27.370	26.237	N/A	13675	N/A	1.201	

#	Peak Name	CH	tR [min]	Area [μV·sec]	Height [μV]	Area%	Height%	Quantity	NTP	Resolution	Symmetry Factor	Warning
1	Unknown	5	8.043	3861151	416331	62.557	64.304	N/A	18323	2.626	1.348	
2	Unknown	5	8.690	2311042	231113	37.443	35.696	N/A	18405	N/A	1.338	

[Condition For **1o**]

Column: CHIRALPAK IH-3 (4.6 mm x 250 mm)

Eluent: hexane/^{i}PrOH = 80:20

Flow rate: 1.0 mL/min

Detection: 254 nm

Temperature: 30 ℃

Peaks: (*S*) t_R = 25.7 min, (*R*) t_R = 34.2 min

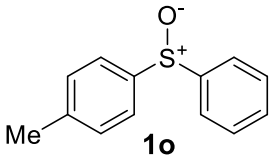

1o

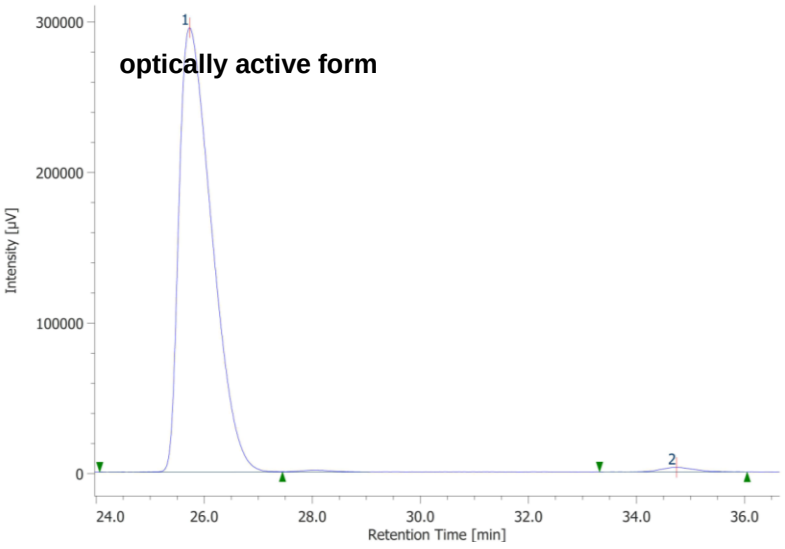

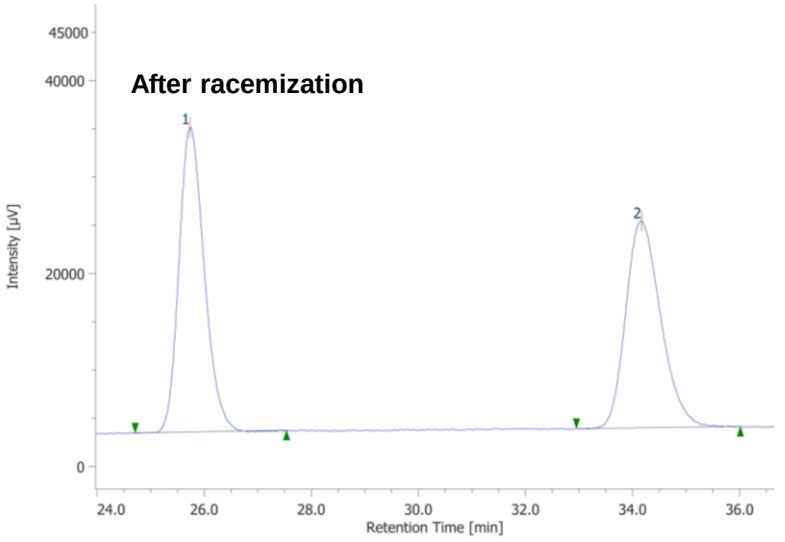

#	Peak Name	CH	tR [min]	Area [μV·sec]	Height [μV]	Area%	Height%	Quantity	NTP	Resolution	Symmetry Factor	Warning
1	Unknown	5	25.730	12392490	295128	98.943	98.995	N/A	8315	7.927	1.806	
2	Unknown	5	34.740	132334	2997	1.057	1.005	N/A	14582	N/A	1.209	

#	Peak Name	CH	tR [min]	Area [μV·sec]	Height [μV]	Area%	Height%	Quantity	NTP	Resolution	Symmetry Factor	Warning
1	Unknown	5	25.737	1034659	31579	51.566	59.609	N/A	14328	8.249	1.227	
2	Unknown	5	34.170	971805	21399	48.434	40.391	N/A	13190	N/A	1.226	

[Condition For **1p**]

Column: CHIRALPAK IK-3 (4.6 mm x 250 mm)

Eluent: hexane/^{i}PrOH = 85:15

Flow rate: 1.0 mL/min

Detection: 254 nm

Temperature: 30 ℃

Peaks: (*S*) t_R = 37.6 min, (*R*) t_R = 39.6 min

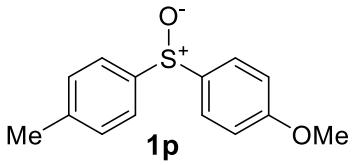

1p

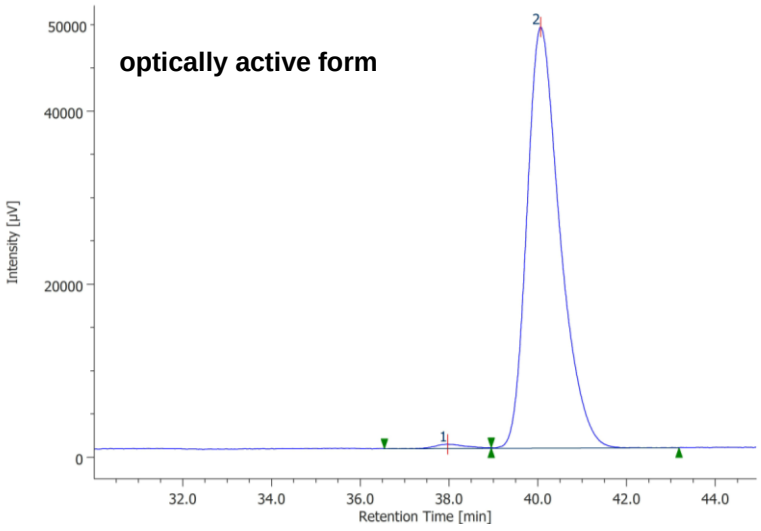

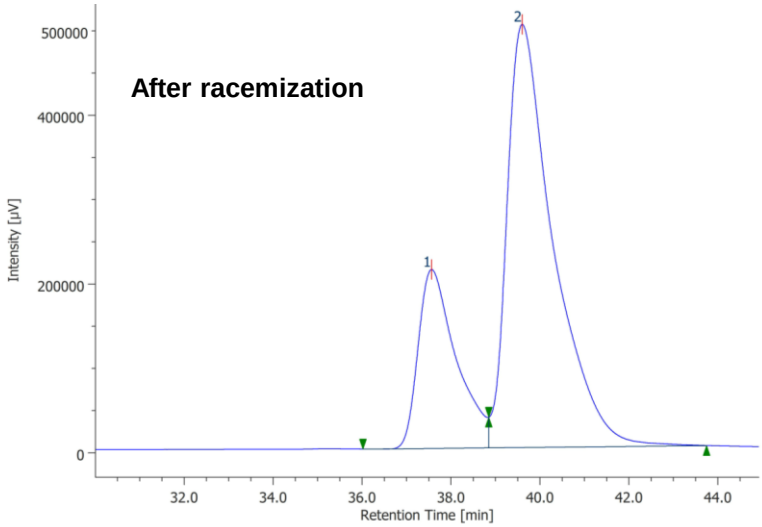

#	Peak Name	CH	tR [min]	Area [μV·sec]	Height [μV]	Area%	Height%	Quantity	NTP	Resolution	Symmetry Factor	Warning
1	Unknown	5	37.967	23562	483	0.928	0.983	N/A	16681	1.678	N/A	
2	Unknown	5	40.060	2516005	48661	99.072	99.017	N/A	14594	N/A	1.351	

#	Peak Name	CH	tR [min]	Area [μV·sec]	Height [μV]	Area%	Height%	Quantity	NTP	Resolution	Symmetry Factor	Warning
1	Unknown	5	37.560	12582471	211922	25.806	29.719	N/A	9977	1.253	N/A	
2	Unknown	5	39.597	36176068	501157	74.194	70.281	N/A	8144	N/A	N/A	

^{1}H and ^{13}C NMR spectra data of products

1-Methyl-4-(methylsulfinyl)benzene (±)-1a

^{1}H NMR spectrum

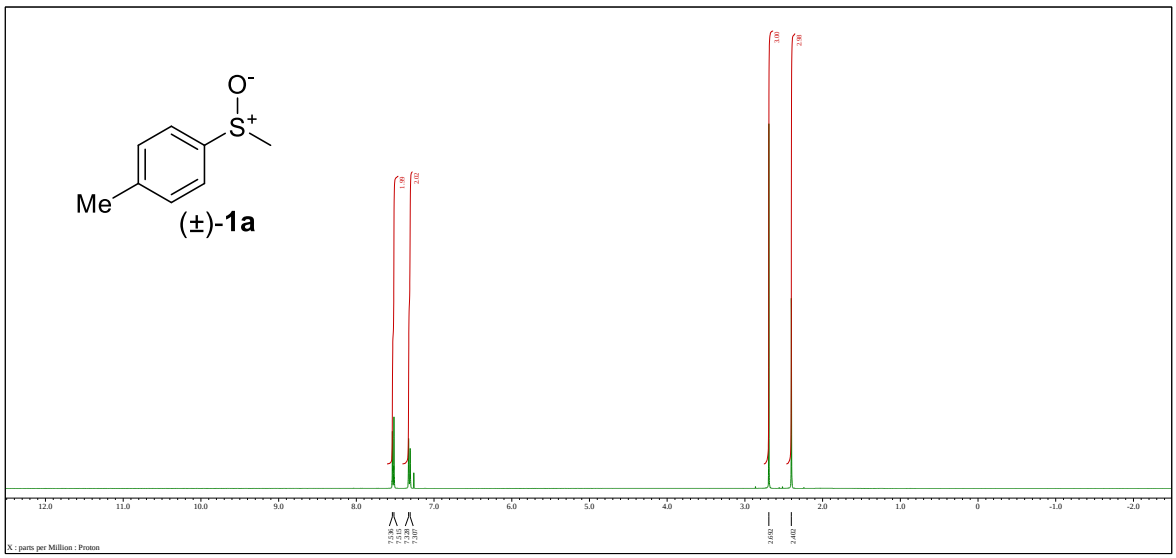

^{13}H NMR spectrum

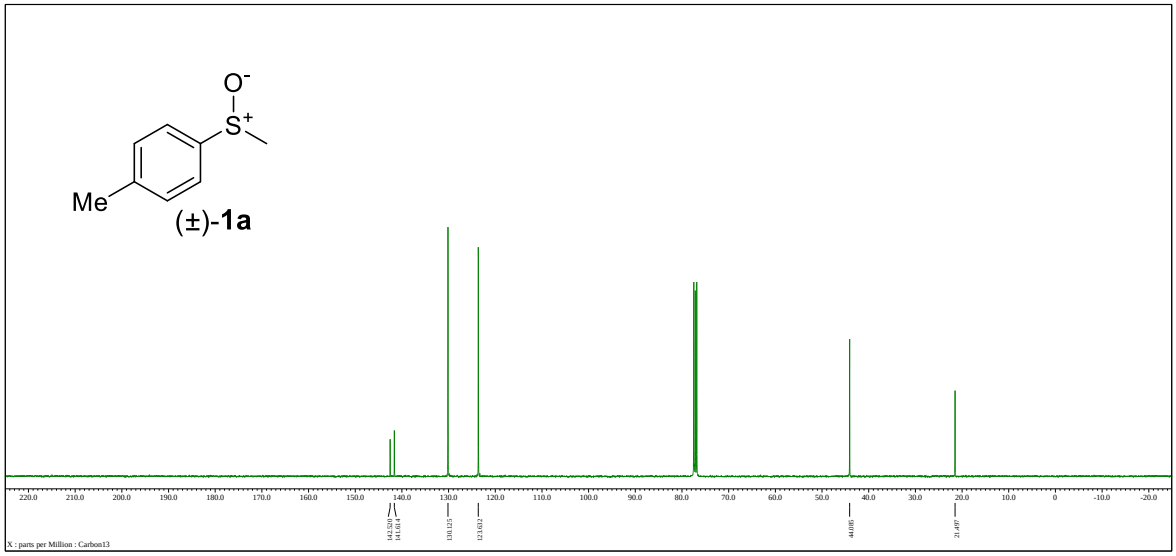

(Methylsulfinyl)benzene (±)-1b

^{1}H NMR spectrum

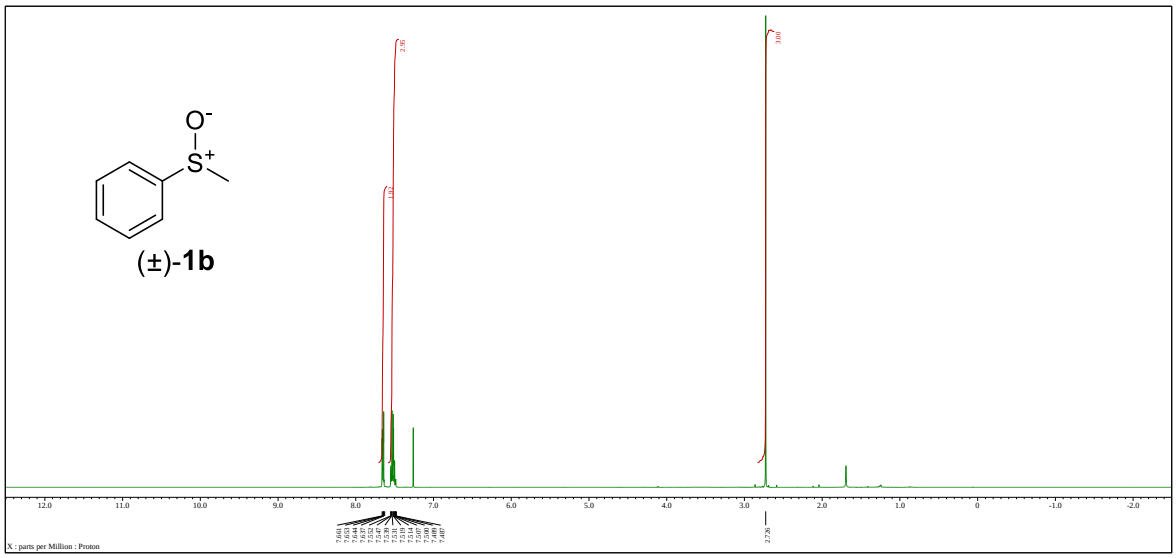

^{13}C NMR spectrum

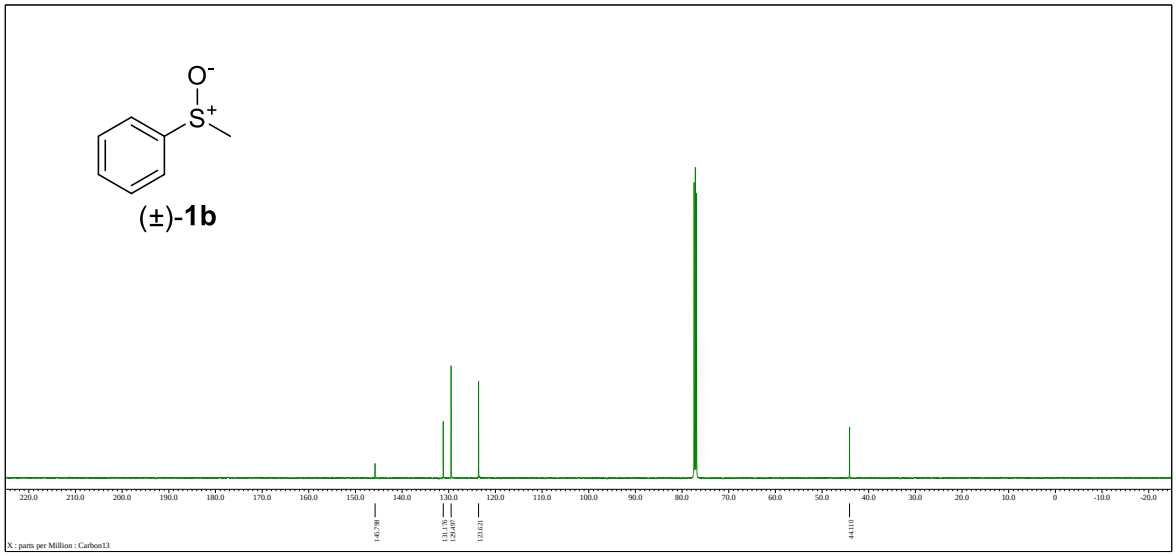

1-Methoxy-4-(methylsulfinyl)benzene (±)-1c

^{1}H NMR spectrum

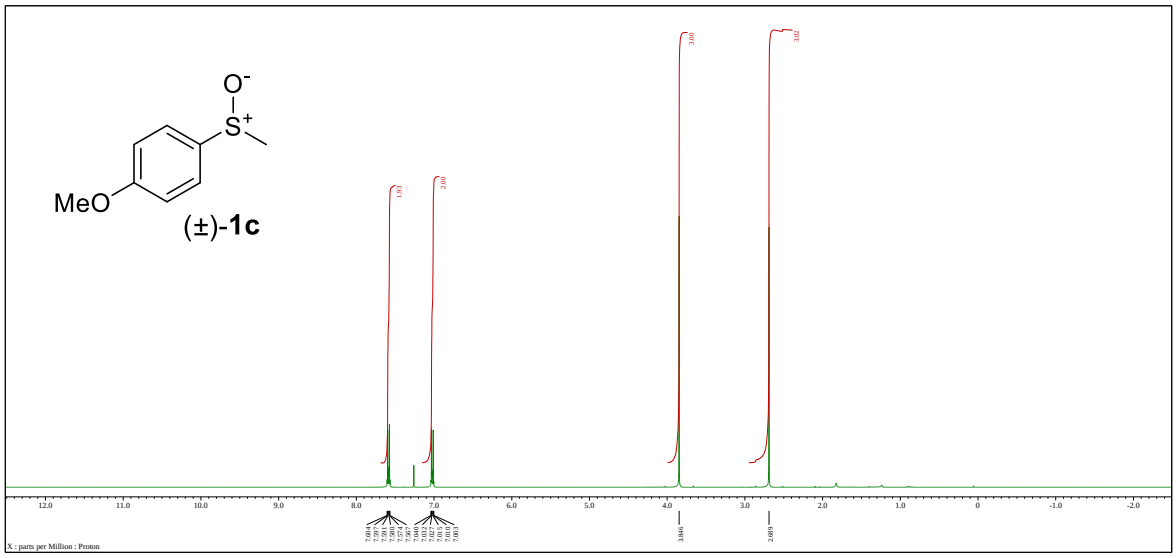

^{13}C NMR spectrum

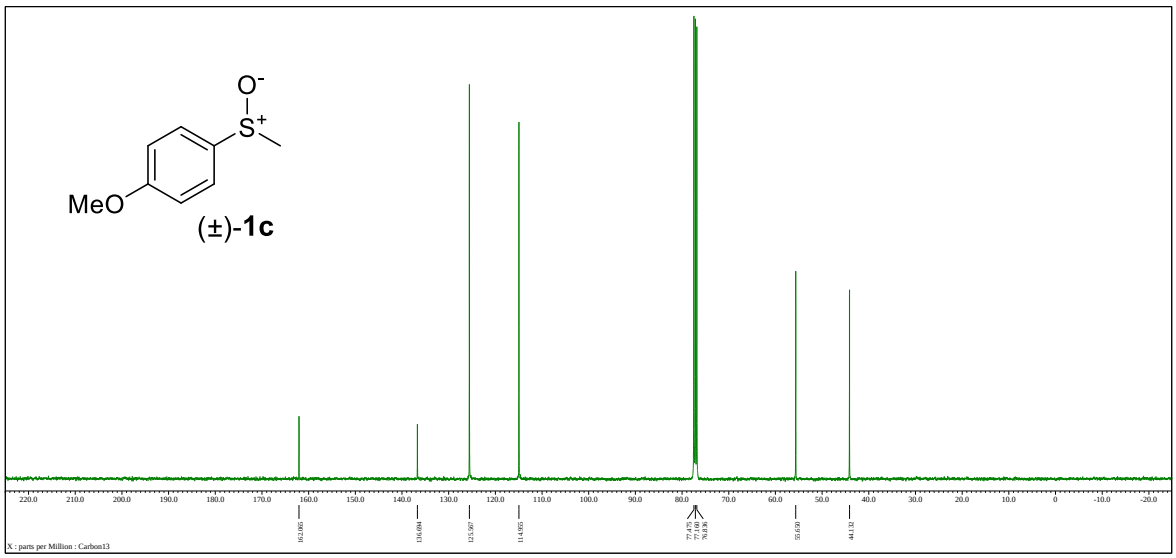

1-Bromo-4-(methylsulfinyl)benzene (±)-1d

^{1}H NMR spectrum

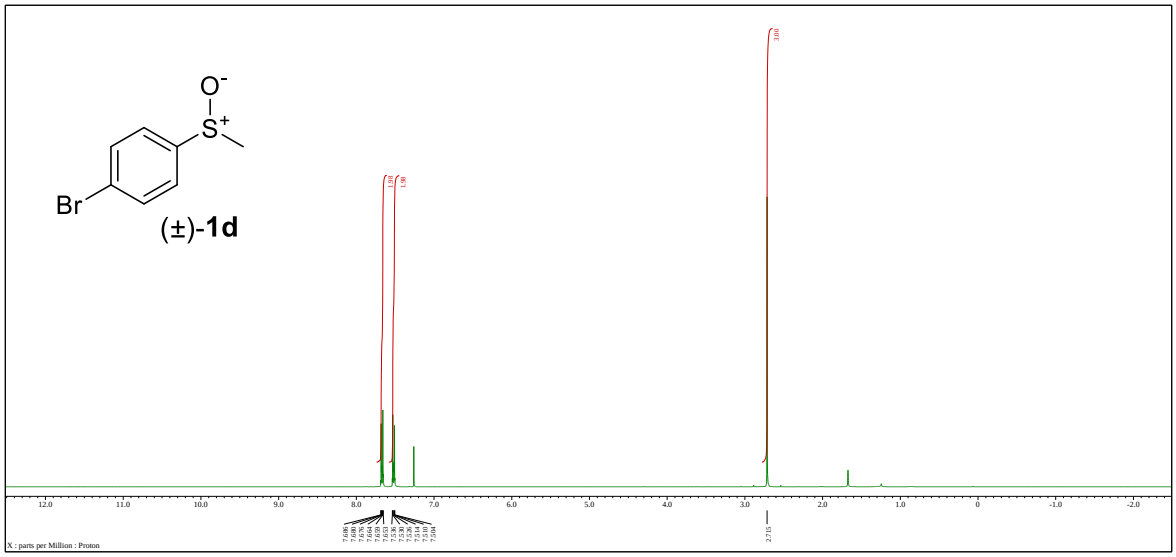

^{13}C NMR spectrum

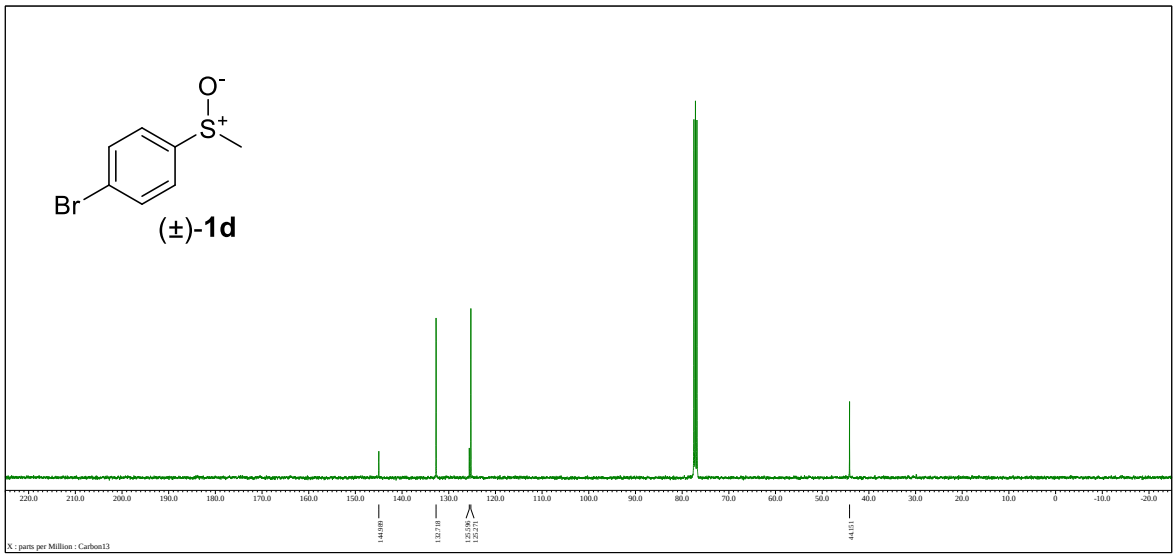

4-(Methylsulfinyl)benzonitrile (±)-1e

^{1}H NMR spectrum

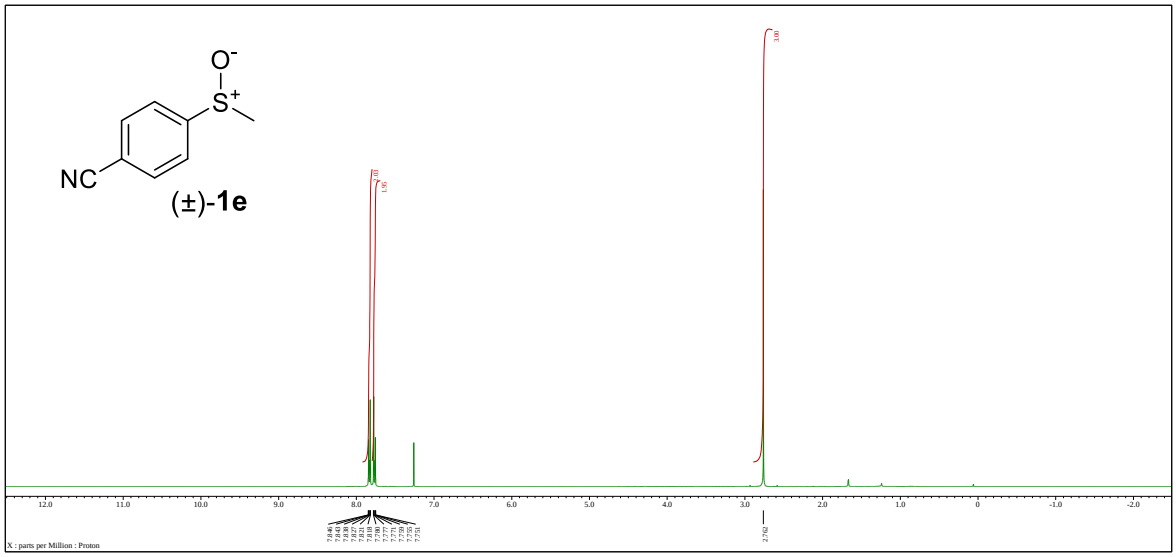

^{13}C NMR spectrum

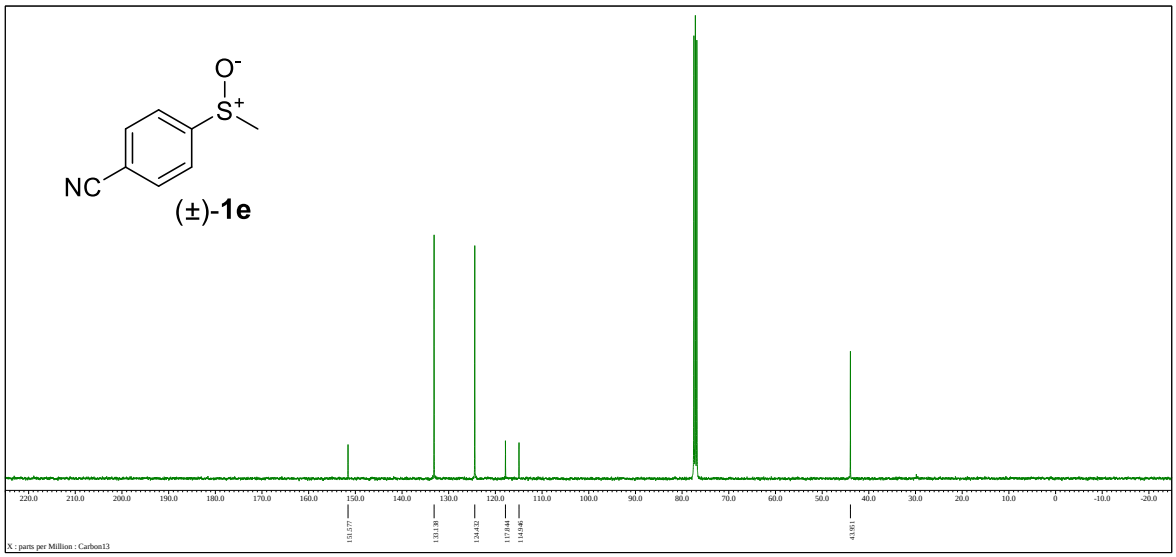

1-(Methylsulfinyl)-4-nitrobenzene (±)-1f

^{1}H NMR spectrum

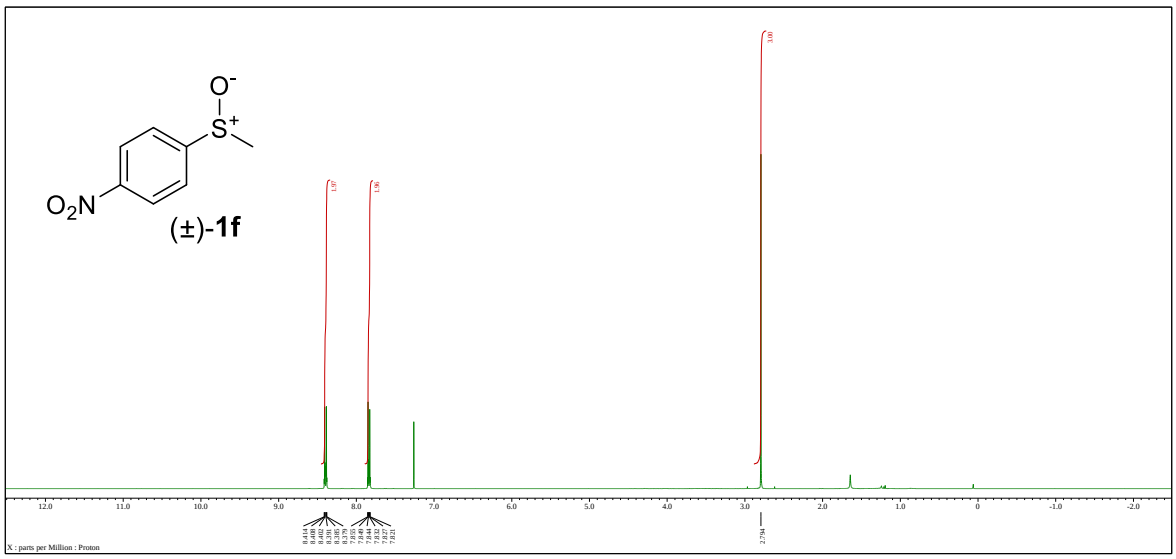

^{13}C NMR spectrum

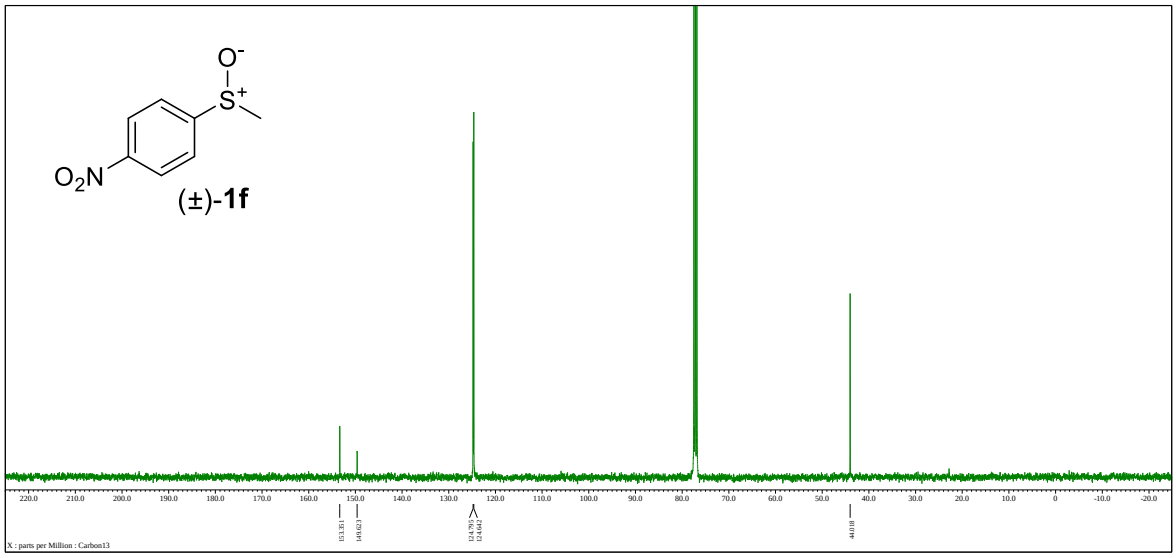

N,*N*-Dimethyl-4-(methylsulfinyl)aniline (*S*)-1g

^{1}H NMR spectrum

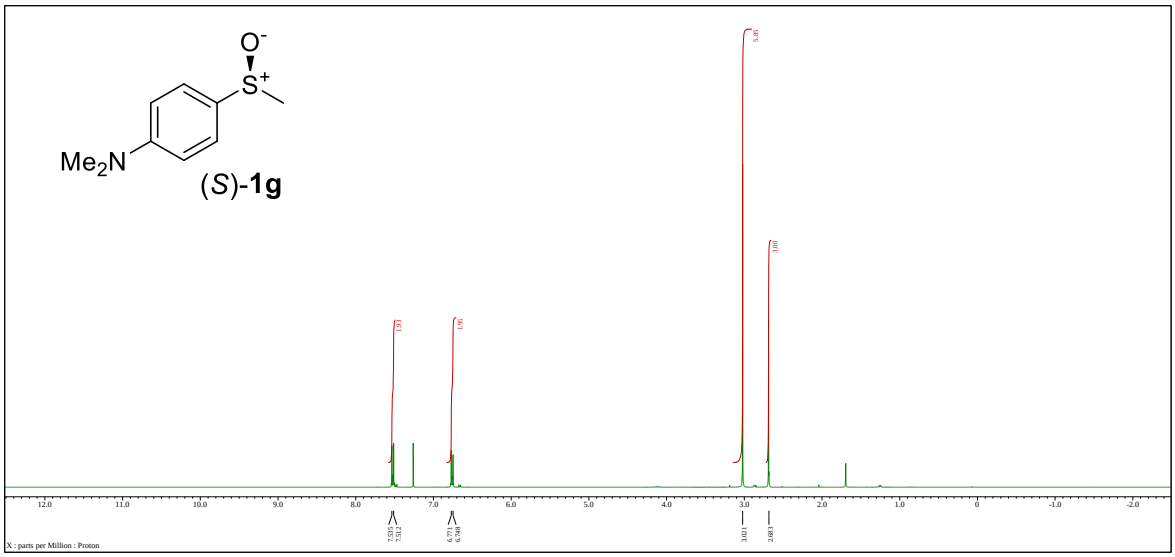

^{13}C NMR spectrum

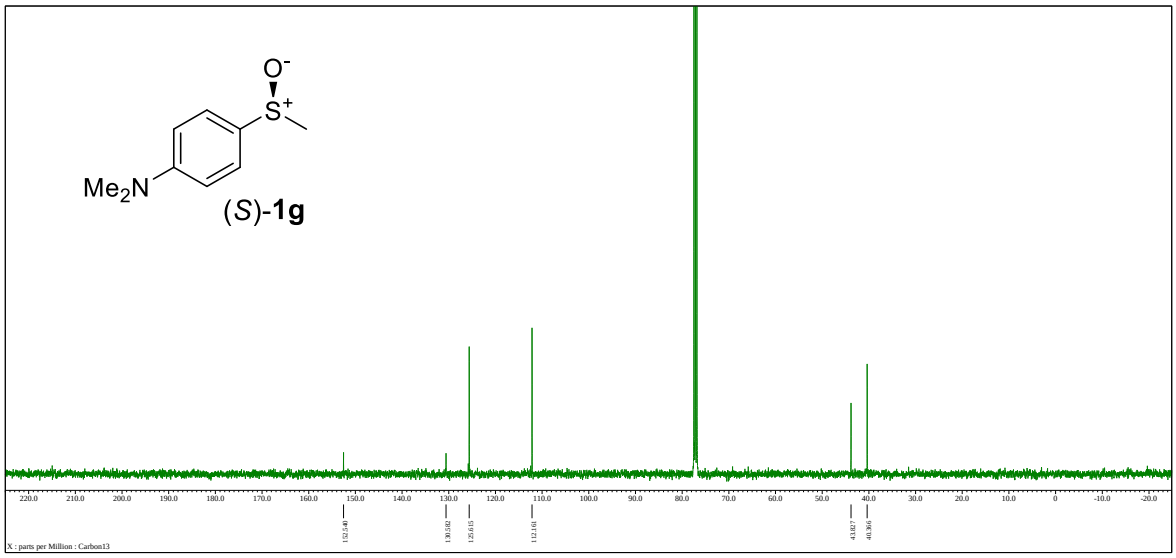

2-Iodo-4-methyl-1-(methylsulfinyl)benzene (±)-1h

^{1}H NMR spectrum

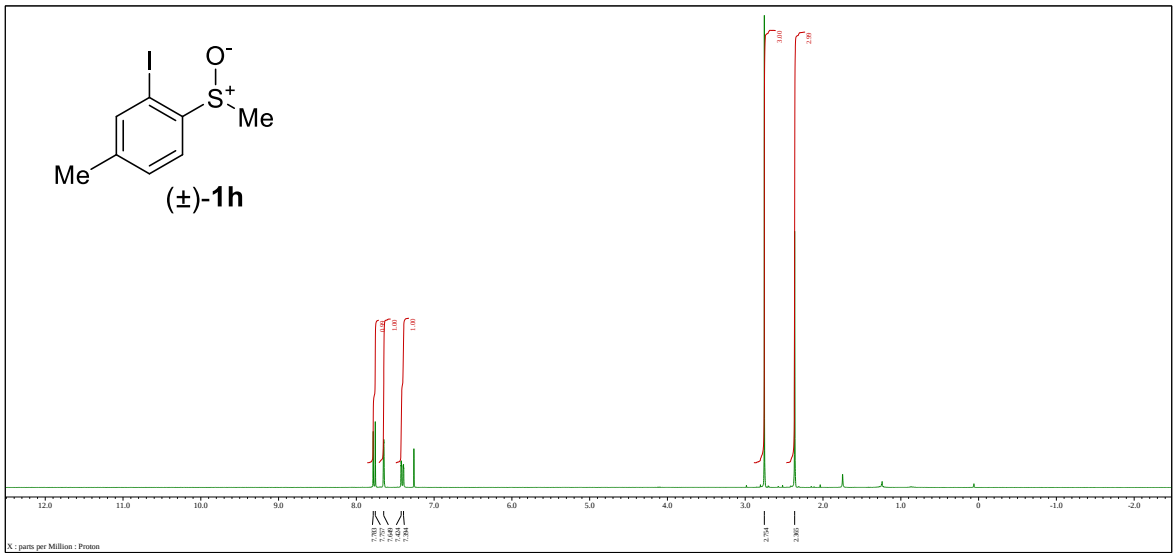

^{13}C NMR spectrum

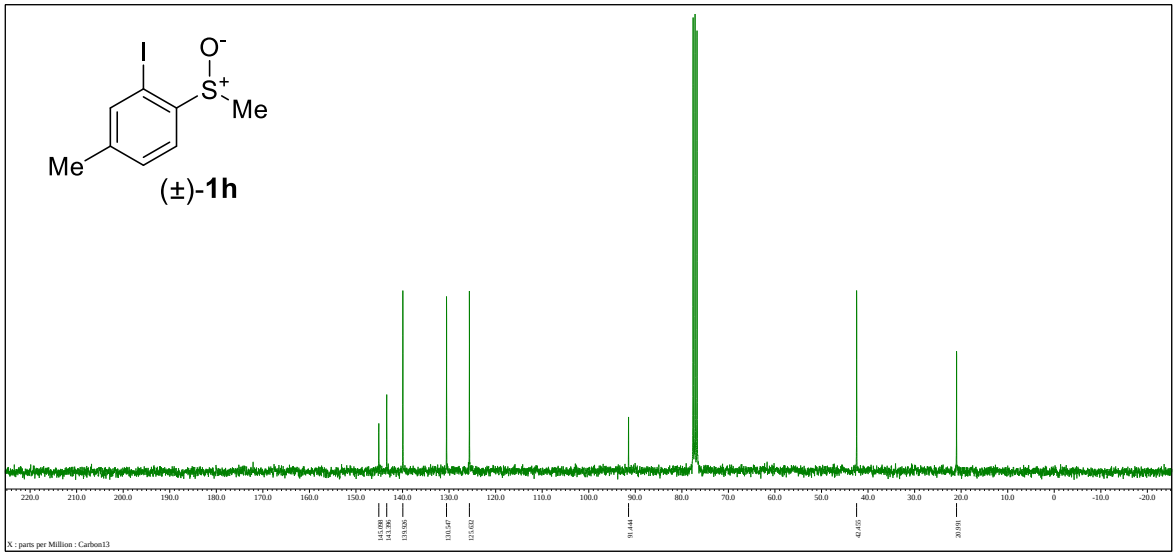

1-(Ethylsulfinyl)-4-methylbenzene (±)-1i

^{1}H NMR spectrum

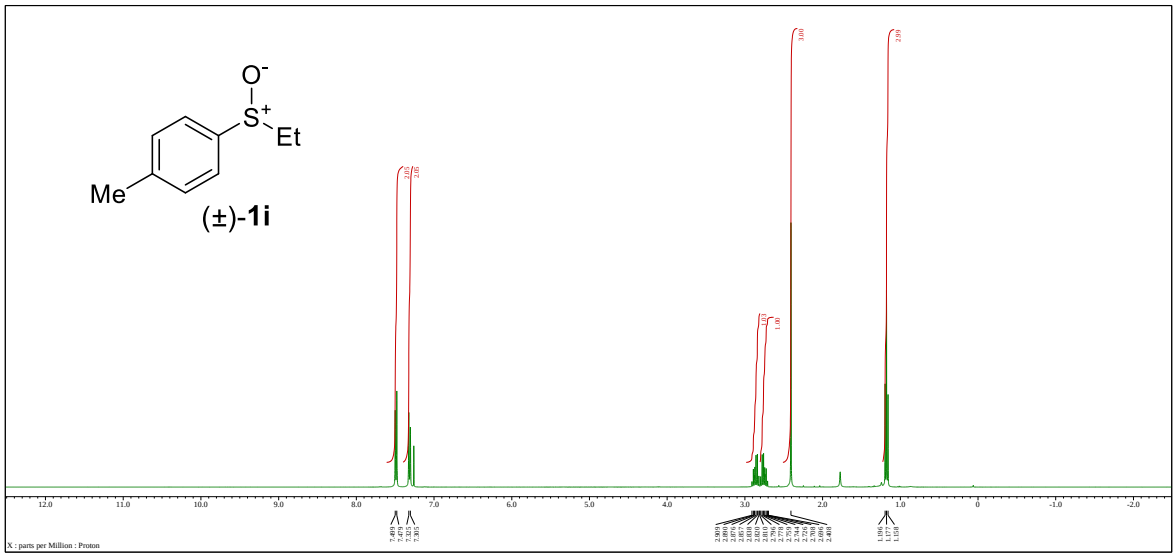

^{13}C NMR spectrum

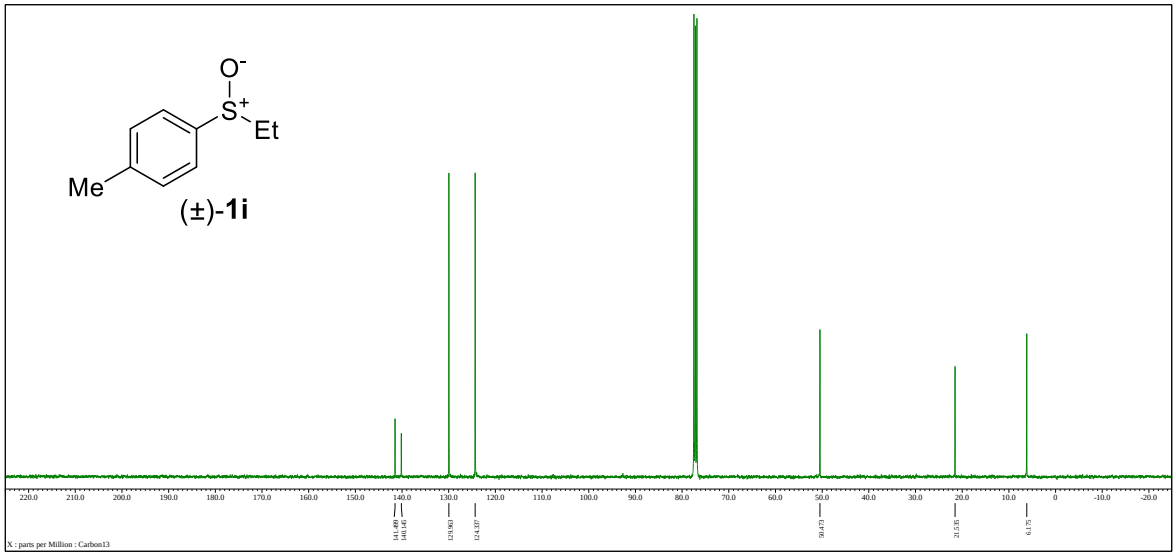

1-(*iso*-Propylsulfinyl)-4-methylbenzene (±)-1j

^{1}H NMR spectrum

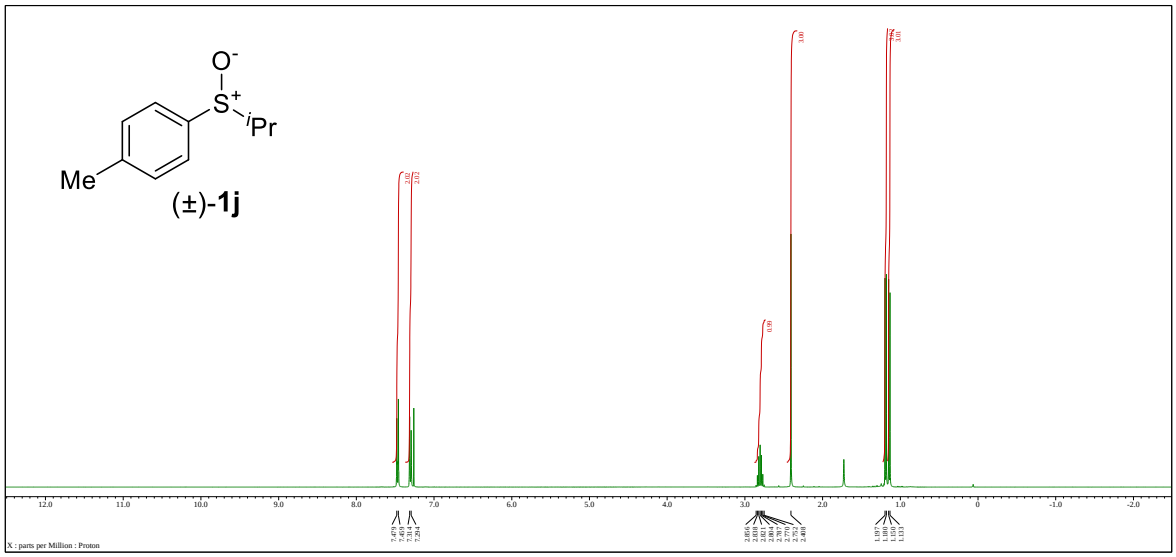

^{13}C NMR spectrum

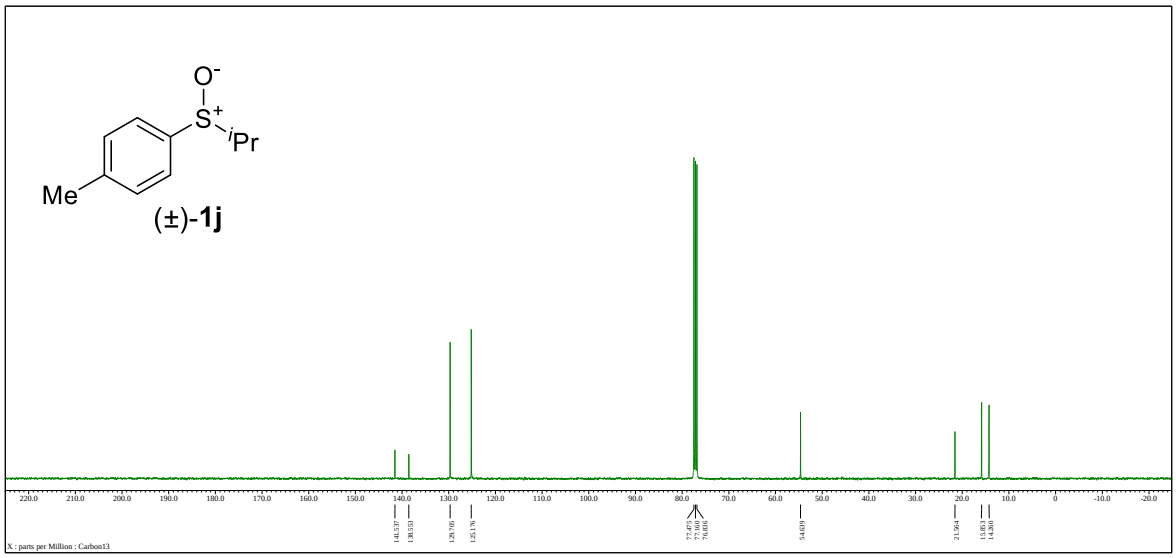

1-(*cyclo*-Propylsulfinyl)-4-methylbenzene (±)-1l

^{1}H NMR spectrum

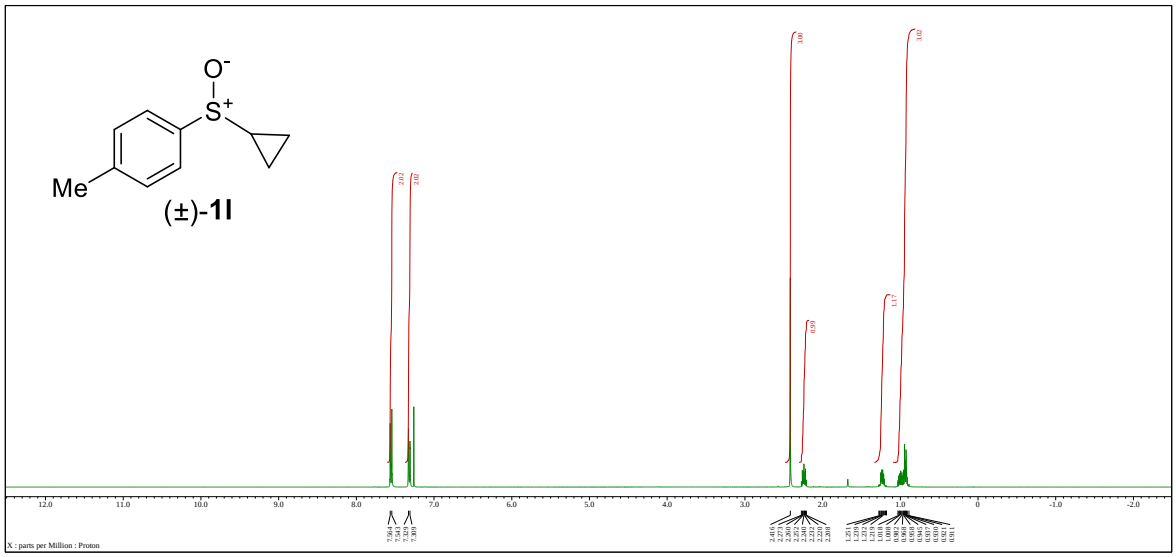

^{13}C NMR spectrum

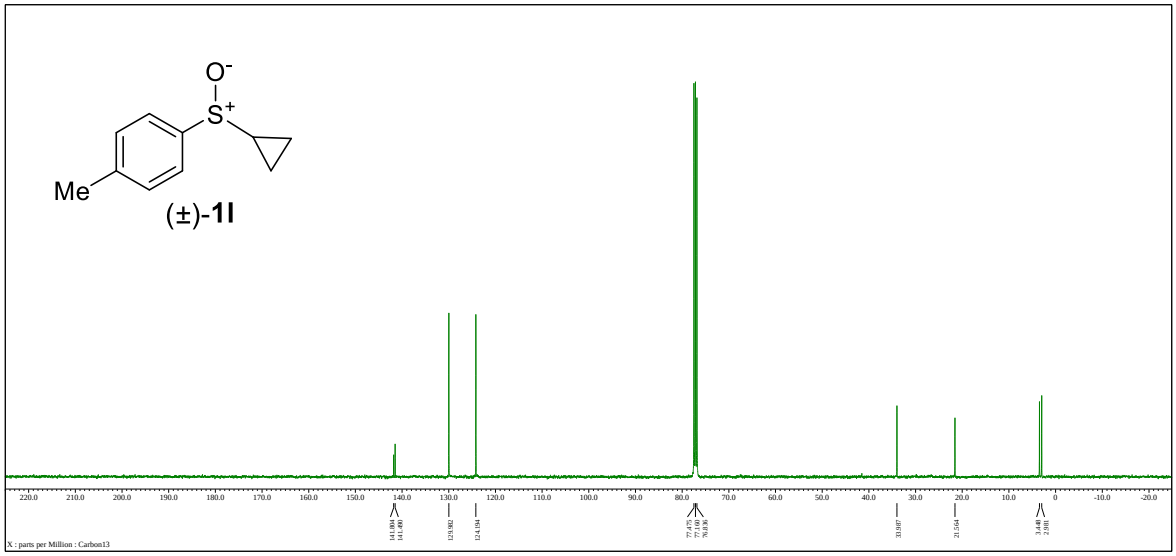

1-(*cyclo*-Pentylsulfinyl)-4-methylbenzene (*R*)-1m

^{1}H NMR spectrum

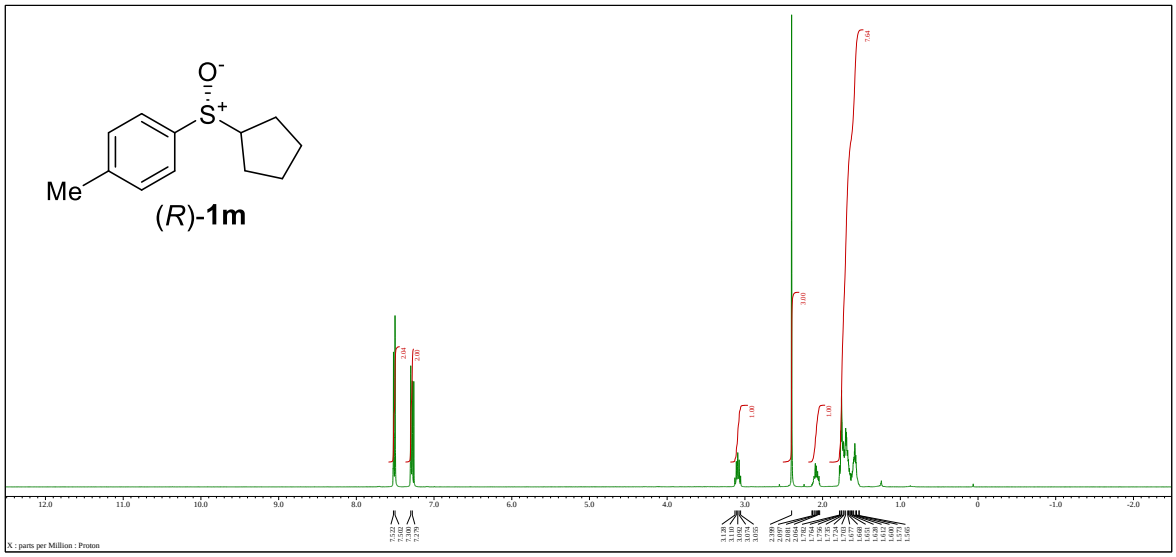

^{13}C NMR spectrum

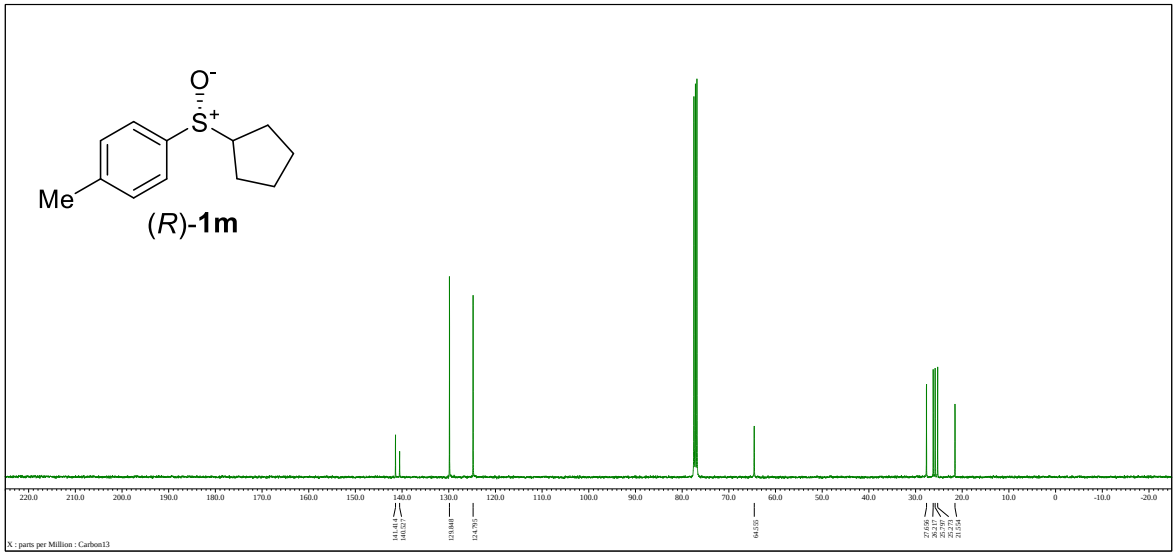

(Vinylsulfinyl)benzene (*R*)-1n

^{1}H NMR spectrum

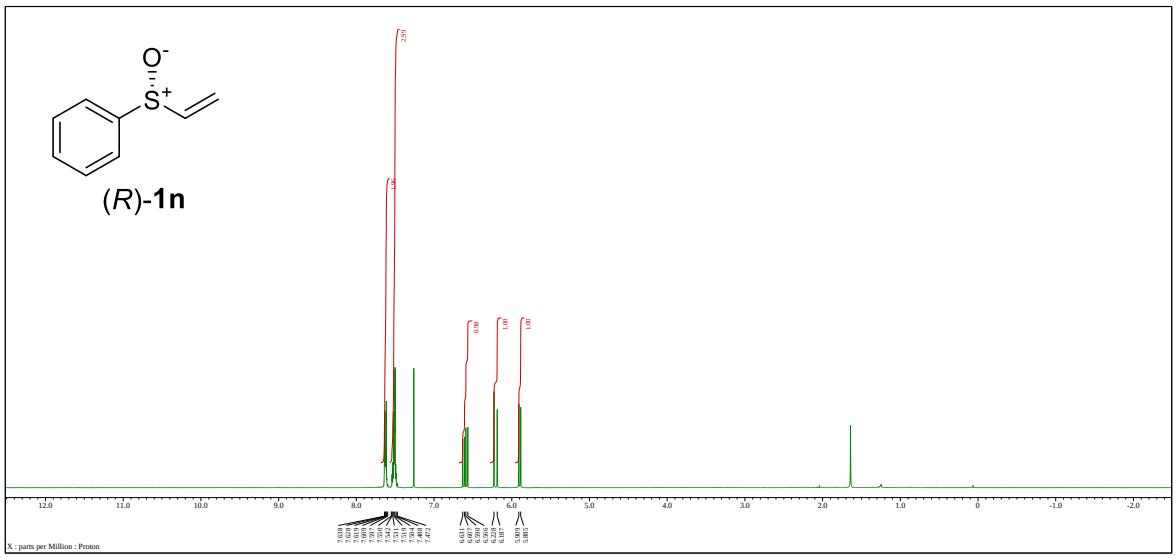

^{13}C NMR spectrum

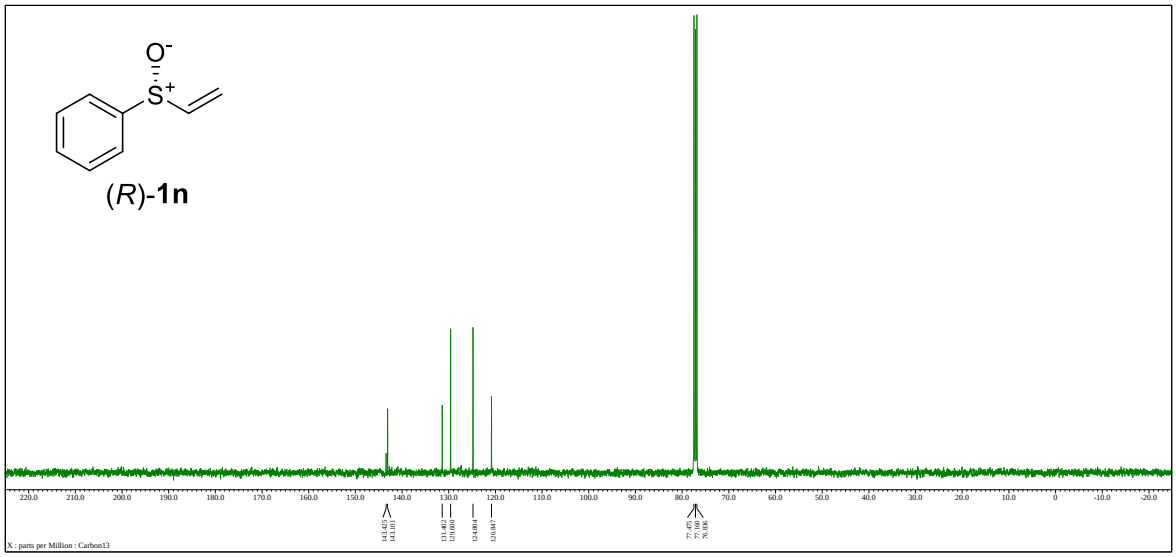

1-Methyl-4-(phenylsulfinyl)benzene (*R*)-1o

^{1}H NMR spectrum

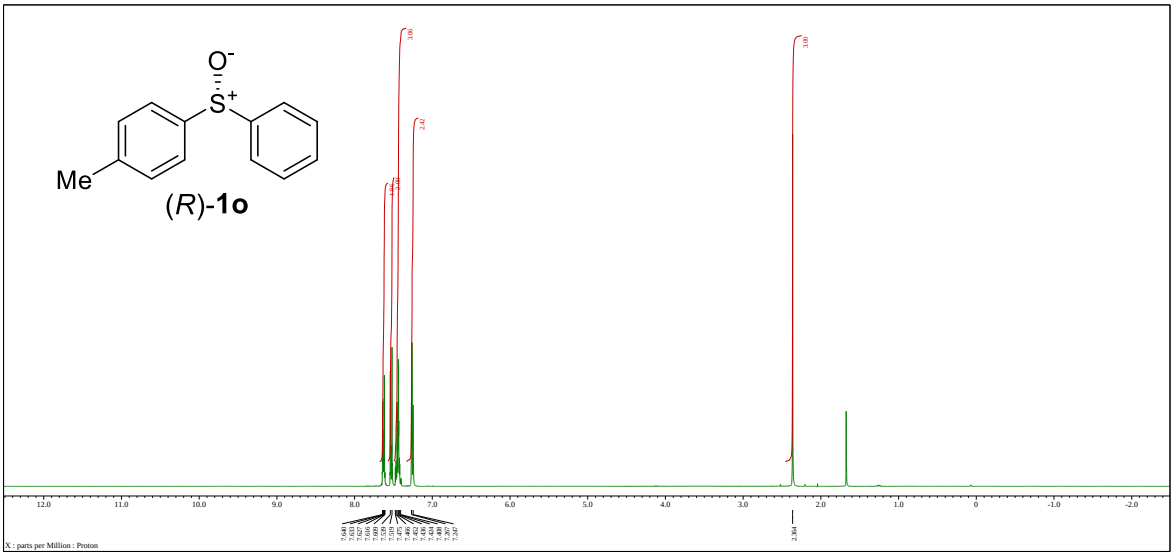

^{13}C NMR spectrum

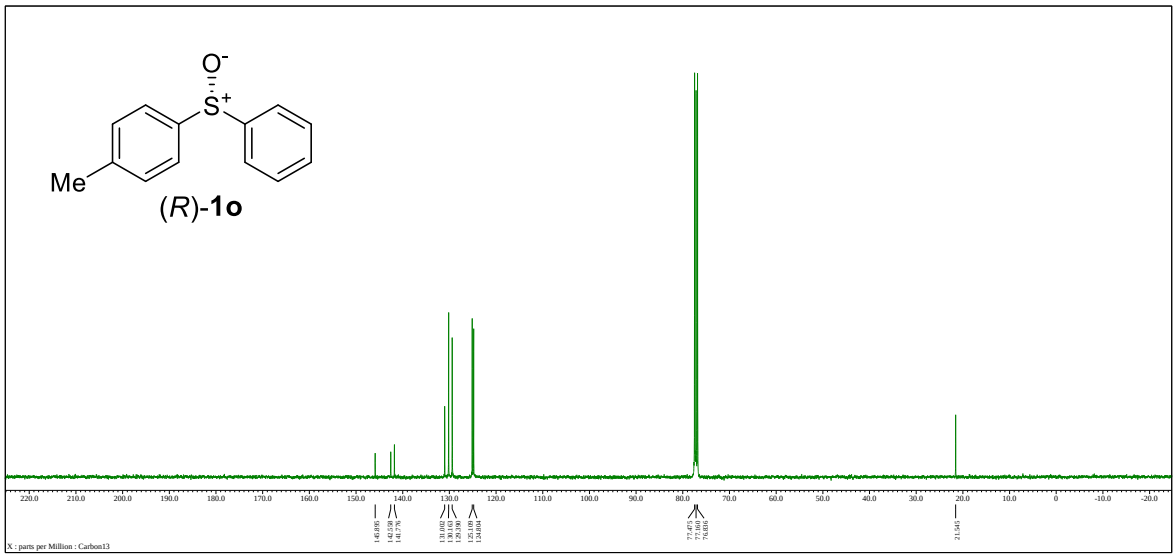

1-Methoxy-4-(*p*-tolylsulfinyl)benzene (*S*)-1p

^{1}H NMR spectrum

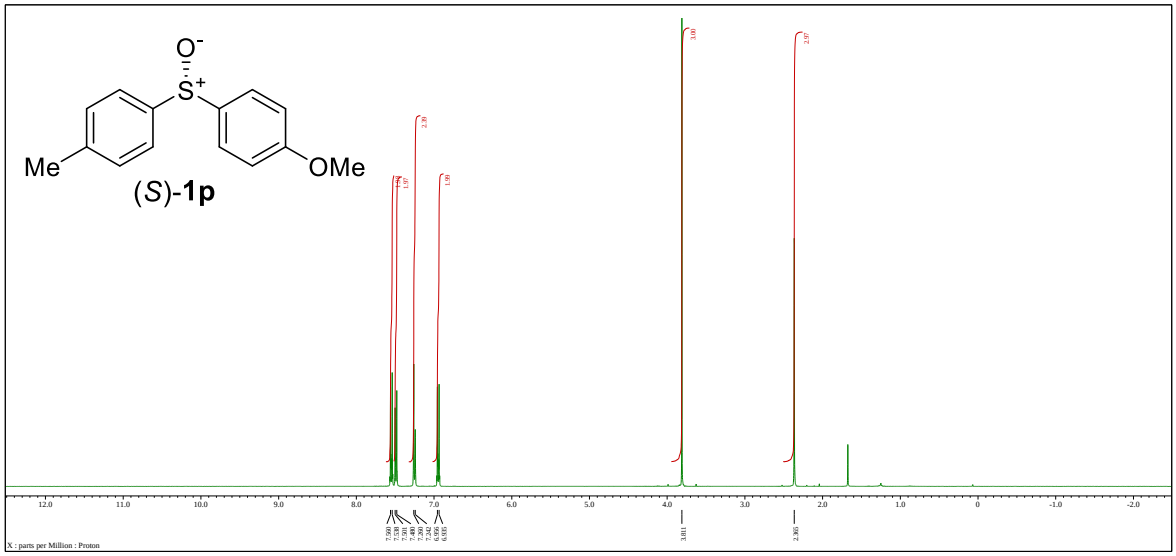

^{13}C NMR spectrum